UNIVERSITY OF CALIFORNIA

Los Angeles

Can an Earth-like Planet have a Titan-like Climate? Exploring the "In-Betweens" of

Terrestrial Planetary Climate States

A dissertation submitted in partial satisfaction

of the requirements for the degree

Doctor of Philosophy in Atmospheric & Oceanic Sciences

by

Matthew Mace McKinney

2022

ABSTRACT OF THE DISSERTATION

Can an Earth-like Planet have a Titan-like Climate? Exploring the "In-Betweens" of
Terrestrial Planetary Climate States

by

Matthew Mace McKinney
Doctor of Philosophy in Atmospheric & Oceanic Sciences
University of California, Los Angeles, 2022
Professor Jonathan Lloyd Mitchell, Chair

The three planets of the Inner Solar System with significant atmospheres, Venus, Earth, and Mars, can be described as representing three "climate archetypes" of terrestrial planets: Venus is hot, dry, and rotates slowly; Mars is cold and dry, with fast rotation similar to Earth; Earth is the "middle ground", warm enough to sustain liquid water on its surface but not so warm it evaporates away. These archetypes can be placed as endpoints on a spectrum of climates, where adjusting one or more planetary parameters can move a climate from one archetype to another, e.g. drying the surface can move an Earth-like planet towards the Venus and Mars archetypes. In addition to the three inner planets, there is one additional body in the Solar System that has a thick atmosphere and solid surface: Titan, a moon of Saturn. Titan presents a unique opportunity in observable planetary climates because it has a volatile liquid, or condensable, on its surface in the form of methane. This methane is able to evaporate to form clouds (Turtle et al., 2018) and likely rain (Turtle et al., 2011), but is mostly restricted to large polar lakes (Lunine and Lorenz, 2009) with the rest of the surface a vast desert (Mitchell and Lora, 2016). This means Titan's climate archetype is between the ocean-dominated Earth and the fully-dry Venus/Mars.

In this dissertation, we seek to further investigate the "in-betweens" of these climate archetypes, focusing on the transition between an Earth-like planet and a Titan-like one. To

accomplish this, we recreate a Titan-like climate using an Earth-like global climate model (GCM) by varying a small set of planetary parameters. We first limit the available water by placing a continental land strip centered on the equator and varying its width. This mimics Titan's dry tropics and wet poles, and could be similar to past continental arrangements in Earth's history. Second, we take three of these land strip widths and vary the rotation period, starting with Earth's rotation and moving towards Titan's (16 Earth days). Third, for the same three land strip widths and using Earth's rotation, we vary the volatility of the condensable via a constant multiplied to the saturation vapor pressure. Titan's condensable, methane, is more volatile under Titan's surface conditions than water is on Earth, resulting in high specific humidities. By artificially increasing the saturation vapor pressure, we can approximate this effect without changing the properties of the condensable.

We find that simply replicating Titan's parameters in our simulations does not fully reproduce Titan-like conditions. In addition, we find that it is possible to reproduce key Titan-like features by varying only the width of the equatorial land strips. This may indicate that there are many possible "in-between" states an Earth-like planet can have that span the gap between the Earth and Titan climate archetypes. It also suggests Titan's current climate is primarily dependent on its surface liquid distribution, meaning an Earth-like planet with similar topography is likely to display the same features.

The dissertation of Matthew Mace McKinney is approved.

David A. Paige

Gang Chen

J. David Neelin

Jonathan Lloyd Mitchell, Committee Chair

University of California, Los Angeles

2022

To my parents

who encouraged me to try new things

To my wife

whose insights were invaluable

to this work

TABLE OF CONTENTS

LIST OF FIGURES

x

LIST OF TABLES

ACKNOWLEDGMENTS

Many people were part of my journey to a Ph.D. degree, and I would not have been able to accomplish this without their presence. First and foremost I would like to thank my parents. They started my path towards pursuing what interested me and gave me the opportunities to see it through.

I want to thank my wife, Yue Huang, for her support during my graduate school career. Her knowledge and expertise were invaluable in navigating my way through the unknowns.

I want to thank my advisor, Jonathan Mitchell, who gave me the chance to work on a project I truly enjoyed and enter a field I will be passionate about for years to come. Additionally, I thank my previous advisors that helped guide my research experience, Chidong Zhang at the University of Miami and Alex Hall at UCLA.

My sincere thanks to my doctoral committee members, Gang Chen, David Neelin, and David Paige, for their patience and feedback on my research.

I want to extend my gratitude to my collaborators at the University of Exeter, Geoff Vallis and Stephen Thomson, who helped me set up and run the model used in this work.

I also want to thank all of my past and current group members who helped give feedback and contributed their expertise to my work, Juan Lora, Sean Faulk, Tersi Arias-Young, Spencer Hill, Hung-I Lee, Francisco Spaulding-Astudillo, Rebecca Lewis, David Moore, and Emery Grahill-Bland.

Vita

2016	B.S., Meteorology, Mathematics, University of Miami.
2016-2022	Teaching Assistant, University of California, Los Angeles.
2017-2022	Graduate Student Researcher, University of California, Los Angeles.
2018	M.S., Atmospheric & Oceanic Sciences, University of California, Los Angeles.

Publications

Effects of Varying Land Coverage, Rotation Period, and Water Vapor on Equatorial Climates that Bridge the Gap between Earth-like and Titan-like. **M. McKinney**, J. Mitchell, and S.I. Thomson. Journal of the Atmospheric Sciences. *Accepted.* (2022).

Effects of Seasonality on Planets with Climates Bridging the Gap between Earth-like and Titan-like. **M. McKinney** and J. Mitchell. *In prep.* (2022).

What is Titan-like? Analysis of Simulations from the Titan Atmosphere Model using Observationally Motivated Criteria for a Titan-like Climate. **M. McKinney** and J. Mitchell. *In prep.* (2022).

CHAPTER 1

Introduction

The three planets of the Inner Solar System with significant atmospheres, Venus, Earth, and Mars, can be described as representing three "climate archetypes" of terrestrial planets. Each archetype characterizes a possible fate for an otherwise Earth-like world:

1. Venus is too close to the Sun, which eventually evaporated its oceans and shut off the weathering process that removes CO_2 from the atmosphere in a process referred to as the "runaway greenhouse" (Ingersoll, 1969). The end result is a thick CO_2 atmosphere and an incredibly hot, dry climate.

2. Earth was not as close as Venus, allowing it to retain its oceans and mild temperatures. It did at times almost become too cold, slipping into "snowball Earth" states when the Sun was younger and dimmer, and will eventually become too hot as the Sun continues to warm (Wolf and Toon, 2015).

3. Mars was too far from the Sun, freezing its oceans and condensing the CO_2 in its atmosphere in a process called "atmospheric collapse". The result is a cold, dry climate with only a thin CO_2 atmosphere and ancient hydrogeologic features to hint at a more Earth-like past.

When taken together, these three archetypes demonstrate key concepts of habitability and atmospheric development that can be applied to other planetary systems. There is, however, one more terrestrial body with a significant atmosphere in the Solar System. A moon of Saturn, Titan possesses both a large N_2 atmosphere and large deposits of surface liquid.

These two features are otherwise unique to Earth, making Titan a key opportunity to expand on our collection of climate archetypes.

The primary distinguishing factor for Earth's climate relative to Venus and Mars is the presence of a volatile liquid, or condensable, on the surface. A condensable in the context of planetary science is a liquid that can evaporate from the surface into the atmosphere, subsequently condense and/or solidify, and then fall back to the surface as precipitation. Earth's condensable, water, is abundant enough and paired with significant enough topography such that over 70% of its surface is an ocean multiple kilometers deep. As previously mentioned, Earth is not alone in having deposits of liquid on its surface. Titan possesses several large methane lakes that can evaporate to form clouds (Turtle et al., 2018) and rain (Turtle et al., 2011), meaning that Titan's condensable is methane as opposed to water. Titan's surface is not dominated by methane, however. Its lakes of liquid methane are concentrated at its two poles (Lunine and Lorenz, 2009) and in a broader polar "wetlands" extending to the midlatitudes (Lora and Mitchell, 2015; Mitchell and Lora, 2016) while the rest of its surface is a vast desert centered on the equator. This presents an interesting contrast to Earth, which is often described as an "aquaplanet", meaning its surface and climate are dominated by deep, global oceans. Titan can be considered its natural counterpart, the "terraplanet", where the surface and climate are dominated by dry land as a single global continent with geographically isolated reservoirs of surface liquid.

Figure 1.1 presents the four archetypal terrestrial planets of the Solar System in relation to each other's characteristics. There are three primary planetary parameters we will consider in this work:

1. How much of the surface is covered by condensable? At the top of the diagram is Earth, which has most of its surface covered with deep oceans. Moving down towards the bottom there is Titan, with a small percentage of its area covered by shallow methane seas, and then the completely dry Mars and Venus.

2. How fast does the planet rotate? Earth and Mars rotate at a similar rate, which is much faster than Titan ($\sim$16 Earth days) and extremely fast compared to Venus ($\sim$243 Earth days).

3. How volatile is the condensable, or in other words, how much of the condensable is found in the atmosphere as vapor rather than as a liquid on the surface? Earth, Mars, and Venus all have (or had) water as their primary condensable. Titan has methane, which is much more volatile under its surface conditions than water is on Earth. This means most of Titan's available methane is found in its atmosphere, where it constitutes a significant proportion ($\sim$4%) of the total mass.
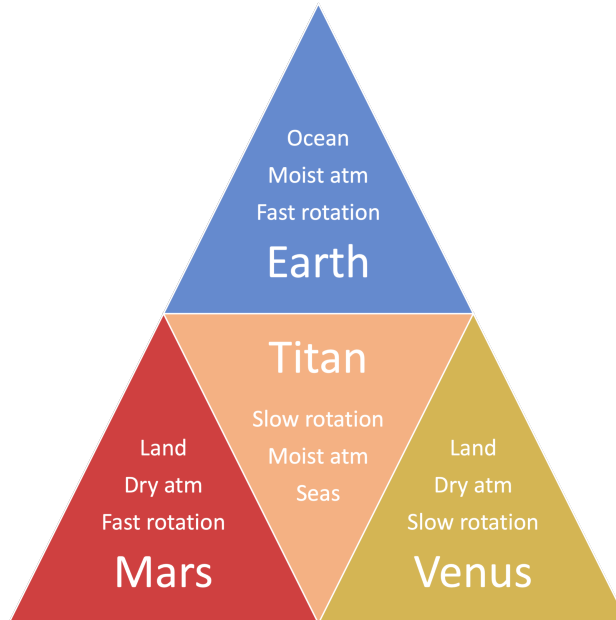
Figure 1.1: TPACE Pyramid

Changing the value of these parameters allows us to move from one archetype to another in a controlled way, but also allows us to explore the "in-between" states. These are represented by the borders between each archetype in Figure 1.1. The border most interesting to us is that between Earth and Titan, which represents a range of possible climates that all

have condenable surface liquid. Earth and Titan are the end-points of this range, acting as the "extremes".

Titan differs from Earth in several important ways. Its tropics are uniformly higher elevation than its midlatitudes and poles, as opposed to topography on Earth which has significant local variation and minimal dependence on latitude. Its condensable, methane, is more volatile under Titan's surface conditions than water is under Earth's. The volatility of a liquid is a measure of how easily it evaporates at a given temperature and pressure; a more volatile liquid will evaporate more readily than a less volatile liquid under the same conditions. In Titan's atmosphere the result is higher specific humidities (i.e the mass of condensable vapor to the total mass of air) of methane in the troposphere than can be achieved on Earth with water. Its rotation period is long, 16 Earth-days, weakening the effects of the Coriolis Force. On Earth the Coriolis force causes moving air parcels and ocean currents to curve in their path. This can be seen in many common weather patterns, including hurricanes and baroclinic storms. The Coriolis Force is zero at the equator and sub-dominant in an area confined to $\sim$10-20°N/S latitude. This sub-dominant area can be referred to as the "tropics" with regards to atmospheric dynamics because the weak Coriolis Force – and correspondingly small temperature gradient – prevents the formation of most large-scale weather systems common to the rest of the planet (Sobel et al., 2001, often referred to as the Weak Temperature Gradient (WTG) approximation). This region is much broader on Titan due to its slower rotation (and to some extent its smaller size), so we can describe Titan as an "all-tropics" planet (Lora and Mitchell, 2015). This means that its Intertropical Convergence Zone (ITCZ), the location where air rises out of the boundary layer (BL) in the summer hemisphere tropics, moves deep into the summer hemisphere (e.g. Mitchell and Lora, 2016, and citations therein; Faulk et al., 2017; Guendelman and Kaspi, 2018; Singh, 2019; Hill et al., 2021, 2022).

The ability of Titan's ITCZ to move well into the midlatitudes suggests there is a significant seasonal cycle. Earth's tropics experience seasons primarily from the movement of the
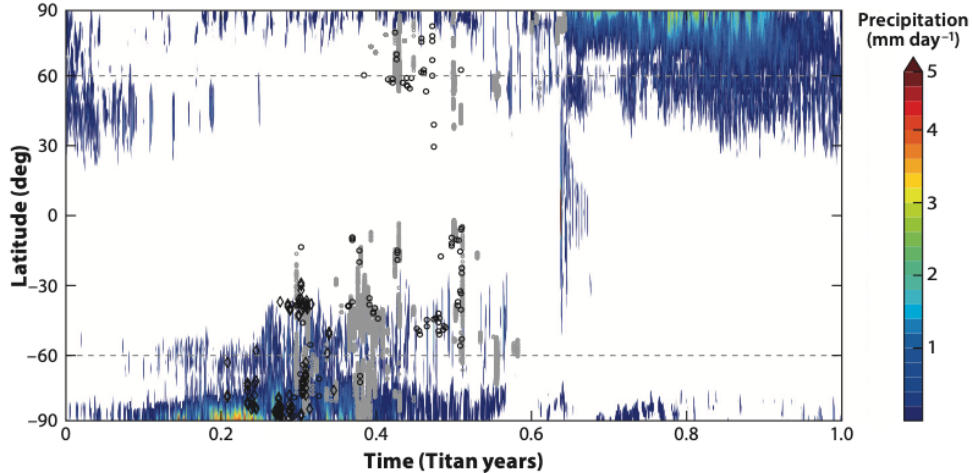
Figure 1.2: Cloud observations and TAM Wetlands simulated precipitation, equivalent to Figure 4 from Mitchell and Lora (2016).

ITCZ, which brings rain to different parts of the tropics as it moves in response to seasonal insolation. Titan's ITCZ is able to bring precipitation to the high latitudes as well, and may be the primary source of precipitation for the entire surface. Figure 1.2 shows simulated precipitation from the Titan Atmosphere Model (TAM; Lora et al., 2015) overlayed with observed clouds on Titan (Figure 4 from Mitchell and Lora, 2016). Both the clouds and precipitation shift between the two poles as the summer season moves between the hemispheres, with only some transient occurrences in the low latitudes. This is rather different from Earth's ITCZ, which is consistently rainy and cloudy throughout its seasonal motions over the equator to the summer hemisphere's tropics. This points to the dry tropical surface on Titan as a key driver of this difference, since on Earth the ITCZ is mostly over warm tropical oceans that provide abundant evaporation. Figure 1.3 shows simulated q_1 for a TAM simulation over an average Titan year. The tropics are notably drier than the high latitudes, despite having higher annual-mean temperatures that would allow air parcels to hold more vapor. This suggests there is either a mechanism for removing moisture from the tropical surface that dominates transport into it, or that the transport itself is restricted. Mitchell and Lora (2016) hypothesizes that the tropical humidity is set from above by sat-

urated parcels descending from the top of the dry boundary layer. They point to Huygens probe observations that the troposphere in Titan's tropics was saturated up to the edge of boundary layer (Niemann et al., 2005; Tokano et al., 2006), which could be maintained by outflow from high-latitude storms. When the saturated parcels sink into the tropical boundary layer, they warm adiabatically and maintain their specific humidity, resulting in an undersaturated tropical surface.
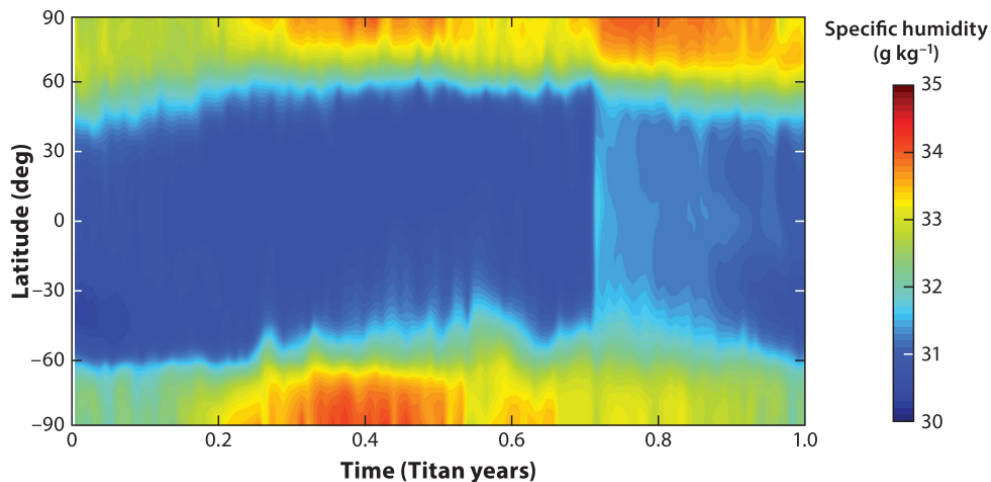
Figure 1.3: TAM Wetlands simulated q_1, equivalent to Figure 9 from Mitchell and Lora (2016).

The term "all-tropics" would suggest that Titan has a singular, global Hadley Cell (HC). As such, it is important to understand the dynamics of the HC and how these have been derived. Held and Hou (1980) (subsequently HH80) developed an initial model for the width of an axisymmetric HC that made three primary assumptions:

1. The flow is in gradient balance,

2. The poleward flow conserves angular momentum, and

3. Energy is conserved within the flow.

The HH80 conception of the HC is a dry, closed circulation where winds rise at the equator

and maintain their angular momentum as they flow poleward. This model was later expanded on by Caballero et al. (2008), who developed a more general model that could be applied to a radiative-convective atmosphere. The height of the tropopause in these approaches was for the most part considered largely invariable in latitude within the HC. Hill et al. (2020) looked at using a fixed tropopause temperature instead, allowing the tropopause height to vary with surface temperature. They found that in Earth-like climates this change in assumptions has little impact on HC structure, as the regions where it might be expected to have the largest effects are also the least sensitive to it. They do note that a fixed tropopause temperature may be more appropriate for smaller, slower-rotating, cooler planets, which would include Titan.

The aforementioned models focused only on an axisymmetric HC, equivalent to a permanent equinox or annual-mean state (Hill et al., 2022). This situation is rare, as both Earth and Titan experience seasonal shifts in insolation due to axial tilt. The most common condition for both planets is thus an off-equatorial peak in solar heating, resulting in an asymmetric, cross-equatorial HC (Lindzen and Hou, 1988). The rising branch, and therefore the ITCZ, moves poleward into the summer hemisphere, bringing seasonal rain to the tropics and subtropics. When this occurs over a continent the lower heat capacity of the dry surface can allow the latitude of peak heating to extend well into the subtropics, forming a monsoon (Bordoni and Schneider, 2008). The descending branch of the HC also moves poleward in the summer hemisphere, but much less than the rising branch (Adam et al., 2016). This creates a small summer cell that is significantly dwarfed by the cross-equatorial winter cell. Despite the greater extent in latitude of the cross-equatorial HC circulation, it appears to be more angular momentum-conserving than the equinoctial HC (Walker and Schneider, 2006; Bordoni and Schneider, 2008). They point to significant eddy momentum flux into the equinoctial HC of the Fall hemisphere as the main driver that allows streamlines to cross angular momentum contours. These fluxes are largely blocked by strong upper-level easterly winds that develop with the formation of a cross-equatorial cell, allowing it to more closely

match the angular momentum-conserving theories of HC circulation.

While it is true that the cross-equatorial cell is closer to angular momentum conservation, it and its equinoctial counterpart are both clearly influenced by eddies. Walker and Schneider (2006) found that neither the angular momentum-conserving approach nor one primarily dominated by eddies is adequate for describing a realistic HC circulation. Instead, a mid-range approach would be necessary that can handle both regions of the circulation dominated by one mode over the other and regions where neither is clearly dominant. Such a closed theory is lacking. Mitchell and Hill (2021) focus on the subsiding branch of the HC that occurs in the subtropical regime, which they define as being the transition point between the convective tropics and quasigeostrophic extratropics. Their theory is that the vertical velocity of the descending branch is largely unaffected by planetary rotation period due to being constrained by the piecewise-constant static stability of the tropics and extratropics. The substropics represent the transition between the two values of static stability on either side, meaning that if it is only weakly influenced by rotation period, the mean value in the subtropics is also weakly influenced. This holds even if the subtropics widen/contract due to a weaker/stronger Coriolis Force that comes with a change in rotation period, since it is the mean value that is relevant to the downward velocity (Mitchell and Hill, 2021).

Hill et al. (2022) presents a unified theory for the location of both the ascending and descending branches of the cross-equatorial HC, which combines the work of Kang and Lu (2012) on the descending branch and Hill et al. (2021) on the ascending branch. They also incorporate the effects of surface heat capacity, which acts to both damp the seasonal change and delay it from the seasonal cycle of insolation. This theory places the ascending branch at the poleward limit of where the gradient wind of the radiative-convective equilibrium state would have an angular momentum maximum (Hide, 1969; Hill et al., 2021, i.e., Hide's Theorem) and the descending branch at the point where the HC's zonal winds become baroclinically unstable (Kang and Lu, 2012). The location of the descending branch did not depend on the ascending branch for planets with fast rotation, such as Earth, matching

8

observations that the descending branch of Earth's HC moves very little over a year. On planets with very slow rotation, the ascending branch would reach the summer pole while the descending branch would only reach into the winter high-latitudes because it depends on different physical parameters (Hill et al., 2022).

Most of this work used highly idealized simulations of an Earth-like planet with homogeneous surface boundary conditions, and typically have no water. Our simulations can expand on this by incorporating a non-homogeneous ocean-atmosphere surface by introducing an equatorial land strip. The presence of land at the equator and ocean on either side is rather unusual from the perspective of Earth. This can allow us to make more general conclusions about the features of the HC in the planetary context, bridging the gap between Earth-based theories of global circulation and lesser-explained planetary settings.

We perform our investigation in three parts. Chapter 2 describes the first set of experiments using the GCM Isca (Vallis et al., 2018), and has been accepted for publication as McKinney et al. (2022). We vary four primary planetary parameters in these experiments: evaporative resistance, equatorial land fraction, rotation period, and condensable volatility. Each parameter starts at an Earth-like value and is moved towards a final Titan-like value. We then apply three observationally motivated criteria to determine if an experiment has a Titan-like climate. These experiments do not include a seasonal cycle, meaning our analysis is based on annual-mean quantities only. We find that high condensable volatility is most effective at creating a Titan-like climate in our simulations. This work provides insight into the individual effects of Titan's specific set of planetary parameters and demonstrates that Titan-like conditions do not require Titan-like constituents.

In Chapter 3, we follow this work with a set of equivalent experiments that include a seasonal cycle, allowing our analysis to expand to sub-annual features and bringing the simulations more in line with Earth and Titan. We add three additional criteria for Titan-like conditions that are connected to seasonality. Contrary to the results in Chapter 2, we find that large equatorial land fraction is most effective at creating Titan-like conditions,

while a large rotation period and high condensable volatility had minimal (or even negative) impacts on meeting the criteria. This suggests much of Titan's unique climate features could primarily be the result of its dry tropics, and that an Earth-like planet with a similar surface liquid distribution might look more like Titan than Earth.

In Chapter 4, we finalize this work by applying the methods used in the previous two steps to three TAM experiments (Lora et al., 2015). This allows us to assess our analysis methods from Chapters 2 & 3, and more completely investigate the characteristics of a Titan-like climate. The three TAM experiments include an aquaplanet case, a "wetlands" case with a prescribed wet region north of 60◦ latitude, and a "hydro" case with dynamic surface and subsurface hydrology combined with realistic topography. We find that the wetlands and hydro cases meet most of our Titan-like criteria, and are close to meeting the rest. This suggests our criteria are robust at identifying Titan-like climate states, while also providing insight on how to improve them. The analyses from Chapters 3 and 4 will be adapted into two manuscripts to expand on McKinney et al. (2022).

CHAPTER 2

McKinney et al. 2022

Since Titan is an all-tropics planet, it may be assumed that polar air would be advected into the tropics on its way to the ITCZ. This would allow for saturated parcels to reach the tropics and set the local specific humidity to levels similar to those at the colder poles, which would be the location of last saturation for these air parcels. Simulations of Titan's global climate Lora and Mitchell (2015) suggest this does not occur, as the specific humidity in the tropics appears to be *lower* than polar values (Figure 6 of Ádámkovics et al., 2016; Lora and Ádámkovics, 2017). Methane cannot condense out of the air moving horizontally away from the poles as the temperatures increase and the relative humidity (RH) of the parcels decreases. This necessitates an alternative hypothesis to explain the lower specific humidity in Titan's tropics relative to its poles. Griffith et al. (2013) suggested that the tropical humidity is set by falling virga from above the lower troposphere. Virga is precipitation that evaporates before reaching the ground, effectively acting as a transfer of specific humidity from one level of the atmosphere to a lower one. There is an additional hypothesis that, when combined with downward vertical flow, virga creates a near-constant specific humidity profile in the lower troposphere, which was observed by the Cassini-Huygens mission (Niemann et al., 2005, Figure 2 therein). At the same time, temperatures in the lower troposphere follow the dry adiabat, meaning relative humidity (RH) falls quickly as you approach the surface (Figure 1 of Tokano et al., 2006). If this hypothesis is true it can be used as a proxy for a Titan-like climate. Mitchell and Lora (2016) alternatively suggest that slantwise, meridional-vertical motion from baroclinic, mid-latitude storms could source the tropics with low-specific-humidity air. The two hypotheses may be distinguishable in simulations,

for instance by estimating the region of last saturation for equatorial parcels (O'Gorman and Schneider, 2006).

Recent work by Fan et al. (2021) showed that high global evaporative resistance can yield near-constant specific humidity in the lower troposphere even in an Earth-like Global Climate Model (GCM). They pointed to the presence of negative surface evaporation as the driver of this extremely dry climate state. Negative evaporation is generally only possible with a surface temperature inversion, but can be achieved much more easily when a high evaporative resistance is applied. One motivating question for this work is whether negative evaporation is necessary to produce the near-constant vertical profiles in specific humidity.

A complementary approach for understanding the controlling factors of Titan-like and Earth-like hydroclimate states is to first define the qualities that distinguish them and study how an idealized climate system behaves as it transitions from one to the other. A number of parameters differ between the Earth and Titan climate systems. Our hypothesis is that four such parameters control the hydroclimate state: evaporative resistance, equatorial land fraction, rotation period, and the volatility of the condensable. In this paper we develop a suite of numerical experiments using an Earth-based climate model that span the parameter range bounded by Earth and Titan, and study the suite of experiments to evaluate under what conditions the Earth-like climate becomes Titan-like. In order to perform this analysis, we will first need to define what counts as "Titan-like". There are several key features of Titan's hydroclimate that have been observed and can be identified in our model runs. We choose three of these to use as our Titan-like criteria:

1. The highest annual-mean near-surface specific humidity is off the equator, which we define as poleward of 5°N/S latitude (referred to herein as the "OffEq" criterion), based on observed near-surface specific humidity shown in Figure 6 of Ádámkovics et al. (2016),

2. The vertical specific humidity at the equator is constant or nearly so (the "ConVQ"

criterion), as shown in Figure 2 of Niemann et al. (2005), and

3. The equatorial climate is significantly drier than an Earth-like aquaplanet. The Huygens probe measured RH values at the surface of around 50-60% (Niemann et al., 2005; Tokano et al., 2006, Figure 1), so experiments with equatorial near-surface RH at or below 60% will meet the "LowRH" criterion.

We introduce the climate model used for the numerical experiments in Section 2 and outline the structure of our numerical experiments and our analysis methods in Section 3. In Section 4, we present and analyze the numerical experiments. We offer some discussion and further insights, plus next steps in Section 5. We summarize the main findings and conclude in Section 6.

2.1 Model Description

Isca is an open-source climate modeling framework, which allows the creation of atmospheric models over a wide-range of complexities (Vallis et al., 2018). It is based on the Flexible Modeling System (FMS) developed at GFDL (www.gfdl.noaa.gov/fms/), but has been modified significantly to include multiple options for various parameterizations, as well as options to simulate various planets and moons.

In the present work we use an idealized configuration of Isca, with mostly Earth-like parameters, but without any Earth-like continents, topography, or seasons. We mainly change the properties of the surface, which in the default Isca setup (referred to herein as "Isca-default") is a mixed-layer ocean with a heat capacity equivalent to 40m of water. For our experiments we have incorporated a novel surface hydrology scheme developed by Faulk et al. (2020) for the Titan Atmosphere Model (Lora et al., 2015, TAM;), referred to herein as "Isca-hydro". This hydrology scheme treats the entire surface of the planet as "land", which can then have water on its surface. This water can run off into neighboring grid cells that are either at a lower elevation or lower relative water level, using the scheme shown in

Figure 2.1. The water is not treated as a separate surface from the solid surface, and instead the model uses the depth of water in a grid cell to calculate the local heat capacity. As such there is only a single "surface" for each grid cell, and all grid cells use the same calculations for surface parameters regardless of water content. The hydrology scheme from Faulk et al. (2020) includes options for infiltration and subsurface flow, but we do not use any subsurface processes in our experiments.

The experiments are run using a suite of physics modules. These include a full Betts-Miller convection scheme (Betts, 1986; Betts and Miller, 1986), the Socrates radiation scheme developed by the UK Met Office (Manners, 2017; Edwards and Slingo, 1996), and a simple large-scale condensation scheme. The settings for the Betts-Miller scheme are equivalent to those used in TAM from Lora et al. (2015) and Faulk et al. (2020), with the RH relaxing to 0.8 over a period of 7200 seconds. There is precipitation produced by the convection and condensation schemes, but there is no cloud module. Re-evaporation is included in the condensation scheme. For these experiments we use the same configuration of Socrates as in their "Global Atmosphere 7" configuration, with 6 bands in the short-wave and 9 in the long-wave (Manners, 2017), as described for Isca in Thomson and Vallis (2019). We use a spectral dynamical core at T21 horizontal resolution (having 64 longitudinal gridpoints and 32 in latitude), and use 40 vertical sigma levels extending up to a top full-pressure level of 0.6hPa. The T21 resolution was chosen to minimize the time needed to run our experiments. We additionally ran a few sample experiments at T42 horizontal resolution to compare, and found similar mean states and convergence times.

The planet is based on Earth, with the same radius, solar constant, orbital period, 1 bar sea-level pressure in an N_2 atmosphere, and water as the condensable, but with 0° obliquity and eccentricity. The albedo is set to a constant value of 0.3 for all experiment setups and without distinguishing between land and water, which is to approximate Earth's mean albedo. The atmosphere is treated as Earth's pre-industrial atmosphere with CO_2, a specified O_3 layer in the stratosphere, and radiative feedback from water vapor that enters

14

the atmosphere through evaporation. We specify the O_3 field to be constant in time, and hemispherically symmetric, using the same setup as in Jucker and Gerber (2017).
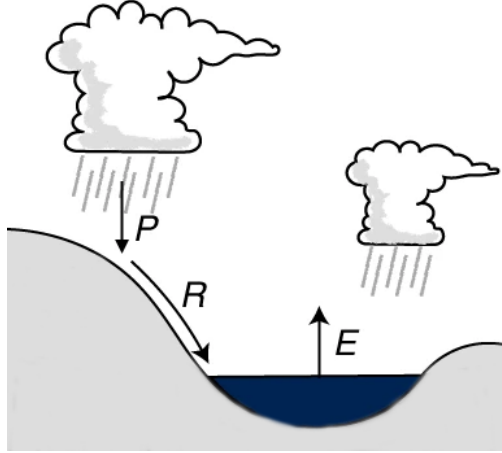
Figure 2.1: Subsection taken from the diagram of the TAM hydrology module from Faulk et al. (2020). We use only the precipitation (P), runoff (R), and surface evaporation (E) from this scheme.

2.2   Methods

To make the baseline Earth-like planet of the model more Titan-like, we vary four parameters:

1. We start by mirroring the approach used in Fan et al. (2021). For this we use an aquaplanet setup with an evaporative resistance, $r_E = 100 \times (1 - \beta)$, where β is a constant inserted into the equation for surface evaporation,

$$E = \rho C_K L_v V_s (\beta q_s^* - q_1) \tag{2.1}$$

where ρ is the surface air density, C_K is a transfer coefficient, L_v is the latent heat of vaporization, V_s is the surface wind speed, $q_s^*(T_s)$ is the saturation specific humidity at the surface temperature T_s, and q_1 is the lowest-model-layer specific humidity. We use the variable r_E, represented as a percentage, in this mansucript for convenience. This

means that $r_E = 100\%$ indicates a complete shutdown of evaporation and $r_E = 0\%$ indicates the absence of evaporative resistance.

Evaporative resistance acts to reduce the surface evaporation without needing to create a dry surface in the model. All aquaplanet simulations have a global surface reservoir 40m deep, 1-day rotation, and water as the condensable. The hydrology scheme calculates evaporation using Equation 1 and specified values of r_E.

As previously mentioned, it is relatively easy to achieve negative evaporation when using a large value of r_E (equivalent to a small, but nonzero, value of β) as the constant is only applied to one term of the difference. Due to the difficulty in connecting this to a physical phenomenon, we will attempt to produce a Titan-like state by varying other parameters that do not directly affect the evaporation equation.

2. We create a strip of land centered on the equator with a variable width in latitude, $\Delta\varphi$. This is accomplished using the Isca-hydro scheme which allows for custom global topography. By raising the solid surface only at a specified location and initializing an ocean elsewhere whose depth is just below the height of the raised area, we can create continents of varying widths. We use a Gaussian curve with a fixed peak elevation,

$$z(\varphi) = \begin{cases} A\cos(f\varphi) & |\varphi| \le \Delta\varphi \\ a\exp\left(\frac{-\varphi^2}{2c^2}\right) + 1 & |\varphi| > \Delta\varphi \end{cases} \tag{2.2}$$

where $z(\varphi)$ is the elevation of the solid surface as a function of latitude (φ), A is the maximum elevation in meters (set to 70), and $\Delta\varphi$ is the latitude of the land strip's edge in both hemispheres. The coefficient f is defined as a separate function of φ,

$$f(\varphi) = \frac{\arcsin\left(\frac{60}{A}\right) - 90}{\varphi} \tag{2.3}$$

while the coefficients a and c are defined as functions of $\Delta\varphi$,

$$a(\Delta\varphi) = \frac{60}{\exp\left(\frac{-\Delta\varphi^2}{2c^2}\right)} \tag{2.4}$$

16

$$c(\Delta\varphi) = \sqrt{\frac{-2\Delta\varphi - 1}{2\ln(0.9)}} \tag{2.5}$$

We use the following values for $\Delta\varphi$: 5°, 15°, 25°, 35°, 45°, 55°, 65°, and 75°. All $\Delta\varphi$ experiments use $r_E = 0\%$, 1-day rotation, and water as the condensable. Grid cells outside of the land strip are initialized with 40m of water.

3. For experiments with $\Delta\varphi$ of 25°, 35°, and 45°, we also vary the rotation period (T_r) to the following values in Earth-days: 1, 2, 4, 8, and 16. All T_r experiments use $r_E = 0\%$ and water as the condensable. Grid cells outside of the land strip are initialized with 40m of water. The upper value is chosen based on previous work by Faulk et al. (2017) who found that even at $T_r = 8$ the ITCZ of an Earth-like planet could reach the poles.

4. For the same $\Delta\varphi$ in 3 we additionally vary ξ, defined as a constant factor applied to the Clausius-Clapeyron equation (as in Frierson et al., 2006), such that

$$e_s(T) = \xi e_0 \exp\left[\frac{L_v}{R_v}\left(\frac{1}{T} - \frac{1}{T_0}\right)\right] \tag{2.6}$$

where e_s is the saturation vapor pressure as a function of temperature, e_0 is a known reference vapor pressure at temperature T_0, L_v is the latent heat of vaporization, R_v is the specific gas constant of water vapor, and ξ takes the values 1, 1.25, 1.5, 1.75, 2, 2.25, and 2.5. The upper value is chosen so that the model does not enter a runaway greenhouse, since our model does include water vapor feedback. Due to this feedback, a doubling of ξ results in at least one order-of-magnitude increase in column water vapor. Titan has two orders of magnitude more methane vapor in its atmosphere than Earth has water, much larger than we can achieve with these values of ξ. As we will show in Section 4, this range is sufficient to transition the Earth-like model to a Titan-like hydroclimate state. All ξ experiments use $r_E = 0\%$ and $T_r = 1$. Grid cells outside of the land strip are initialized with 40m of water.

To facilitate comparison between the equatorial hydroclimates of aquaplanet and terra-planet simulations, we diagnose the components of the zonal-mean atmospheric moisture

17

budget due to large-scale condensation, convection, diffusion, and convergence of the moisture flux $(-\nabla \cdot F_Q)$. The latter is further divided into mean $(-\nabla \cdot \overline{F_Q})$ and eddy components $(-\nabla \cdot F'_Q)$, where

$$-\nabla \cdot F_Q = -\nabla \cdot \overline{F_Q} - \nabla \cdot F'_Q \tag{2.7}$$

We compare regions of moisture flux divergence and convergence to the effective surface of last saturation for equatorial, surface-level air, which we define as the dew point temperature of a parcel at the equatorial surface, $T_{d,eq}$. Overplotting the $T_{d,eq}$ isotherm on moisture flux divergence/ convergence allows us to inspect for equatorial surface moisture source regions.
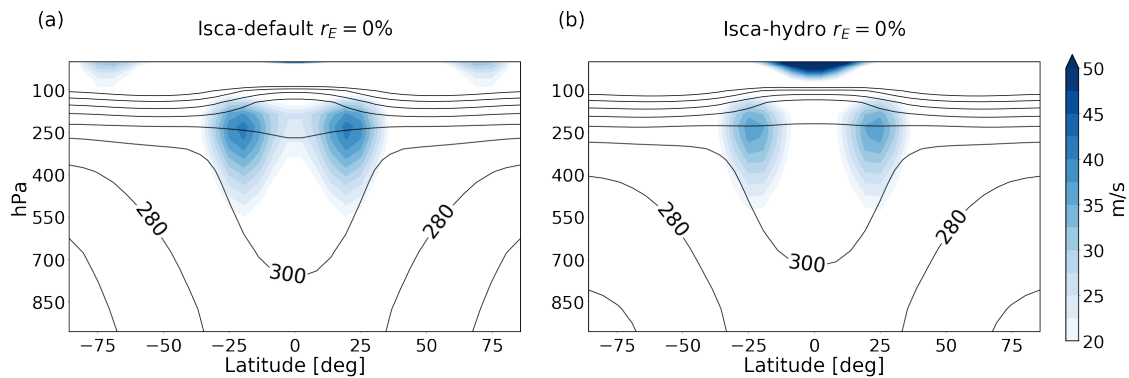
Figure 2.2: Zonal- and time-mean zonal wind overlaid with the potential temperature field for (a) the Isca-default aquaplanet experiment with $r_E = 0$ and (b) the equivalent Isca-hydro experiment. Filled contours show the zonal wind values in (m/s), while the black contour lines show the potential temperature in (K). Temperature contours are spaced 20K apart.

Simulations are performed for 25 years, and all diagnostics are averaged over the last 10 years. We observed that all experiments reached a steady state within 15 years, but do not demonstrate this herein for length considerations. Figure 2.2 shows the zonal wind and potential temperature fields for two aquaplanet simulations with $r_E = 0\%$ using the Isca-default (a) and Isca-hydro (b) surface schemes. This figure shows similar jet locations and peak winds for the two hydrology schemes with minor differences. The potential temperature values in our sample cases are somewhat cooler than those from Held and Suarez (1994,

subsequently HS), but the shape of the distribution is similar. The jet locations are closer to the equator, around 25° latitude, compared to approximately 40° in HS. While the peak magnitudes of the jets are similar both between the two cases in Figure 2.2 and the HS cases, we do find some superrotation at the equator. In the Isca-default case it is found in the upper troposphere, while in the Isca-hydro case it is in the stratosphere. Based on the comparison in Figure 2.2, we are confident that the Isca-hydro scheme is functional and effective for our analysis. Using model diagnostics of the hydrology, we then apply our three criteria for Titan-like climate states to assess whether a given parameter set has transitioned to a Titan-like hydroclimate.

2.3 Results

The results of our numerical experiments provide new insight into the transition from an Earth-like to Titan-like hydroclimate regime. We group the experiments by single parameter variations, i.e. keeping all others fixed.

2.3.1 Variable r_E Experiments

We first run a set of aquaplanet experiments using the Isca-default hydrology scheme. These experiments are used to establish a baseline Earth-like state and the effect of a uniform evaporative resistance. In Figure 2.3 we take an initial look at the global circulation and specific humidity of the two end-member experiments for this experiment set, $r_E = 0\%$ and $r_E = 99.9\%$. The $r_E = 0\%$ case has an Earth-like circulation (2.3(a)) and specific humidity field (2.3(c)), while the other case demonstrates a nearly-dry atmosphere (2.3(d)). Its Hadley Cell (HC) has contracted in the vertical dimension, extending only up to 600hPa (2.3(b)), indicating weak convection likely caused by the lack of moisture and subsequent latent heating.

To assess the three Titan-like criteria, we look at the near-surface specific humidity.
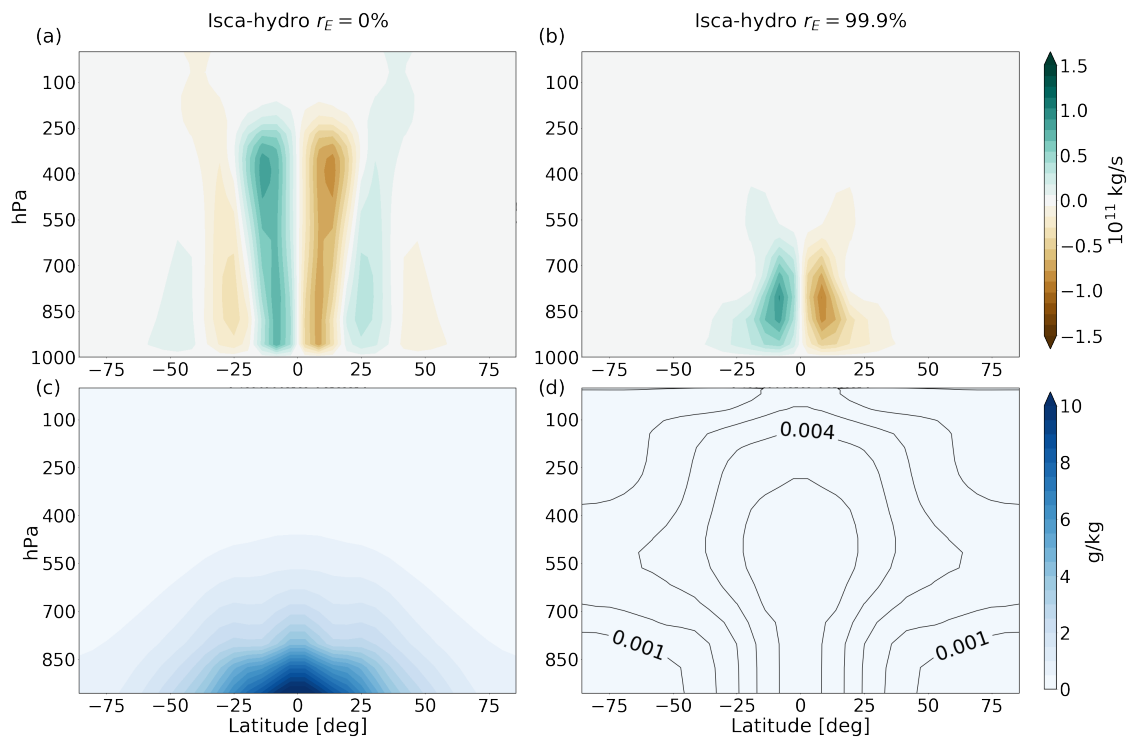
Figure 2.3: Top row: Zonal- and time-mean stream function for the Isca-hydro aquaplanet experiments with (a) $r_E = 0\%$ and (b) $r_E = 99.9\%$. Bottom row: Equivalent to the top row but for the specific humidity fields of each experiment. In order to show the specific humidity distribution in (d), we include black contour lines showing values in g/kg and spaced 0.001 g/kg apart. We find a significant contraction in the vertical extent of the Hadley Cell (HC) with higher r_E, in accordance with an almost fully-dry atmosphere.
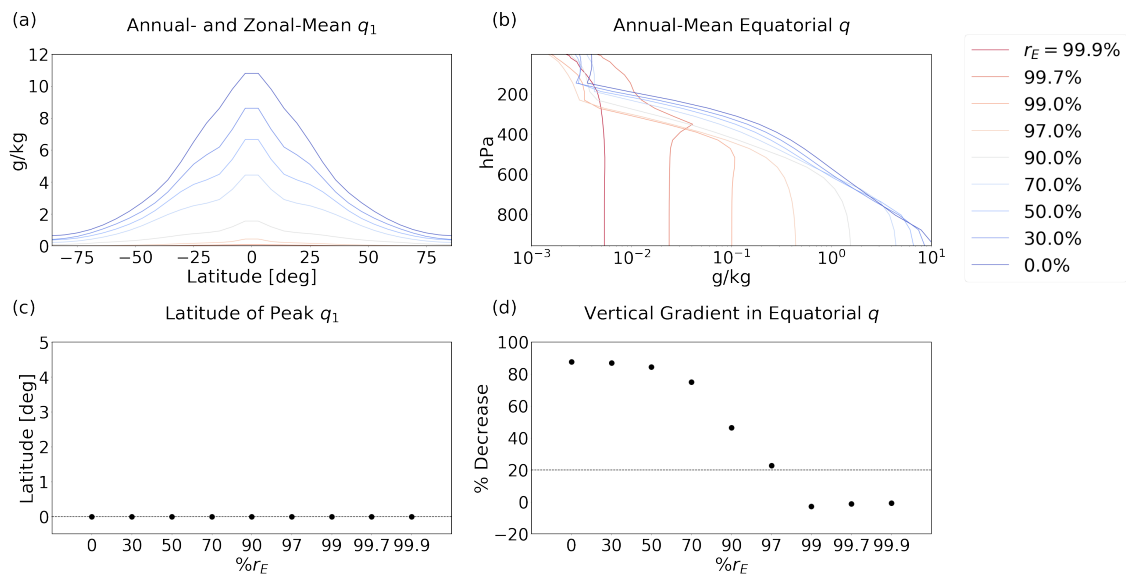
Figure 2.4: Specific humidity analysis for the r_E experiments. Figure (a) shows the zonal- and time-mean near-surface specific humidity, while (b) shows the time-mean vertical profile of specific humidity at the equator. Figure (c) shows the latitude of peak specific humidity from (a) as a function of r_E. The dotted line denotes 0° latitude. Since all experiments have their peaks at 0°, none meet the OffEq criterion. Figure (d) shows the vertical gradient in specific humidity from (b) between the surface and 600hPa pressure level, calculated as a percent decrease from the surface value. The dotted line shows the 20% threshold, and any experiments with gradients at or below that threshold meet the ConVQ criterion.

Figure 2.4(a) shows zonal- and time-mean q_1 for each r_E experiment using the Isca-hydro scheme, while 2.4(c) shows the latitude of peak q_1 as a function of r_E for the same experiments. All cases in the Isca-hydro setup have their peak humidity at the equator, failing to meet the OffEq criterion. Drier cases do have smaller gradients between the equator and poles, but since the r_E parameter is applied uniformly everywhere on the surface the equator never becomes drier than the midlatitudes.

Next we assess the vertical profile of specific humidity for the equatorial column to see if any experiments meet the ConVQ criterion. Figure 2.4(b) shows the vertical profile of time-mean specific humidity at the equator for the r_E experiments, while 2.4(d) shows the percent decrease in specific humidity moving from the surface to the 600hPa pressure level. The 20% threshold to meet the ConVQ criterion is indicated by a dotted line. The percent decrease in specific humidity only begins to decrease once $r_E > 50\%$, and only goes below the 20% threshold in experiments with $r_E \geq 99\%$. We conclude that the ConVQ criterion is only met for high values of r_E, which would indicate a very dry surface.

For the final criterion, LowRH, we show the equatorial time-mean RH for all r_E experiments in Figure 2.5. RH drops quickly with increasing r_E, reaching values below 60% for $r_E \geq 70\%$. We conclude that experiments with $r_E \geq 99\%$ meet both the ConVQ and LowRH criteria.
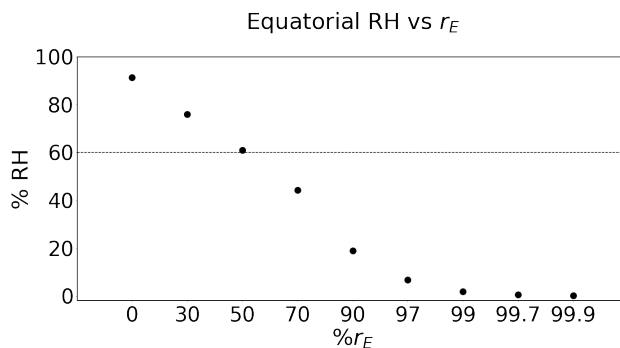
Figure 2.5: Time-mean equatorial RH for the r_E experiments as a function of r_E. The dotted line denotes 60% RH, meaning experiments below it meet the LowRH criterion.

The results for the r_E experiments are summarized in Table 2.1. We find that no experiments meet the OffEq criterion, but experiments with higher r_E are more likely to meet the ConVQ and LowRH criteria. We infer that the r_E experiments cannot meet the OffEq criterion because we apply a uniform r_E value everywhere, whereas Titan is not uniformly dry over its surface. As such, we require a surface that includes a mix of dry and wet regions to develop more realism toward the Titan-like regime.

	Criteria		
	OffEq	ConVQ	LowRH
$r_E = 0\%$			
30%			
50%			
70%			X
90%			X
97%			X
99%		X	X
99.7%		X	X
99.9%		X	X

Table 2.1: Criteria matched by each r_E experiment.

2.3.2 Variable $\Delta\varphi$ Experiments

As detailed in Section 2, we add a hemispherically symmetric strip of land to the Isca-hydro scheme by introducing global topography with a moderately elevated equatorial region. The width of said strip is adjusted by adjusting the topography, and runoff is self-consistently simulated while surface infiltration is prohibited. We first analyze the effect of the land strip's width on the stream function and specific humidity fields in Figure 2.6. We find a
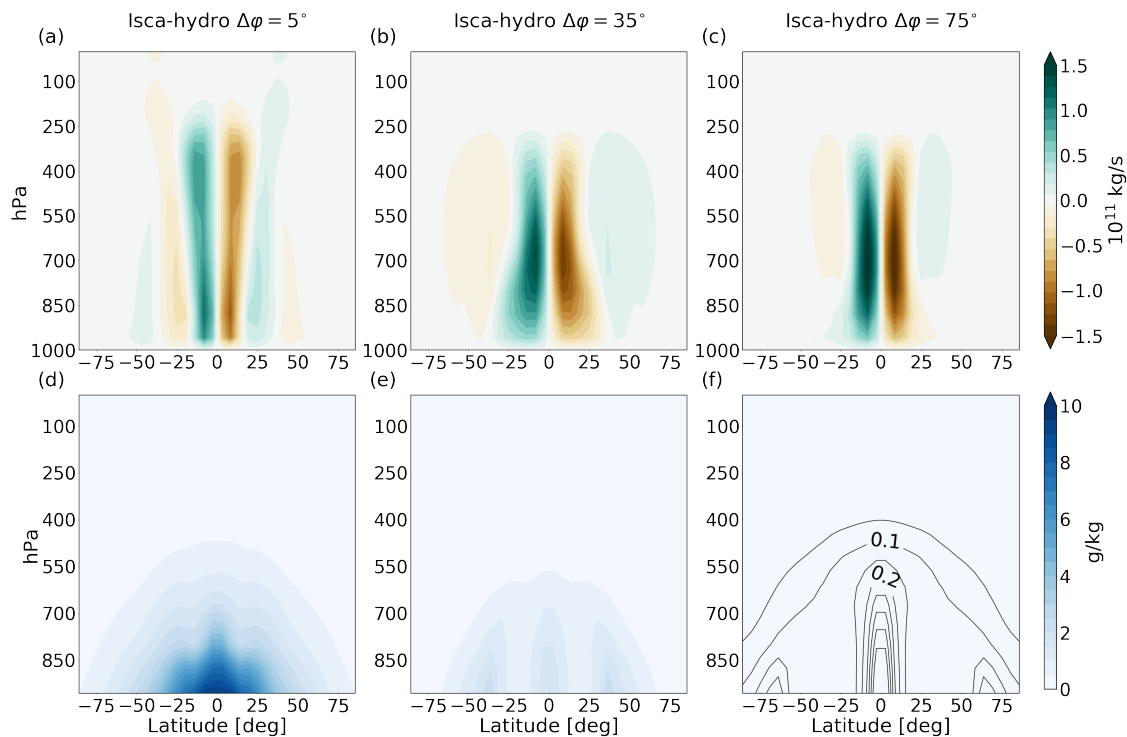
Figure 2.6: Top row: Zonal- and time-mean stream function for the Isca-hydro experiments with (a) $\Delta\varphi = 5°$, (b) $\Delta\varphi = 35°$, and (c) $\Delta\varphi = 75°$. Bottom row: Equivalent to the top row but for the specific humidity fields of each experiment. As in Figure 2.3(d), we add black contour lines in (f) to show the specific humidity distribution. These contours show values in g/kg and are spaced 0.05 g/kg apart. Similar to the effect of high r_E, we find the vertical extent of the HC decreases with larger $\Delta\varphi$ as the atmosphere becomes dry.

similar vertical contraction and strengthening of the HC with higher $\Delta\varphi$ (2.6(a-c)) as in Figure 2.3 with higher r_E. In both cases the driest end-member is almost completely dry relative to the first, meaning the presence of a large land strip has a comparable effect to high evaporative resistance, as might be expected.
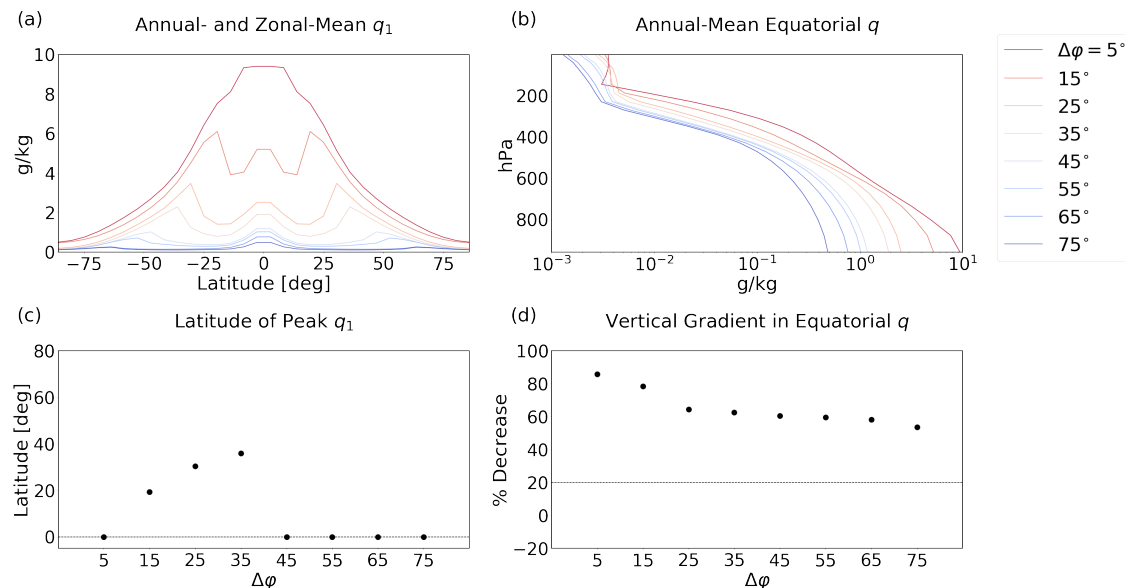
Figure 2.7: Specific humidity analysis for the $\Delta\varphi$ experiments. Figures (a) and (b) are equivalent to Figures 2.4(a) and (b), respectively, for these experiments. Figures (c) and (d) are equivalent to Figures 2.4(c) and (d), respectively.

We assess the first two Titan-like criteria, OffEq and ConVQ, in Figure 2.7. We find that the presence of the land strip lowers the equatorial value of q_1 significantly for experiments with $\Delta\varphi > 5°$ and $\leq 35°$. Figure 2.7(c) shows the latitude of peak q_1 moving outward from the equator with larger $\Delta\varphi$ until $\Delta\varphi = 45°$, after which it returns to the equator. The equatorial value appears to decrease less quickly than the midlatitude value for higher $\Delta\varphi$ in 2.7(a), which allows it to reclaim the overall peak. The midlatitude peaks in specific humidity are similar to the values at those latitudes in cases with smaller $\Delta\varphi$. This means they are dependant on the surface temperature at the shorelines, which decreases as $\Delta\varphi$ increases and the shorelines move further poleward. This effect becomes more important than the effect

of the land strip on the equatorial peak in specific humidity for $\Delta\varphi \geq 45°$. We hypothesize that the equatorial peak is primarily dependant on the HC's access to midlatitude moisture, which would be largely cut off once $\Delta\varphi$ exceeds 35°. In contrast, the midlatitude peak's dependence on local surface temperature would continue to be relevant for values of $\Delta\varphi$ well past 45°, allowing for the observed switch in which peak dominates.

Figure 2.7(b) shows the vertical profile of specific humidity at the equator while 2.7(d) shows the percent decrease from the surface to 600hPa pressure level as in Figure 2.4(c), d. None of the experiments develop the near-vertical profile of the highest r_E cases, however there is a general trend toward deeper, more uniform vertical profiles with increasing $\Delta\varphi$.

Despite having no experiments meet the ConVQ criterion, the $\Delta\varphi$ experiments almost all meet the LowRH criterion. Figure 2.8 shows the near-surface equatorial- and time-mean RH as a function of $\Delta\varphi$. The RH quickly drops below the 60% threshold once $\Delta\varphi$ exceeds 5°, and dips below 20% for $\Delta\varphi \geq 45°$. The jump between $\Delta\varphi = 5°$ and 15° certainly moves the hydroclimate to the drier equatorial hydrology expected for Titan-like climates.

The results of the $\Delta\varphi$ experiments are summarized in Table 2.2. As with the r_E experiments, the LowRH criterion is met by the most experiments, but in contrast the OffEq criterion is met by some experiments while none meet the ConVQ criterion. We conclude that the mixture of dry and wet surfaces has a different impact on the equatorial climate state than a uniform evaporative resistance. In addition, the most Titan-like criteria are only met by experiments with moderately-sized land strips, suggesting there are competing effects of $\Delta\varphi$ and simply increasing it does not produce a fully Titan-like state. We expand on this set of experiments by including two extra parameters, rotation period and condensable volatility. We vary these for a subset of the land strips ($\Delta\varphi = 25°$, 35°, and 45°), moving from Earth-like values to Titan-like ones.

26
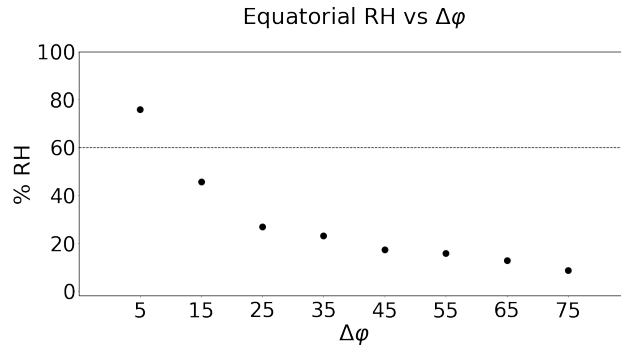
Figure 2.8: RH analysis for the variable-$\Delta\varphi$ experiments, equivalent to Figure 2.5.

	Criteria		
	OffEq	ConVQ	LowRH
$\Delta\varphi = 5°$			
15°	X		X
25°	X		X
35°	X		X
45°			X
55°			X
65°			X
75°			X

Table 2.2: Criteria matched by each $\Delta\varphi$ experiment.
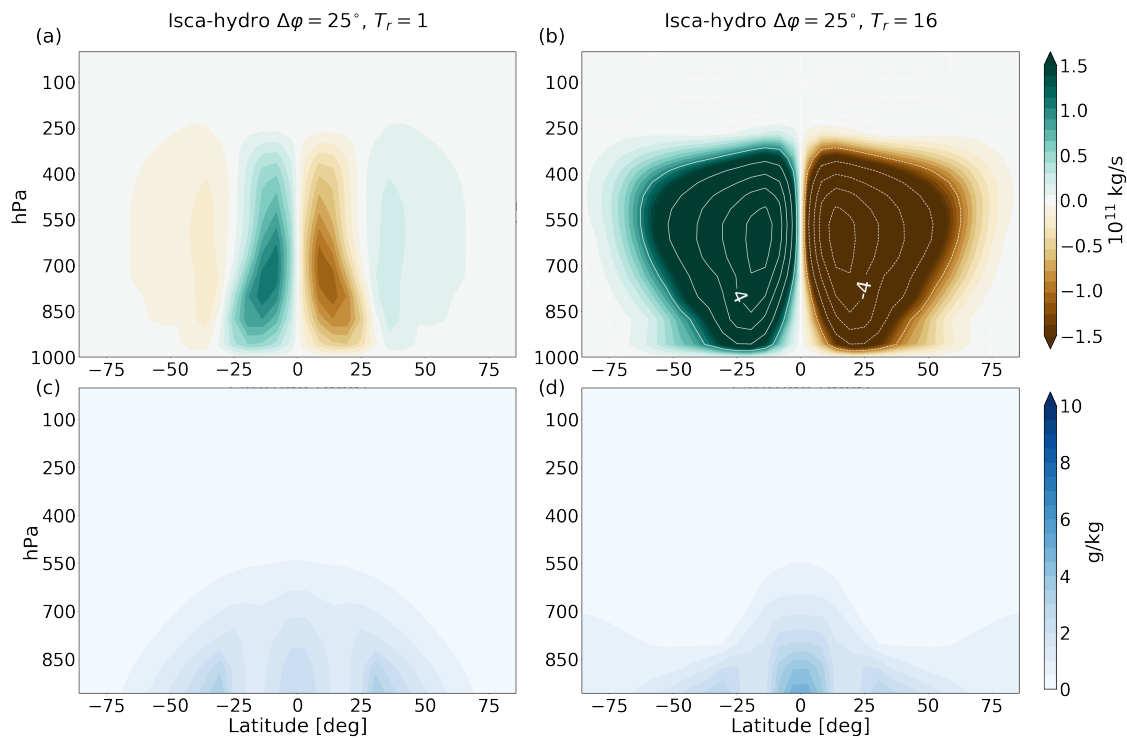
Figure 2.9: Top row: Zonal- and time-mean stream function for the Isca-hydro $\Delta\varphi = 25°$ experiments with (a) $T_r = 1$ and (b) $T_r = 16$. We add white contour lines to (b) to show values beyond the range of the filled contours. These contour lines show values in 10^{11} kg/s and are spaced 10^{11} kg/s apart. Bottom row: Equivalent to the top row but for the specific humidity fields of each experiment. We find a significant increase in HC strength with larger T_r and a corresponding increase in equatorial specific humidity.

2.3.3 Variable T_r Experiments

Two significant atmospheric circulation patterns affecting the water cycle – the width of the Hadley circulation and the location of the baroclinic zone – depend on T_r (Kaspi and Showman, 2015). We then expect that varying the rotation period will influence the equilibrium distribution of water vapor by influencing the origin of moisture transport relative to shorelines. In the next set of experiments, we vary the rotation period across the values $T_r = 1$, 2, 4, 8, and 16-days for three land-strip widths of $\Delta\varphi = 25°$, $35°$, and $45°$, and holding all other parameters fixed. As with previous experiments sets, we begin with a look at two end-member cases to assess the broad affects of rotation. Figure 2.9(a) (b) shows the zonal- and time-mean stream function for the experiment with $\Delta\varphi = 25°$ and $T_r = 1$ ($T_r = 16$). The intensity of the HC is much greater in the $T_r = 16$, as is the equatorial specific humidity. The high equatorial humidity suggests that the higher T_r is allowing the equator greater access to midlatitude moisture by expanding the HC. We will keep this in mind as we analyze the three Titan-like criteria.

Figures 2.10(a), c, and e show zonal- and time-mean q_1 for the T_r experiments. Only two experiments meet the OffEq criterion, the $\Delta\varphi = 25°$ and $35°$ cases where $T_r = 1$ day. The equatorial peaks in q_1 appear to increase with higher T_r, while the midlatitude peaks are constant or slightly decreasing. This allows the equatorial peak to dominate in all experiments with $T_r \geq 2$. We hypothesize this is due to the width of the Hadley circulation in relation to the width of the land strip. In the 1-day cases, the HC extent is more likely to be contained by the land strip, cutting it off from midlatitude moisture and allowing it to accumulate in the midlatitudes.

Similar to the $\Delta\varphi$ experiments, no T_r experiments meet the ConVQ criterion. There is in fact a trend away from the threshold (Figure 2.10(h)) with higher T_r, despite Titan itself having $T_r = 16$. In fact it is possible that for values of $T_r < 1$ an experiment could meet the ConVQ criterion. Reconciling this with Titan's high value of T_r brings us back to the land strip itself: the relevant determiner for the ConVQ criterion is the relation between the HC
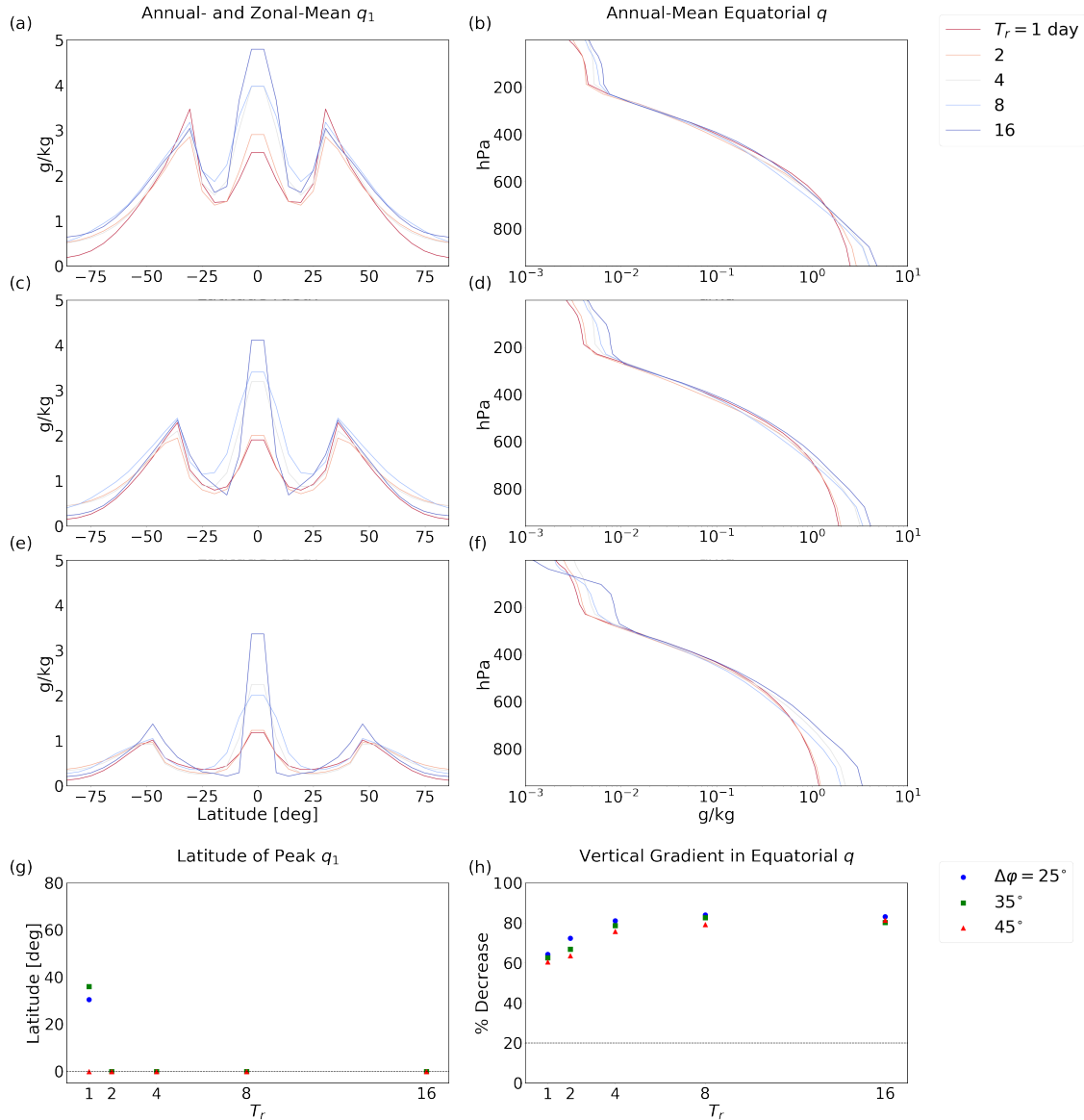
Figure 2.10: Specific humidity analysis for the T_r experiments. Figures (a), (c), and (e) show the zonal- and time-mean q_1, as in Figure 2.7(a). Figures (b), (d), and (f) show the time-mean equatorial vertical profile of specific humidity, as in Figure 2.7(b). First row is for the experiments with $\Delta\varphi = 25°$, second row for $35°$, and third row $45°$. Figure (g) shows the latitude of peak q_1 as a function of T_r for each value of $\Delta\varphi$, while (h) shows the percent decrease in specific humidity between the surface and 600hPa pressure level as a function of T_r.
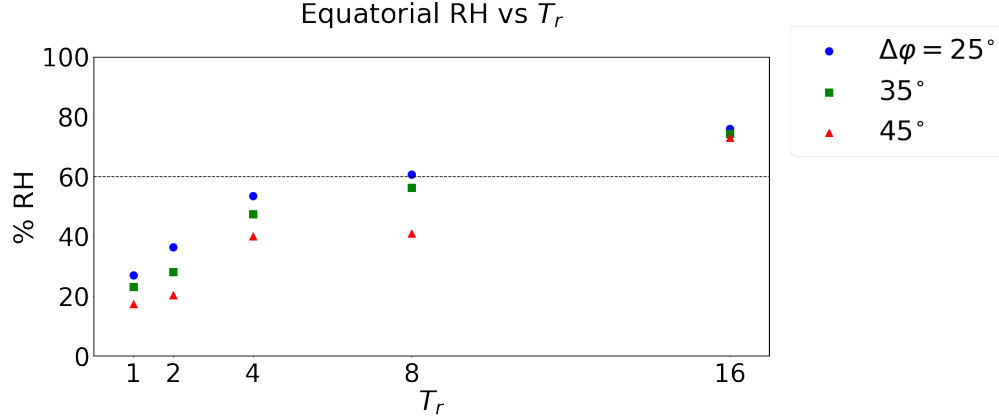
Figure 2.11: RH analysis for the T_r experiments, equivalent to Figure 2.5.

and land strip, rather than either in isolation. The effect of a wider land strip (increasing $\Delta\varphi$, Figure 2.7(d)) should be equivalent to the effect of a narrower HC (decreasing T_r, Figure 2.10(h)). This means that even though Titan has a large T_r, it is made up for by an also large $\Delta\varphi$ which dominates the overall hydroclimate.

Figure 2.11 shows that all but one experiment with $T_r \leq 8$ meet the LowRH criterion, with that one experiment, $\Delta\varphi = 25°$ and $T_r = 8$, narrowly missing. All experiments with $T_r = 16$ fail to meet the LowRH criterion, and all have very similar values. In addition, their RH values are close to those of the $\Delta\varphi = 5°$ experiment, suggesting their equatorial regions have access to abundant moisture despite the land strips.

Overall, experiments with smaller T_r and larger $\Delta\varphi$ were more likely to meet the three criteria. The latter is within expectations, as Titan has a dry tropics and subtropics which mirrors our land strips. The former, though, is unexpected in that Titan is a slow rotator, $T_r = 16$, but in our experiments slow rotation moved the equatorial climate *away* from being Titan-like. We discuss this further in Section 5.

$\Delta\varphi$	T_r	Criteria		
		OffEq	ConVQ	LowRH
25°	1-day	X		X
	2			X
	4			X
	8			
	16			
35°	1-day	X		X
	2			X
	4			X
	8			X
	16			
45°	1-day			X
	2			X
	4			X
	8			X
	16			

Table 2.3: Criteria matched by each T_r experiment.
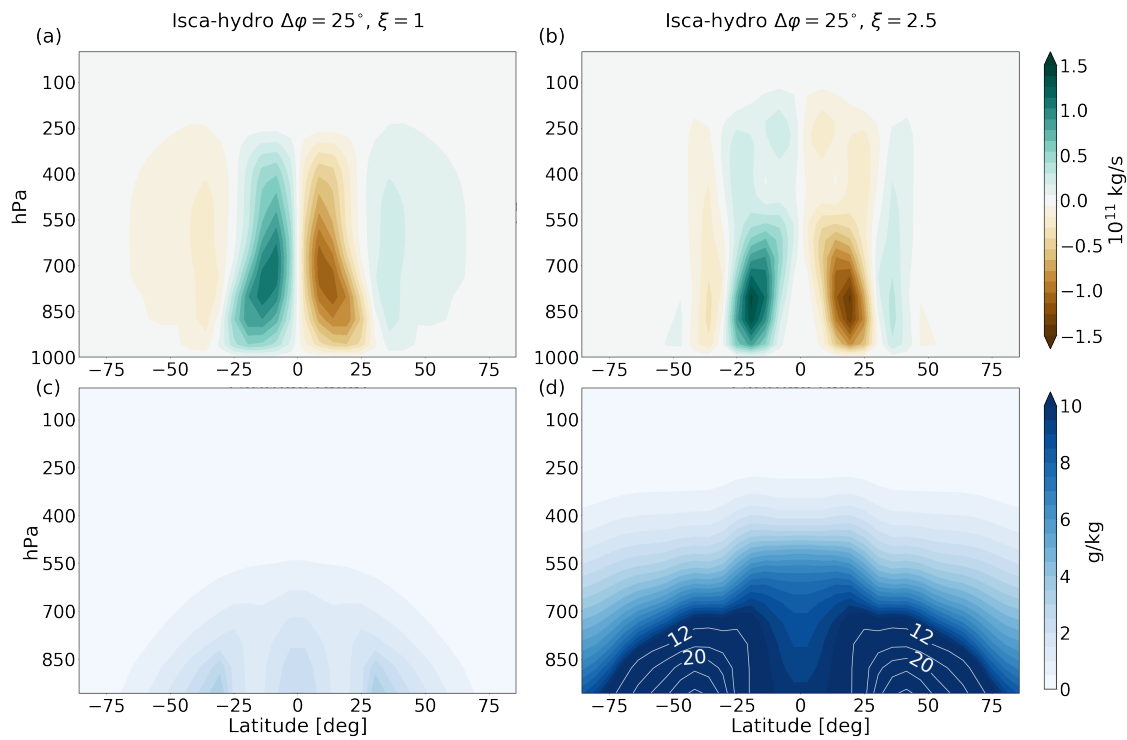
Figure 2.12: Top row: Zonal- and time-mean stream function for the Isca-hydro $\Delta\varphi = 25°$ experiments with (a) $\xi = 1$ and (b) $\xi = 2.5$. Bottom row: Equivalent to the top row but for the specific humidity fields of each experiment. We add white contours in (d) to show the specific humidity structure. These contours show values in g/kg and are spaced 4 g/kg apart. We find that the HC both contracts vertically and moves outward from the equator with higher ξ.

33

2.3.4 Variable ξ Experiments

In the final set of experiments, we vary the water volatility parameter, ξ, to mimic the higher volatility of methane on Titan. Based on in-situ measurements of Titan's atmosphere by the Huygens probe (Niemann et al., 2005), we can approximate the surface mole fraction of methane to N_2 on Titan as 0.05 and the RH as 50%. We can convert this to a specific humidity value by multiplying the ratio of the molecular masses of methane and N_2,

$$q_{Titan} \approx 0.05 \times \frac{16}{28} \approx 30\text{g/kg} \tag{2.8}$$

If we take 25°C (298.15K) as an arbitrary but representative value for Earth's surface temperature, we can apply the Clausius-Clapeyron equation to get a representative saturation vapor pressure e_s, which in turn can be converted into a saturation specific humidity, q_s,

$$e_s = e_0 \exp\left[\frac{L_v}{R_v}\left(\frac{1}{T_0} - \frac{1}{298.15}\right)\right] \tag{2.9}$$

$$q_s = \frac{e_s R_d}{p_s R_v} \tag{2.10}$$

where $e_0 = 611$ hPa, $L_v = 2.25 \times 10^6$ J/kg, $R_v = 462$ J/kg/K, $T_0 = 273.15$ K, $R_d = 287$ J/kg/K, and $p_s = 1000$ hPa. This yields $q_s \approx 20$ g/kg, so if we assume 50% RH as in the Titan observations we are left with $q_{Earth} \approx 10$ g/kg for our Earth value of specific humidity. This means we can calculate an effective ξ value for Titan, ξ_{eff},

$$\xi_{eff} = \frac{q_{Titan}}{q_{Earth}} \approx 3 \tag{2.11}$$

This is slightly above the maximum ξ value of 2.5 used in this work, but this is a highly approximate value and based on the following results this difference does not have a significant impact on our analysis.

We use the $\Delta\varphi = 25°$ experiments with $\xi = 1$ and $\xi = 2.5$ as the end-members for comparison in Figure 2.12. Figures 2.12(a) and b are the zonal- and time-mean stream functions for each case, while c and d are the equivalent specific humidity fields. Unlike in

previous comparisons, we find that the vertical contraction of the HC in 2.12(b) corresponds to an increase in specific humidity in 2.12(d). In fact, the specific humidity is far higher than any previous case, as might be expected with high values of ξ. The effect on the HC may instead be connected to the RH, which does not increase in line with specific humidity. Another interesting feature is the shift in the HC peak away from the equator with higher ξ. The peak latitude moves from roughly $10°$ latitude to $20°$, with the lower part of the circulation moving further out than the upper. There is also a suggestion of an equatorial reversal near the surface.

Figures 2.13(a), c, and e show q_1 for each ξ experiment. All cases except for one have their humidity maximum off of the equator (2.13(g)), although for most the equator is a local maximum. q_1 increases everywhere with higher ξ, although this effect is less significant at the equator compared to the midlatitudes. The increased trend is expected given that higher ξ represents an increase in the amount of water vapor needed to saturate air, while the smaller effect at the equator is likely due to the land strips limiting access to moisture. We conclude that all but one case ($\Delta\varphi = 45°$, $\xi = 1$) meet the OffEq criterion.

Figures 2.13(b), d, and f show the vertical specific humidity profiles at the equator. Multiple experiments have nearly vertical profiles in the lower atmosphere, and three just reach the 20% gradient threshold (2.13(h)). These three experiments all have $\xi = 2.5$, demonstrating an inverse relationship between meeting the ConVQ criterion and the magnitude of specific humidity when compared to the aquaplanet experiments, i.e. the experiments with the highest humidities are the ones with constant vertical profiles. While seemingly contradictory, Titan itself has a more volatile condensable in methane than water on Earth, and a correspondingly higher specific humidity of methane in its atmosphere despite being "drier" in RH terms.

Figure 2.14(a) shows the time-mean equatorial near-surface RH. All cases are well below the 60% threshold to meet the LowRH criterion. There is a weak trend towards lower RH with higher ξ. The fact that the higher ξ experiments have both low RH and high q_1 means
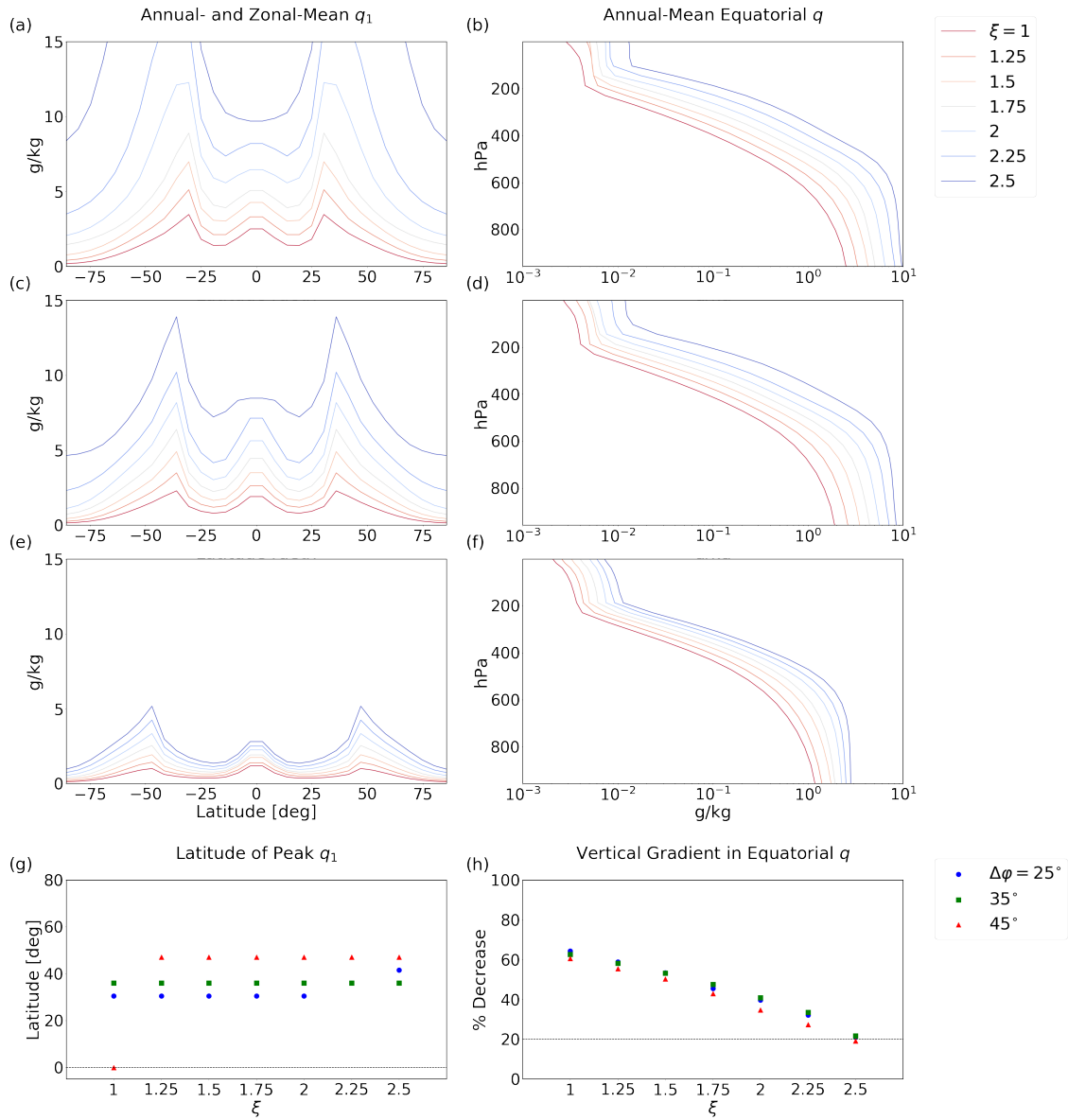
Figure 2.13: Left column: Equivalent to Figures 2.10(a), (c), (e), and (g) but for the ξ experiments. Right column: Equivalent to Figures 2.10(b), (d), (f), and (h).

that the temperature, and thus the q_s^*, are more strongly increasing with ξ than q_1. We can see the increase in equatorial surface temperature in Figure 2.14(b) as a function of ξ. Even in the cooler $\Delta\varphi = 45°$ experiments there is an increase of over 10K between $\xi = 1$ and $\xi = 2.5$. The net effect is a "drier" (lower RH) climate in the high-ξ cases despite having correspondingly higher q_1.

We find that only the cases with $\xi = 2.5$ meet the ConVQ criterion, while all but one of the ξ experiments meet the OffEq and LowRH criteria. We conclude that the primary effect of ξ is on the ConVQ criterion, with the OffEq and LowRH criteria influenced more by the presence of the land strips. The full results of the ξ experiments are summarized in Table 2.4.
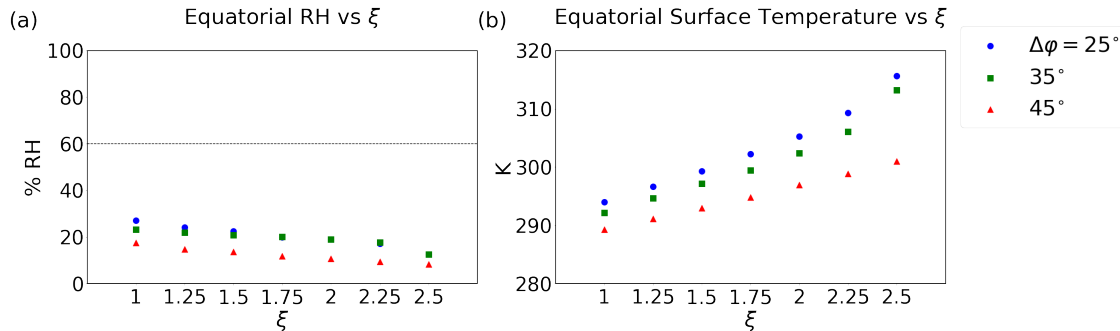
Figure 2.14: (a): RH analysis for the ξ experiments, equivalent to Figure 2.5. (b): equivalent to (a) but for surface temperature.

2.4 Discussion

Overall, the parameter most effective at achieving the three Titan-like criteria was ξ. The only experiments to meet all three criteria had $\xi = 2.5$, the highest value we used for the parameter. The other parameters allowed experiments to meet two of the three criteria, but never had any meet all three. The r_E experiments met more criteria with higher r_E, but were unable to meet the OffEq criterion due to r_E being applied uniformly to the entire surface. The $\Delta\varphi$ experiments met two criteria for $\Delta\varphi = 15°$, $25°$, and $35°$, but only one for higher

		Criteria		
$\Delta\varphi$	ξ	OffEq	ConVQ	LowRH
25°	1.00	X		X
	1.25	X		X
	1.50	X		X
	1.75	X		X
	2.00	X		X
	2.25	X		X
	2.50	X	X	X
35°	1.00	X		X
	1.25	X		X
	1.50	X		X
	1.75	X		X
	2.00	X		X
	2.25	X		X
	2.50	X	X	X
45°	1.00			X
	1.25	X		X
	1.50	X		X
	1.75	X		X
	2.00	X		X
	2.25	X		X
	2.50	X	X	X

Table 2.4: Criteria matched by each ξ experiment.

values of $\Delta\varphi$. This makes it hard to define a clear correlation between $\Delta\varphi$ and our Titan-like criteria. As $\Delta\varphi$ increases, the peaks in q_1 associated with the continent's shorelines decrease (Figure 2.7(a)). This decrease roughly follows the curve of the $\Delta\varphi = 5°$ case, from which we infer the peaks represent the temperature at the shoreline and closely match the value at that latitude in experiments with narrower land strips. For land strips with shorelines well into the midlatitudes the local temperature is cold enough to suppress the local peak in q_1 to the point where it is no longer larger than the equatorial value. The equatorial values change more slowly than the shoreline values for $\Delta\varphi \geq 35°$, perhaps reflecting the HC being cutoff from the ocean (Figure 2.18(a)).

The final parameter, T_r, also had experiments in its set meet at most two criteria. The experiments that met two criteria all had $T_r = 1$, while experiments with $T_r = 16$ met none of the criteria. This means that smaller T_r correlates with meeting more Titan-like criteria, despite Titan itself having $T_r = 16$. It is then, perhaps, surprising that its equator is able to maintain such a dry climate. Based on our experiments, the volatility of the surface condensable may be the primary factor in setting Titan's low-q_1 equatorial climate. The highest-ξ experiments all met the three criteria, and were the only ones to do so. Expanding the experimental range to include experiments with simultaneously high ξ and T_r will allow us to better understand Titan's climate, which we leave to future work.

2.4.1   Moisture Transport Analysis

We have identified three experiments that meet all of our Titan-like criteria, but do not know how closely they match Titan-like dynamics. Titan's equatorial humidity is hypothesized to be set either by virga and vertical advection downward from the upper troposphere or slantwise, horizontal-vertical moisture transport by baroclinic eddies. It is unlikely to be the result of surface evaporation with low-level moisture advection. In order to identify the source of equatorial moisture in our experiments, we first look at the vertical wind above the equator. Figure 2.15 shows the time-mean vertical wind at the 850hPa pressure level over

the equator for the ξ experiments. We find that the upward winds weaken with higher ξ, and even shift direction for the experiments with $\Delta\varphi = 25°$ and $35°$ at high enough values of ξ. There is a subsequent weakening of these downward winds between the $\xi = 2.25$ and 2.5 cases for both $\Delta\varphi$ sets, meaning the relation between ξ and vertical wind velocity is non-monotonic for the narrower land strips. Considering that the experiments with the strongest downward vertical winds did not meet all three criteria while at least one experiment with upward winds did, we conclude that this alone does not determine whether an experiment will be Titan-like.
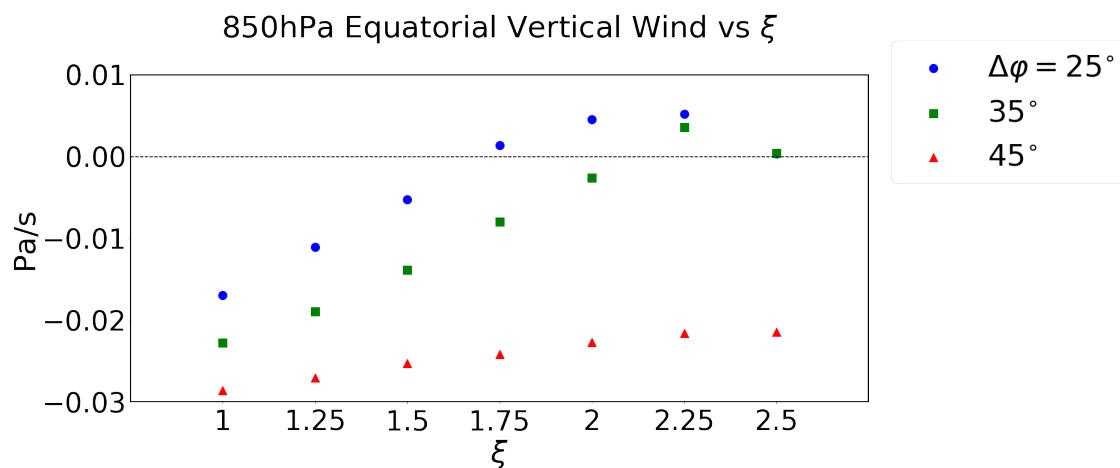
Figure 2.15: Zonal- and time-mean vertical winds at the 850hPa pressure level for the ξ experiments. Units are in Pa/s, so positive values (above dotted line) mean downward motion.

In order to better understand the experiments with upward vertical winds and those that met the three criteria, we take two experiments from each group and plot the zonal- and time-mean moisture convergence with the corresponding moisture transport vectors overlaid (Figure 2.16). For additional comparison, the Isca-hydro experiment with $r_E = 0\%$ is also included in Figure 2.16. We overlay the atmospheric isotherm at the dew point temperature of the equatorial surface, $T_{d,eq}$. This isotherm is only just above the equatorial surface in the $r_E = 0\%$ experiment (2.16(a)-c), as might be expected for an aquaplanet with abundant

water at the equator. However, for the two ξ experiments this isotherm is well above the surface at the equator and only meets the surface at latitudes greater than 50°. Considering that the widest land strip of these two is only $\Delta\varphi = 45°$, this strongly suggests that air parcels are not moving into the equator horizontally from the continent's edge.
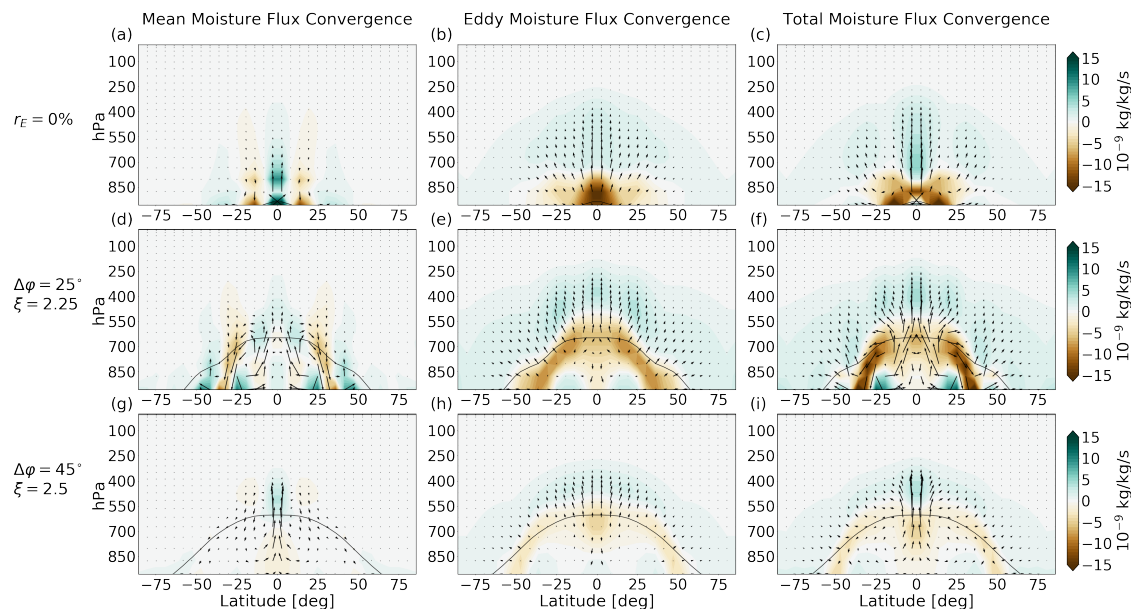
Figure 2.16: Left column: The convergence of the mean moisture flux term with the vector-field overlaid for the Isca-hydro $r_E = 0\%$ aquaplanet experiment and two ξ experiments. Center column: The equivalent plots of the eddy term of the moisture flux. Right column: The equivalent plots of the total moisture flux. Additionally overlaid in each plot is the isotherm of last saturation at the equator, equivalent to the equator's mean surface dew point temperature. The top row shows the Isca-hydro $r_E = 0\%$ experiment, the middle row the $\Delta\varphi = 25°$, $\xi = 2.25$ experiment, and the bottom row the $\Delta\varphi = 45°$, $\xi = 2.5$ experiment.

If moisture is not coming into the equator horizontally, then where is it coming from? Looking at the mean moisture flux vectors in Figures 2.16(d) and g, there are many arrows showing horizontal movement into the near-surface equator. But these arrows all originate at latitudes within the land strips of their respective experiments. As such, the actual source of the moisture must be elsewhere. In 2.16(d) the flux vectors in the near-surface equatorial

region are downward, in line with the winds shown in Figure 2.15. This is also true for the eddy terms in 2.16(e). This suggests the only possible source of moisture for the equatorial surface is from above, advected in by downwelling air. There is a region of weak moisture flux divergence in the mean term at around the 700hPa level, with weak convergence below. The flux vectors at this level also show primarily horizontal flux into the equator, leading us to conclude that moisture in the $\Delta\varphi = 25°$, $\xi = 2.25$ experiment is first brought to the equator aloft in the mid-troposphere before sinking to the surface.

The above case seems to match one hypothesis for Titan's constant specific humidity profile, specifically that the equatorial surface moisture is sourced from above and supplied by downward moisture flux. It does not, however, match all three Titan-like criteria, in contrast to the case shown in Figures 2.16(g)-i. We find no such downward flux in the mean terms (2.16(g)), and instead there is a fairly straightforward circulation of moisture up at the equator and downward in the subtropics. This belies the fact that $\Delta\varphi$ is well beyond the subtropics in this experiment, meaning the return flow to the equator has no access to oceanic moisture except at the very edges of the land strip. The eddy fluxes appear to compete with the mean, even showing downward flux at the equator despite the lack of downward vertical winds. The mean terms dominate in the flux vectors while the eddy terms dominate in the convergence (2.16(i)). Based on the total terms, moisture diverges from a near-surface region close to the edge of the land strip and then flows equatorward. However, this divergence aligns with the dewpoint isotherm slightly above the surface, around 800hPa, where flux vectors are pointing downward as part of the sinking branch of the HC. This could mean that the moisture source for the equator is not the shoreline, but rather an elevated region of the subtropics. This would suggest that the equatorial surface is largely cut off from outside moisture, and its local humidity would match that of the entire HC circulation. We can see evidence of this in 2.16(i), as the flux vectors flowing out from the equator closely follow the dewpoint isotherm as they descend towards edge of the land strip.

We further explore the mechanisms of this transport in Figure 2.17. This figure shows
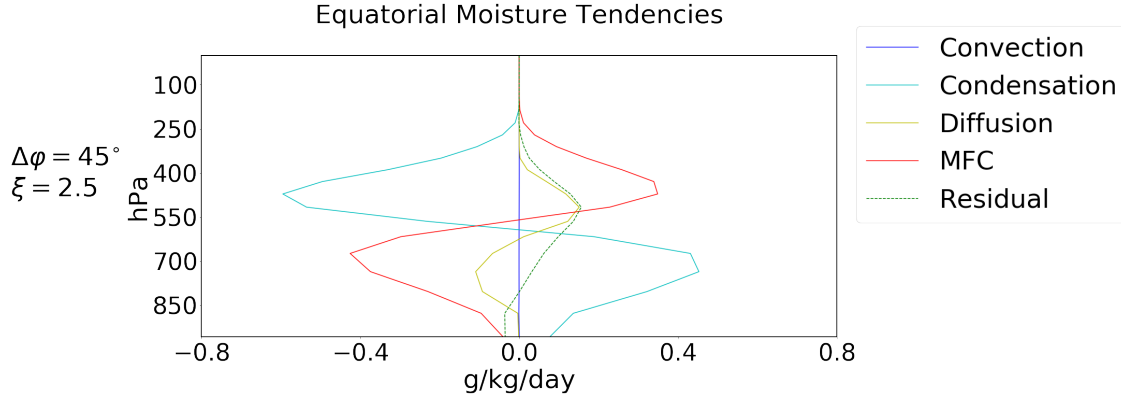
Figure 2.17: Zonal- and time-mean moisture tendencies in the equatorial column for the $\Delta\varphi = 45°$, $\xi = 2.5$ experiment from Figure 2.16. Positive values mean moisture is being added to the air at that level. The Residual is defined as the value necessary to balance the other four tendencies.

the moisture tendency terms for each vertical level at the equator of the $\Delta\varphi = 45°$, $\xi = 2.5$ experiment. Positive values mean moisture is being added to the atmosphere while negative means moisture is being removed. The first three tendency terms are convection, condensation, and diffusion, which are all directly diagnosed in the model. The fourth term is the moisture flux convergence (MFC), which is the 5°N/S mean of the Total Moisture Flux Convergence from Figure 2.16. We also add a Residual, which is the value necessary to balance the four tendencies and represents the error of the MFC.

We find that, unlike the Earth-like state, the equatorial convection tendency is zero at all levels – convection has fully shut off in this experiment. The lower troposphere is primarily characterized by moisture flux divergence (shown as negative MFC in the figure) balanced by re-evaporation (shown as positive condensation), with the roles swapping in the upper troposphere. This means moisture is added to the lower troposphere only via evaporation of rain from the condensation scheme and then removed primarily via MFC and a small amount of diffusion. The opposite then is true of the upper troposphere, where moisture is transported in and then condensed out to produce the rain that supplies the lower levels. The

lower atmosphere of this system is only supplied with moisture via re-evaporation, which must necessarily come from above. This may confirm our hypothesis that the equatorial surface is not supplied with moisture via low-level horizontal transport but rather exclusively by downward moisture flux from the upper troposphere. In Figure 2.16(i) the flux vectors showing horizontal transport into the upper (lower) troposphere at the equator are diverging (converging) in an area of overall convergence (divergence). This means the MFC is primarily due to the vertical component of moisture flux. A consistent interpretation is that falling precipitation completely re-evaporates and the upward transport returns moisture in a closed loop, further supporting our hypothesis that the equatorial water cycle is largely cut off from the high-latitude oceans.

2.4.2 Effect of HC Width on Equatorial Moisture

Our simulations indicate that one way to achieve a Titan-like state on an Earth-like planet may be to have a large equatorial continent ($\Delta\varphi$) and high condensable volatility (ξ). Another, potentially complementary influence is the relative width of the HC and this area of dry land at the equator. The HC widens as T_r increases, as is well-known from theoretical and numerical considerations (e.g. Hide, 1969; Schneider, 1977; Held and Hou, 1980; Schneider, 1987; Lindzen and Hou, 1988; Plumb and Hou, 1992; Emanuel et al., 1994; Emanuel, 1995; Caballero et al., 2008; Kaspi and Showman, 2015; Guendelman and Kaspi, 2018; Hill et al., 2019, 2020). With constant $\Delta\varphi$, this can allow the HC to "reach" the edge and provide a moisture source to the equator.

This can be used to explain the results shown in Figures 2.10(g), 2.10(h), and 2.11. The plots appear to show an unexpected paradox, that being smaller T_r correlates with meeting more Titan-like criteria. As mentioned previously, Titan is a slow rotator, with one Titan-day equaling approximately 16 Earth-days ($T_r = 16$). Yet our experiments with variable T_r show that fast rotators (small T_r) are more likely to meet our Titan-like criteria. Applying the concept that larger T_r corresponds to a larger HC, we would in fact predict

that experiments with smaller T_r and similar $\Delta\varphi$ would be drier and thus more likely to meet our Titan-like criteria. This means that Titan itself must have a competing effect on its equatorial climate. This may be a large $\Delta\varphi$, since if $\Delta\varphi$ is also increased rather than held constant, then it would compete with the wider HC that comes with a larger T_r.

We quantify the ratio between the HC width (defined as the latitude where the zonal-mean mass flux first drops below 10% of its maximum value while at the level of the maximum value) to $\Delta\varphi$ as R_{HC}, shown in Figure 2.18. For $R_{HC} < 1$ the HC is contained by the land strip, while for $R_{HC} \geq 1$ the HC reaches the shoreline. Each row shows one of the three humidity quantities used to determine the Titan-like criteria as a function of R_{HC}. The left column shows data points for the $\Delta\varphi$ experiments, the middle column shows the T_r experiments, and the right column shows the ξ experiments. Each set of markers is colored based on its experimental control parameter value, as indicated in color bars in the top row. Overall, there is a general trend toward meeting more Titan-like criteria with smaller R_{HC}, with some caveats. For the $\Delta\varphi$ experiments, the peak latitude of q_1 (Figure 2.18, top-left) is off the equator for R_{HC} values between ~ 0.75 and ~ 2. Despite having HC widths that are smaller than the land strip width ($R_{HC} < 1$), the experiments with the largest $\Delta\varphi$ have their peaks at the equator. This apparent paradox is due to the high latitude of their shorelines and correspondingly lower mid-latitude values of q_1 outpacing any reduction in q_1 at the equator (see Figure 2.7(a)). For the $\Delta\varphi$ experiments, the percent decrease in the vertical profile of specific humidity (Figure 2.18, middle-left) and equatorial RH (Figure 2.18, bottom-left) both increase with larger R_{HC} and do not have a clear transition at $R_{HC} = 1$. Experiments with varying rotation period, T_r, have only two outlier cases with off-equatorial peaks in q_1 around $R_{HC} = 1$ (Figure 2.18, top-middle); for all others, the peak in q_1 stays at the equator. For the T_r experiments, the percent decrease in SH (Figure 2.18, middle) and equatorial RH (Figure 2.18, bottom-middle) follow similar patterns to the corresponding panels for the $\Delta\varphi$ experiments. There is a similar range in R_{HC} between the $\Delta\varphi$ and T_r experiments, even though the latter only use three values of $\Delta\varphi$ (25°, circles; 35°, squares;
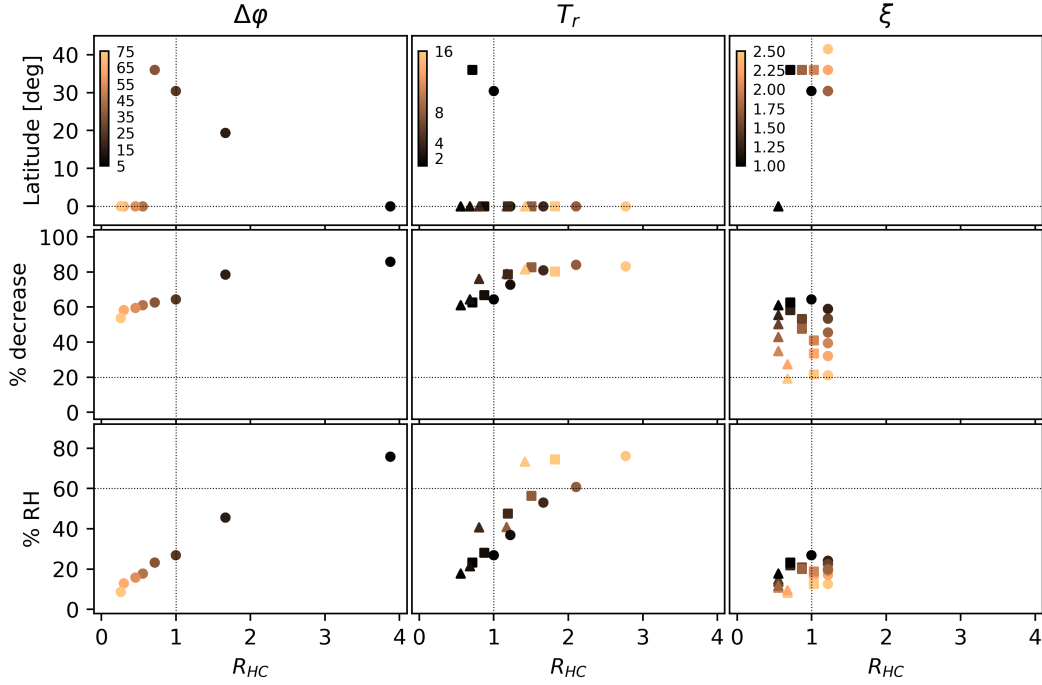
Figure 2.18: Ratio of time-mean HC width to $\Delta\varphi$, R_{HC}, vs: (Top row) Latitude of peak zonal- and time-mean q_1; (Middle row) percent decrease in time-mean specific humidity at the equator between the surface and 60hPa pressure level; (Bottom row) time-mean RH at the equatorial surface. Left column shows data for the $\Delta\varphi$ experiments; Middle column shows data for the T_r experiments; and Right column shows data for the ξ experiments. The marker colors show the respective paramter values of each experiment set. Dashed horizontal lines denote the relevant criteria thresholds (Top: OffEq, Middle: ConVQ, Bottom: LowRH). Dashed vertical lines denote the 1:1 ratio, below which the HC is narrower than the land strip and thus cutoff from the ocean. Symbols in the middle and right columns have the values of $\Delta\varphi = 25°$ (circles), $35°$ (squares) and $45°$ (triangles).

and 45°, triangles). This shows the widening of the HC with increasing T_r is playing the dominant role in determining R_{HC}. In contrast with $\Delta\varphi$ and T_r, R_{HC} varies only slightly, from roughly 0.5 – 1.25, in the ξ experiments. The peak in q_1 (Figure 2.18, top-right) is off the equator for all but one experiment, with that experiment having R_{HC} close to 0.5 and the others having larger values. Excluding this outlier, all experiments meet the OffEq and LowRH criteria. The percent decrease in specific humidity (Figure 2.18, middle-right) and equatorial RH (Figure 2.18, bottom-right) show little dependence on R_{HC}, the scatter being almost entirely from the range of $\Delta\varphi$ used for these experiments. In contrast, increasing ξ decreases the percent decrease in specific humidity (Figure 2.18, middle-right) without changing R_{HC}; only the highest ξ values meet the ConVQ criterion. This suggests that ξ does not significantly affect the extent of the HC, despite affecting the apparent shape of the circulation (Figure 2.16).

To summarize, R_{HC} is moderately predictive of meeting our Titan-like criteria for the $\Delta\varphi$ and T_r experiments, but not at all for the ξ experiments. Figure 2.18 confirms our previous analysis, that large values of ξ associated with Titan's abundant methane vapor are likely responsible for Titan's nearly uniform SH in the lower troposphere. It also makes clear the competing effects of Titan's mid- or high-latitude shorelines and its wide HC on meeting the OffEQ criterion. For fixed T_r, Titan's smaller radius would make its HC fractionally wider than it is on Earth, i.e. it would extend to higher latitudes and exacerbate the problem. Titan's surface liquids would need to be tightly constrained to the very highest latitudes, which given the colder conditions there would make it even more difficult for q_1 at the shoreline to exceed even a small bump in equatorial q_1. A decent approximation is $R_{HC} \sim 1$ on Titan, and while there are a number of our simulations with $R_{HC} \sim 1$ that meet at least two criteria, only the very largest ξ values meet all three. So it seems that while the relative widths of Titan's dry equatorial belt and HC width are important, it is the abundant methane that is key to establishing our three Titan-like criteria.

2.5 Conclusions

We have presented a suite of idealized GCM experiments of an Earth-like climate while varying four parameters to investigate the transition to a Titan-like climate at the equator. We created three criteria to determine if the equatorial climate was Titan-like: (1) The peak in q_1 is not at the equator, despite the peak in near-surface temperature being there; (2) The specific humidity is approximately constant through the lower troposphere at the equator; (3) The annual-mean near-surface RH at the equator is below 60%, indicating a climate that is significantly moisture limited. The first parameter we varied is the width of a land strip centered on the equator that was initialized using a novel model of land hydrology (Faulk et al., 2020). We found that varying the land strip ($\Delta\varphi$) alone did not allow any experiments to meet all three criteria. We then varied the rotation (T_r) for experiments with $\Delta\varphi$ between 25-45°. Similarly to the experiments with only a varied land strip, we found that varying T_r did not meet all three criteria. Notably, the trend is such that lower T_r created more Titan-like conditions, which is in contradiction to Titan's high T_r relative to Earth. This apparent contradiction will require further investigation, most likely by varying T_r and ξ in tandem. The fourth control parameter of our experiments is the volatility of the condensable (ξ), which we varied for the same land strip widths as with the T_r experiments. We found that varying ξ did achieve all three criteria for $\xi = 2.5$. Titan's condensable, methane, is much more volatile than water on Earth, so this finding indicates that the volatility itself may have a significant influence on Titan's low-q_1 climate. We also found a competition between $\Delta\varphi$ and ξ, in that wider land strips were less Titan-like for the same ξ. Our ξ experiments only go up to $\Delta\varphi = 45°$, which is likely narrower than the desert region on Titan. To compensate, the effective ξ on Titan may be higher than the maximum ξ used in our experiments, potentially around 3. While it is feasible to study larger $\Delta\varphi$, we are limited to a maximum ξ because of the water vapor feedback, and expanding the range in ξ will require an adjustment to the radiative transfer. We will explore this in future work.

Our experiments identify several outstanding questions.

1. Can larger T_r allow us to achieve higher values of ξ in our model for the same land-strip widths?

2. How high does ξ need to be to achieve Titan-like conditions on a land strip that covers a similar area to Titan's large equatorial desert?

3. Will varying three parameters ($\Delta\varphi$, T_r, and ξ) simultaneously be necessary to create a more Titan-like climate?

In addition to understanding a Titan-like climate, these experiments can be used to shed light on Earth-like climates, including our own planet's past. Earth has had several continental arrangements through its history, and our hydrology module can be used to investigate them in detail by specifying global topography. As demonstrated by our experiments with a land strip of varying width, the presence, location, and size of a continent can have significant effects on global climate. With the addition of a seasonal cycle and more complex continental arrangements, many points in Earth's history can be simulated and compared to provide better understanding of the range of possible climate states.

CHAPTER 3

Seasonal Parameter Sweep

Earth's tropics experience seasonal transitions between "wet" and "dry" periods as the ITCZ moves over a particular latitude band. The same is true for Titan, but over a much larger part of the surface. The movement of the ITCZ on Titan is thus important for both the equatorial and high-latitude climate, and acts to connect these two regions. In our previous study on the transition states between an Earth-like and Titan-like climate (Chapter 2), we neglected seasonality to explore the annual-mean climate of the equator. This was sufficient for an initial understanding of the global climate impacts of evaporative resistance, equatorial land fraction, rotation period, and condensable volatility, but to create a robust representation of a Titan-like state we need to include seasonality. We hypothesize that the addition of seasons will have a significant effect on the equatorial climate of our experiments that include an equatorial land strip. One characteristic effect of the land strips in an aseasonal simulation was to prevent oceanic moisture from reaching the equator. Wider land strips isolated the equator more effectively as the Hadley Cell (HC) circulation was fully contained by the land. The addition of seasonality would allow the HC circulation to move off the equator and access moisture even for wider land strips. It is likely that the widest land strips will see less effects from the addition of seasonality since their width will mitigate the expansion of the HC, and similarly experiments with long rotation periods will see less impact from seasonality as their HC was already wide enough to reach the ocean due to the weak Coriolis Force.

3.1   Methods

We vary the same four parameters as in Chapter 2, these being evaporative resistance (r_E), equatorial land fraction ($\Delta\varphi$), rotation period (T_r), and condensable volatility (ξ), but with the addition of a seasonal cycle. We use Earth-like obliquity and season lengths, only deviating from Earth values in the four varied parameters. Surface heat capacity is dynamic, varying with the amount of surface liquid up to a prescribed mixed-layer depth of 40m. For experiments with an equatorial land strip, surface liquid and topography are initialized as described in Chapter 2. Simulations are performed for 15 years, and all diagnostics are averaged over the last 10 years.

In addition to the three Titan-like criteria used in Chapter 2 (OffEq, ConVQ, and LowRH), we add three new criteria for determining if an experiment is Titan-like:

1. The annual-mean temperature gradient is small. Observations of Titan's surface temperature show that the equator is only about 3K warmer than the poles (Jennings et al., 2009). In contrast, Earth's equator is roughly 30K warmer than its poles. Given the much higher absolute temperatures on Earth we can instead compare the percent change between the equatorial and polar temperatures. For Titan this is approximately a 3% decrease from the equatorial temperature, versus 10% for Earth. Experiments with an annual-mean equator-to-pole temperature decrease of 5% or less will meet the TGrad criterion.

2. The ITCZ reaches into the high latitudes of the summer hemisphere. Observations of clouds on Titan have shown they are most likely to form near the point of maximum insolation, which reaches close to the pole during summer solstice (Turtle et al., 2018). We use two definitions for the ITCZ extent into the summer hemisphere. The first is based on the stream function at 850hPA. Taking the annual zonal-mean climatology of the Northern Hemisphere and starting on July 1st, we find the daily location where the stream function first becomes 0 moving north from the equator. The maximum latitude

value over the average year is the ITCZ extent for that experiment. Experiments where this calculated extent reaches at least 60° latitude will meet the SF-ITCZ criterion.

3. The second definition for the ITCZ is based on the precipitation. On Earth there is a near-constant band of precipitation associated with the low-level convergence of the ITCZ. However, for experiments with large land strips and small T_r, this region of convergence can have little to no associated precipitation. As such, it is important to acknowledge that such a planet can appear to match observations of Titan's high-latitude cloud formation despite having a more Earth-like HC structure. As such, we calculate a latitude of peak solsticial precipitation for each experiment. Once again starting with an annual zonal-mean climatology of the Northern Hemisphere, we take a running mean for each day starting on May 21st and ending on October 10th. Each daily mean includes the 20 days before and after, and is calculated for each gridpoint in latitude. We then find the overall maximum 41-day mean in precipitation and take its latitude as the precipitation-based ITCZ extent. Experiments where this value is at least 60° latitude will meet the P-ITCZ criterion.

3.2   Results

3.2.1   Variable r_E Experiments

We present the results for the first four Titan-like criteria in Figure 3.1. Since these criteria are based on the annual-mean climate, it is not surprising that they look similar to the results from the equivalent aseasonal experiments in Chapter 2. No experiments meet the OffEq criterion (3.1(a)) since the uniform surface and deep mixed-layer keep the peak humidity at the equator. Experiments with $r_E \geq 99\%$ meet the ConVQ criterion (3.1(b)), while experiments with $r_E \geq 70\%$ meet the LowRH criterion (3.1(c)). Both of these criteria are met once the atmosphere has reached a minimum level of dryness. The first of our new criteria, the TGrad criterion, is not met by any experiments, and instead the climate moves away
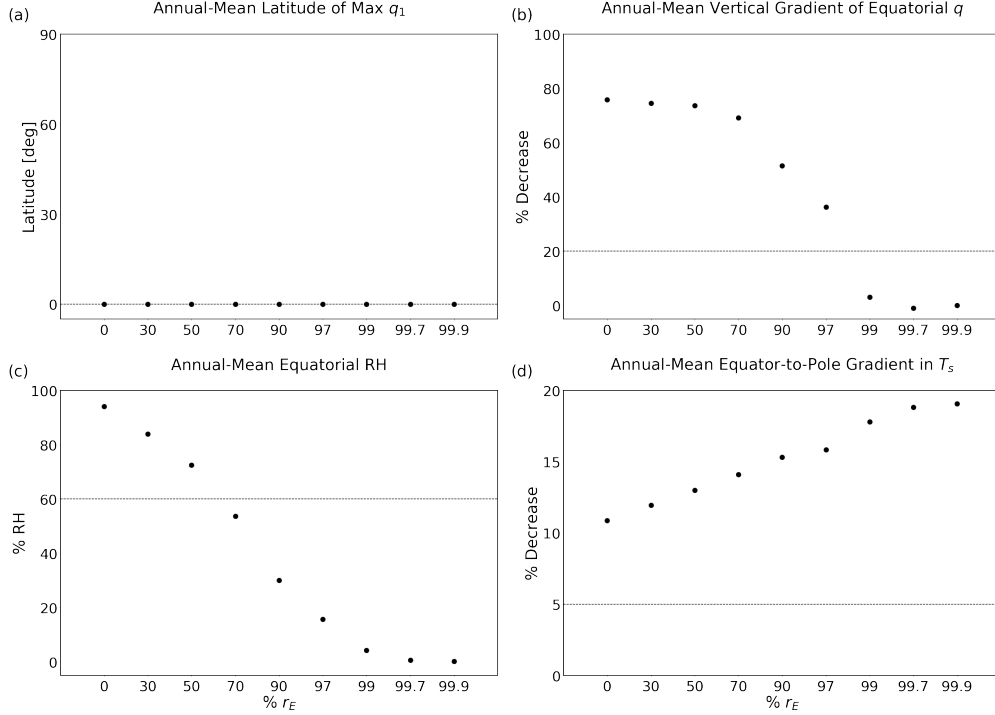
Figure 3.1: Analysis for the OffEq (a), ConVQ (b), LowRH (c), and TGrad (d) criteria for the r_E experiments. Horizontal dashed lines denote the relevant threshold for meeting each criterion.

from the threshold as r_E increases. This may be from the reduced water vapor feedback in the drier experiments allowing more cooling, which has the greatest effect at the poles during polar night. The cooler poles increase the temperature gradient to the equator, moving the climate away from being Titan-like despite moving it towards Titan-like conditions for the ConVQ and LowRH criteria.

Given the large mixed-layer used in our experiments, the seasonal cycle is heavily damped in our aquaplanet cases. As such, the ITCZ extent is tightly constrained to the equator for all values of r_E (Figure 3.2(a)). We include three sample climatologies of the 850hPa stream function in Figures 3.2(b-d), with a black dotted line demarcating the extent shown in 3.2(a). The primary change as r_E increases is a general weakening of the stream function, but the relative positioning of the seasonal summer circulation is nearly identical.
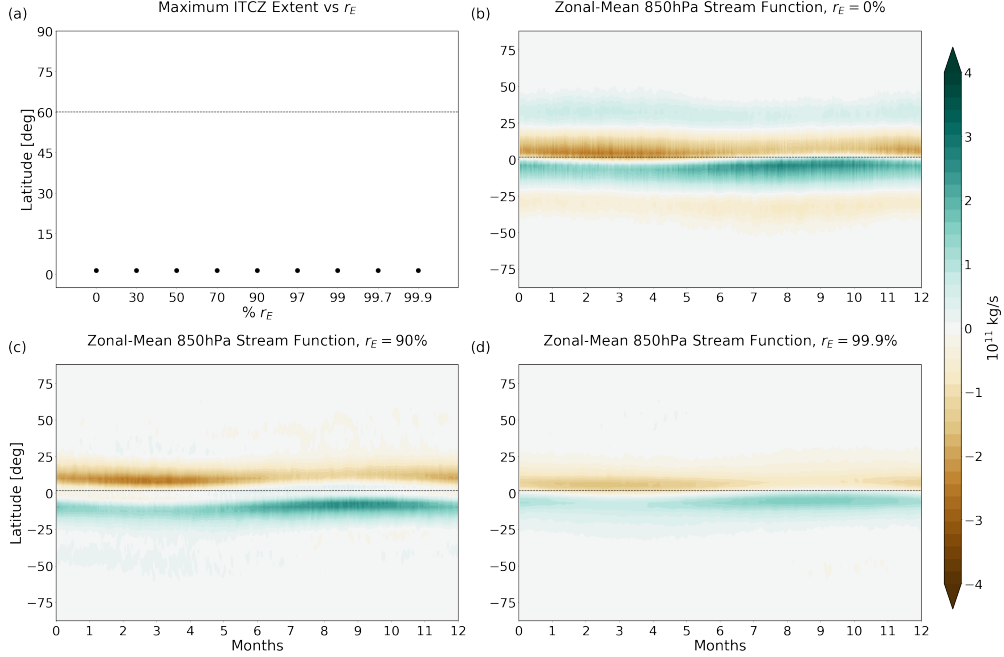
Figure 3.2: SF-ITCZ criterion analysis for the r_E experiments (a) and the zonal-mean 850hPa level stream function over an average year for the $r_E = 0\%$ (b), 90% (c), and 99.9% (d) cases.

As with the ITCZ extent, the precipitation maximum is generally constrained to the deep tropics with the exception of the highest r_E experiment. Without the presence of a land strip, the location of the ITCZ based on the stream function and based on the precipitation should be quite close. This makes the $r_E = 99.9\%$ case particularly interesting, as it concentrates its peak precipitation at the poles. Polar precipitation dominating the tropics should be difficult on an aquaplanet, even with a dry atmosphere, since the uniform surface will still favor evaporation at the warmest location, the equator. But this does not mean it favors condensation at the same point, and this is hinted at by the polar precipitation peaking in the winter months. The atmosphere has reached such a dry regime that the location best able to condense water is the coldest, i.e. the winter poles. The magnitude of precipitation in this experiment is extremely small, peaking at the level of 10^{-20}mm/day. This is almost 20 orders of magnitude smaller than even the $r_E = 90\%$ case, which was only one order of magnitude

54
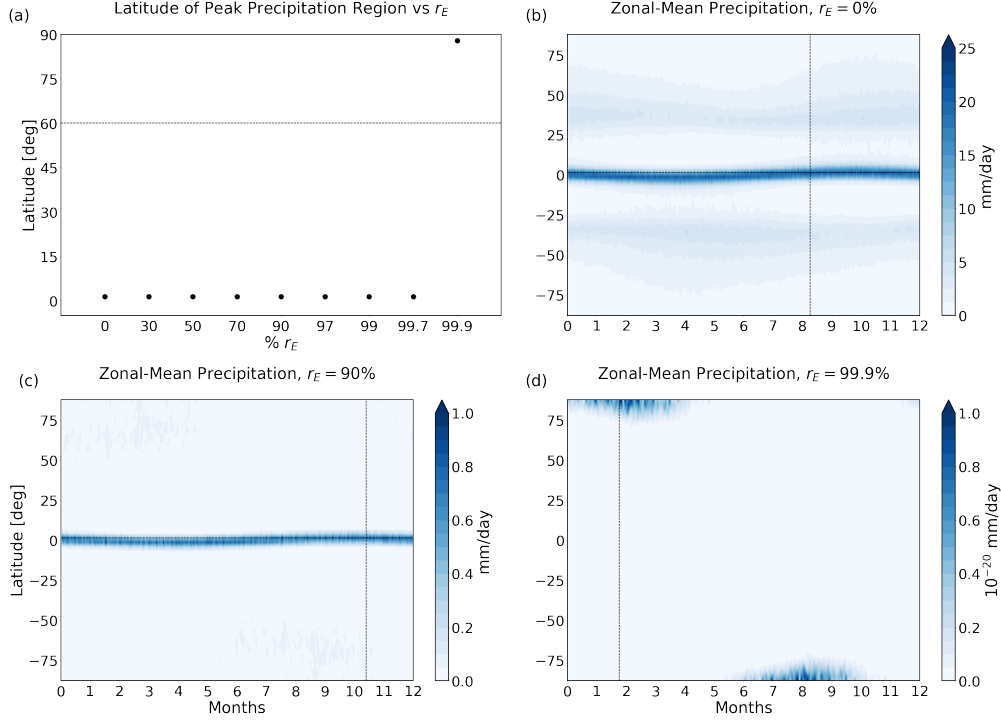
Figure 3.3: P-ITCZ criterion analysis for the r_E experiments (a) and the zonal-mean precipitation over an average year for the same cases as in Figure 3.2 (b-d).

smaller than the $r_E = 0\%$ experiment. The shift to polar precipitation and extremely small magnitudes occurs at the very limit of the r_E range, suggesting it could represent a transition state between a fully dry climate and a "wet" one. Table 3.1 summarizes the results for the r_E experiments.

3.2.2 Variable $\Delta\varphi$ Experiments

As described in Chapter 2, we add a hemispherically symmetric strip of land by introducing global topography with a moderately elevated equatorial region. The width of said strip is adjusted by adjusting the topography, and runoff is self-consistently simulated while surface infiltration is prohibited. We also include the aquaplanet experiment with $r_E = 0\%$ as the $\Delta\varphi = 0$ case.

	Criteria					
	OffEq	ConVQ	LowRH	TGrad	SF-ITCZ	P-ITCZ
$r_E = 0\%$						
30%						
50%						
70%			X			
90%			X			
99%		X	X			
99.7%		X	X			
99.9%		X	X			X

Table 3.1: Criteria matched by each r_E experiment.

Unlike the r_E experiments, all $\Delta\varphi > 0$ cases meet the OffEq criterion (Figure 3.4(a)). The relationship between $\Delta\varphi$ and the location of peak q_1 is approximately linear. Since the q_1 peak in the annual mean is dominated by the summer/winter season, it is expected that the observed trend is based on the expanding shorelines keeping oceanic moisture further away from the equator while also allowing it to move over the warmer near-shore land. Similarly, the expansion of the shorelines acts to dry out the equatorial column and lower its vertical gradient in q to near-zero (Figure 3.4(b)). Unlike in the aseasonal cases from Chapter 2, we conclude that increasing $\Delta\varphi$ does allow the experiments to meet the ConVQ criterion in the annual mean. In fact, only three cases with positive $\Delta\varphi$ do not meet the criterion, suggesting a constant vertical profile is a robust feature of simulations with both a seasonal cycle and a land strip.

In contrast to the OffEq and ConVQ criteria, the results for the LowRH criterion are close to what we found in our aseasonal experiments: equatorial RH drops quickly with increasing $\Delta\varphi$, falling below the 60% threshold immediately after the $\Delta\varphi = 5$ case. The aseasonal
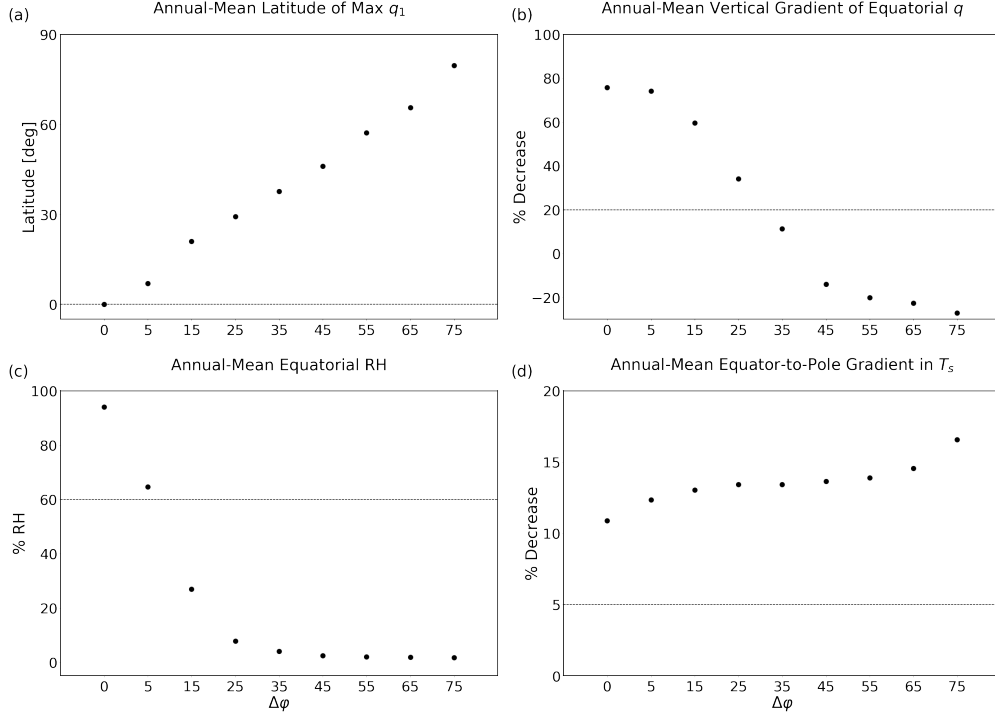
Figure 3.4: Criteria analysis as in Figure 3.1 but for the $\Delta\varphi$ experiments.

experiments do not see such low RH values for $\Delta\varphi \geq 25$, meaning the seasonal cycle does have at least a small effect on all three original criteria for the $\Delta\varphi$ experiments. This effect appears to be a drying of the equator in the annual mean, which may be unexpected given the seasonal cycle allowing the HC to expand poleward during the summer season, theoretically providing greater access to oceanic moisture. This is most notable in the LowRH criterion, which would be dependent only on the moisture advected into the equatorial column and the local surface temperature. Yet we find that even the smallest land strip is close to meeting the 60% RH threshold. We hypothesize that the mechanism for this is the interaction between the ITCZ and the dry land at the equator during the summer/winter seasons, and expand on this topic in Section 4.

No experiments meet the TGrad criterion, and the presence of a land strip appears to push the annual-mean climate away from the 5% threshold. This matches the r_E experiments, which we speculated is due to a reduced water vapor feedback in experiments with large $\Delta\varphi$.
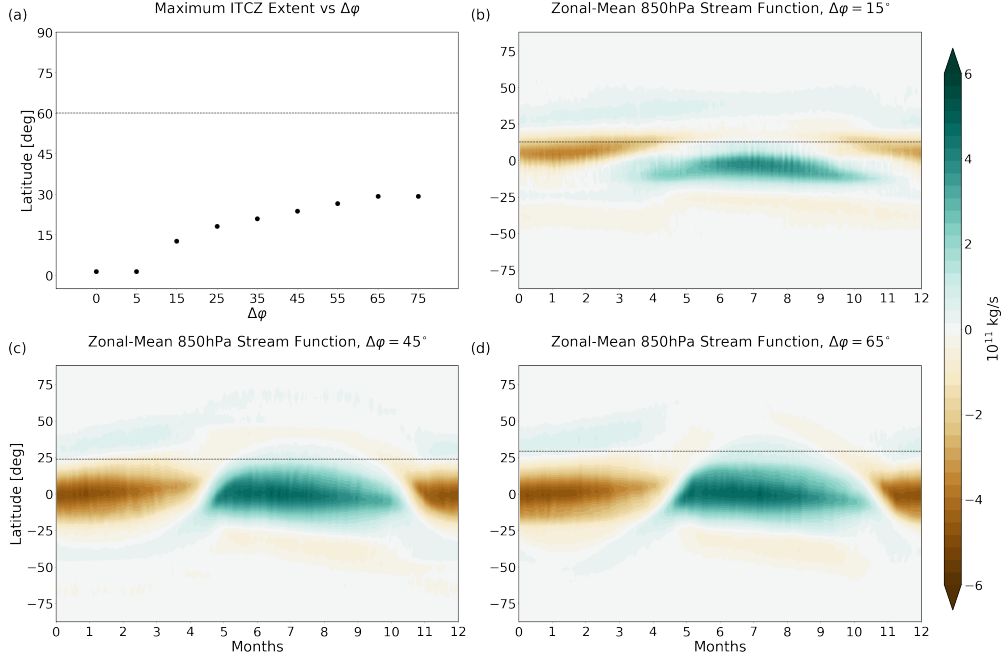
Figure 3.5: As in Figure 3.2, but for the $\Delta\varphi$ experiments (a) and the $\Delta\varphi = 15°$, $45°$, and $65°$ cases (b-d).

At the same time, there is minimal correlation between the gradient in T_s and $\Delta\varphi$ between the values of 15 and $55°$, meaning the actual width of the land strip is unimportant for much of the parameter range. Since global T_s decreases fairly consistently with increasing $\Delta\varphi$, the equatorial and polar values decrease by equivalent amounts in these experiments. Only once the land strip itself begins to move above the Arctic Circle ($r_E \geq 65$) does the gradient begin to increase significantly with larger $\Delta\varphi$. This might be explained by the relative location of water and land; since the equator is dry while the poles are wet, it is reasonable to infer that the global decrease in water vapor feedback is relatively mitigated at the poles where there is an abundant source of evaporation.

Figure 3.5(a) shows the ITCZ extent as a function of $\Delta\varphi$, while 3.5(b-d) show three sample climatology plots of annual-mean 850hPa stream function for different values of $\Delta\varphi$. Each climatology includes a dashed line demarcating the peak ITCZ extent calculated for that experiment. We find in 3.5(a) that ITCZ extent increases significantly with larger $\Delta\varphi$

58
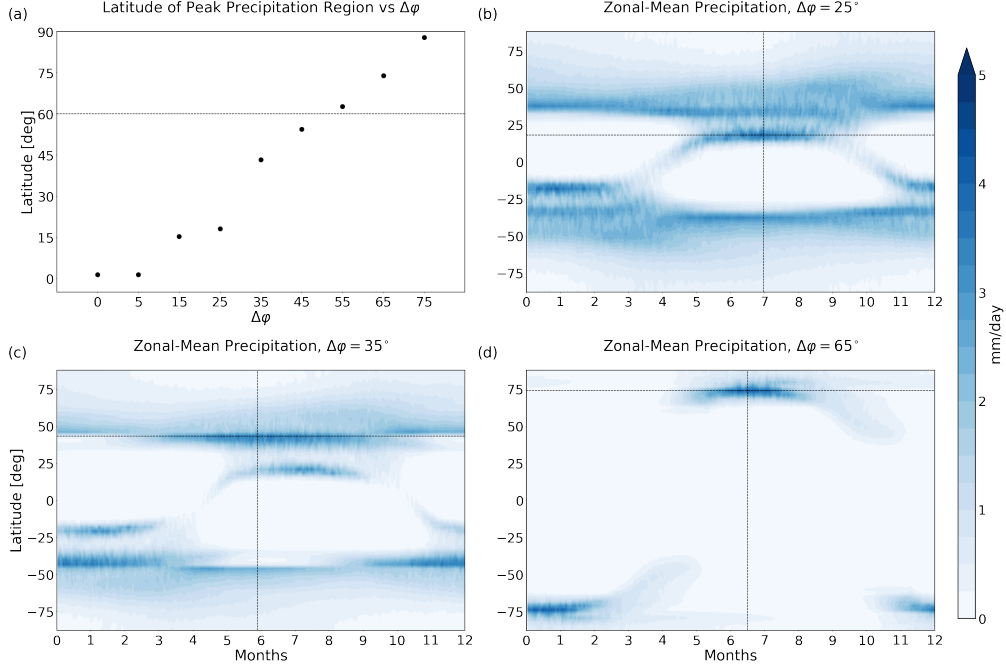
Figure 3.6: As in Figure 3.3, but for the $\Delta\varphi$ experiments (a) and the $\Delta\varphi = 25°$, $35°$, and $65°$ cases (b-d).

up to $\Delta\varphi = 65$. The peak extent reached is approximately $30°$ latitude, much further than expected for $T_r = 1$. We see a widening of the cross-equatorial circulation with larger $\Delta\varphi$ in 3.5(b-d), with this widening occurring in the peak summer months of July and August. This may be similar to the monsoonal HC that occurs over Eastern Asia on Earth, where strong heating over the large land mass of the Asian continent allows the ITCZ to locally move deep into the Northern Hemisphere. Provided a global version of such a continent, it is not surprising to see an even stronger version of this phenomenon. Despite getting much closer to the $60°$ latitude threshold than might be expected, none of the $\Delta\varphi$ experiments meet the SF-ITCZ criterion.

In contrast to the stream function-based ITCZ, the peak solsticial precipitation is much more sensitive to the presence of the land strip (Figure 3.6(a)). Once $\Delta\varphi > 5$, the latitude of the peak increases almost linearly with $\Delta\varphi$, reaching the $60°$ threshold in the $\Delta\varphi = 55$ case. The only deviation is the $\Delta\varphi = 25$ experiment, which is only moderately larger than the

59

$\Delta\varphi = 15$ case but significantly smaller than $\Delta\varphi = 35$. Figure 3.6(b) shows the precipitation climatology for the $\Delta\varphi = 25$ experiment. The peak precipitation region appears to still be the conventional ITCZ, which oscillates between the edges of the land strip at roughly the latitude it would be at on Earth. In the $\Delta\varphi = 35$ case, however, the peak precipitation region has moved from the remnants of the conventional ITCZ to the midlatitudes, where it remains for larger values of $\Delta\varphi$. This transition is fairly significant as it represents a shift from a hydrological cycle dominated by the tropics to one dominated by the midlatitudes. This midlatitude precipitation is not the same as the winter storm track variety, as it still occurs in summer and is seemingly driven by local heating. As shown in 3.6(d), once $\Delta\varphi$ is large enough the tropical precipitation is minimal and summer precipitation is concentrated at the poles. This shows it is possible to match the observations of Titan's polar cloud formation even on planets with small T_r. Table 3.2 summarizes the results for the $\Delta\varphi$ experiments.

	Criteria					
	OffEq	ConVQ	LowRH	TGrad	SF-ITCZ	P-ITCZ
$\Delta\varphi = 0°$						
5°	X					
15°	X		X			
25°	X		X			
35°	X	X	X			
45°	X	X	X			
55°	X	X	X			X
65°	X	X	X			X
75°	X	X	X			X

Table 3.2: Criteria matched by each $\Delta\varphi$ experiment.

3.2.3 Variable T_r Experiments
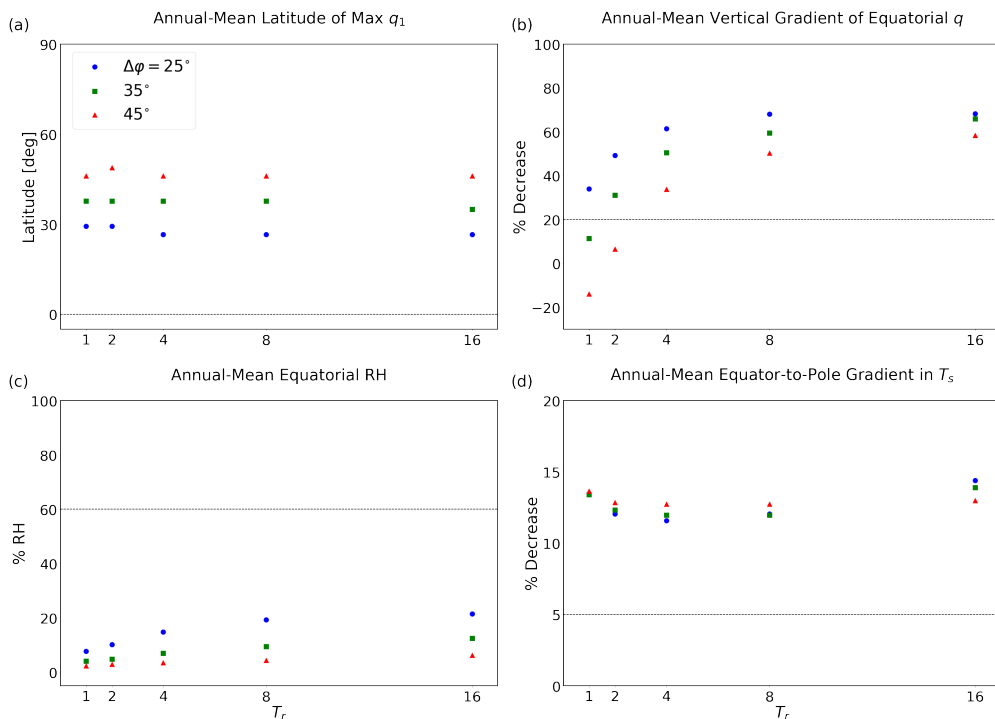
Figure 3.7: As in Figure 3.1, but for the T_r experiments. Experiments are additionally differentiated by $\Delta\varphi$, as described in the legend in (a).

In the aseasonal simulations from Chapter 2, we found that increasing T_r moved the equatorial climate away from Titan-like conditions. The expanded HC circulation allowed more access to oceanic moisture and broadly increased the humidity of the equator. In the seasonal simulations, there is much less an effect on the OffEq and LowRH criteria by T_r (Figure 3.7(a,c)). The values of these criteria are fairly constant with increasing T_r, and all experiments meet the associated thresholds. The TGrad criterion (3.7(d)) is similarly insensitive to increasing T_r, and in this case no experiments meet the criterion. The ConVQ criterion (3.7(b)) is the only one of those shown in Figure 3.7 with a clear pattern in T_r, moving away from the Titan-like threshold as T_r increases. This closely matches the relation between the ConVQ criterion and T_r in the aseasonal experiments.

Surprisingly, no T_r experiments meet the SF-ITCZ criterion (Figure 3.8(a)). There is
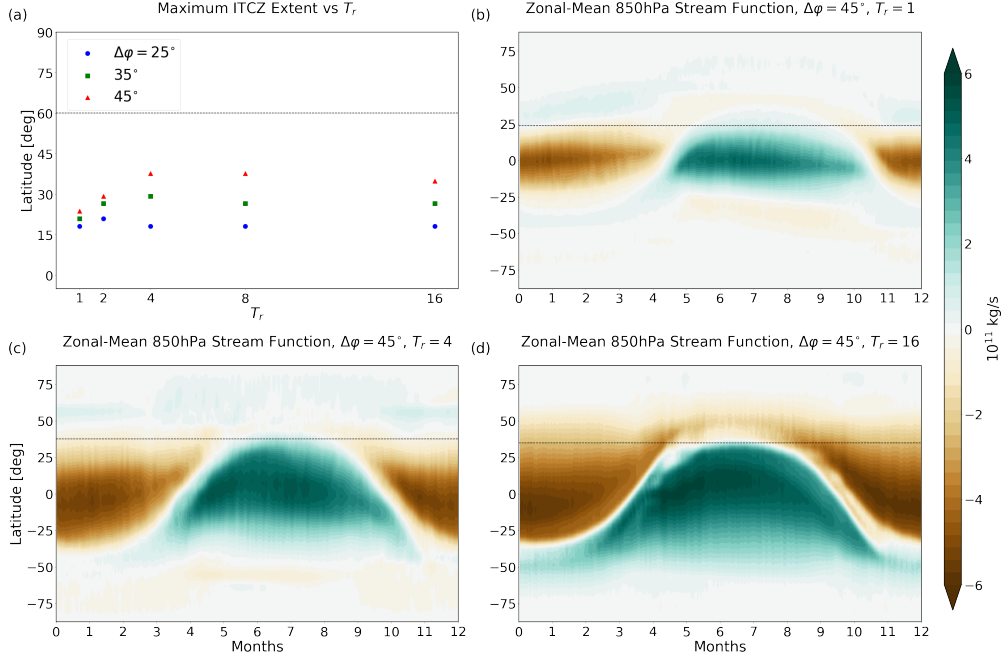
Figure 3.8: As in Figure 3.2, but for the T_r experiments (a) and the cases with $\Delta\varphi = 45°$ and $T_r = 1$, 4, and 16 days (b-d).

minimal correlation between the ITCZ extent and T_r, and even some negative correlation for $T_r \geq 4$. This seems to contradict our hypothesis that larger T_r allows the HC circulation to expand and reach the shorelines of the land strips. It also conflicts with past work on variable rotation in an Earth-like GCM that found global ITCZs for $T_r \geq 8$ (Faulk et al., 2017). Figure 3.8(b-d) shows the 850hPa stream function for three experiments with $\Delta\varphi = 45$ and varied T_r. The peak ITCZ extent maximizes in the $T_r = 4$ case, with further increases in T_r primarily correlating to a stronger circulation rather than a change in extent. The location of the maximum extent appears to stop expanding roughly in the region of the shoreline (3.7(a)), which suggests the difference in surface properties between the land and ocean are working to constrain the HC. The most likely cause is a surface temperature difference, which would mean the shoreline region does not comply with the WTG Theory of the tropics. Even with large T_r the contrast in temperature between the land strip and ocean is maintained, making the ITCZ extent largely insensitive to rotation once it reaches the shoreline. There is a small

trend towards greater ITCZ extents with larger T_r while $T_r \leq 4$ (3.8(a)), corresponding to the ITCZ moving within the continent towards the shoreline. Once it reaches the shoreline the extent remains fixed, or even decreases slightly as the circulation strengthens.
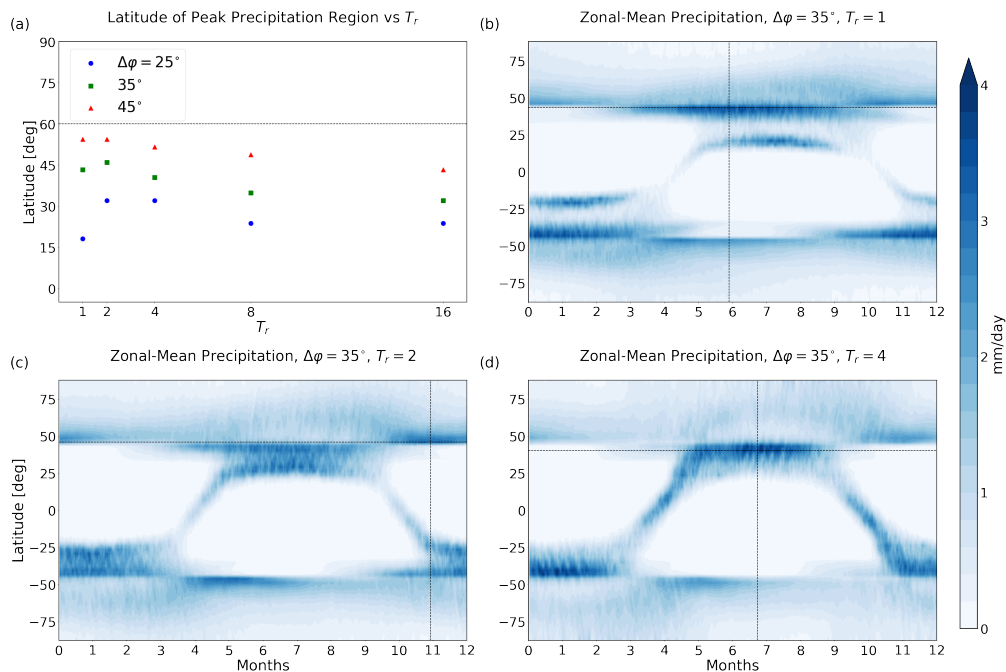
Figure 3.9: As in Figure 3.3, but for the T_r experiments (a) and the cases with $\Delta\varphi = 35°$ and $T_r = 1$, 2, and 4 days (b-d).

As with the SF-ITCZ criterion, no T_r experiment meets the P-ITCZ criterion, although several get within 15° latitude of the 60°N threshold (Figure 3.9(a)). Also similar to the SF-ITCZ, the latitude of peak seasonal P first moves poleward with increasing T_r, up to $T_r = 4$, but then has a slight trend back towards the equator as T_r continues to increase. Figures 3.9(b-d) show the lead up to this transition in the $\Delta\varphi = 35$ cases. There is a shift in the dominant precipitation season from summer in the $T_r = 1$ case (3.9(b)) to late fall/early winter in the $T_r = 2$ case (3.9(c)). Both of these precipitation regions are at similar latitudes, clearly above the conventional ITCZ that is found over the land strip. The shift towards dominant winter precipitation may be due to the interaction between the ITCZ and midlatitude summer peaks in 3.9(b), which are spatially close but still distinct.

63

The magnitude of precipitation is generally lower in this experiment, suggesting the winter peak became dominant due to the summer precipitation weakening. The return to dominant summer precipitation in 3.9(d) seems to be from these two regions fully merging, allowing the new single region of peak summer precipitation to easily dominate the winter peak. Table 3.3 summarizes the results for the T_r experiments.

$\Delta\varphi$	T_r	Criteria					
		OffEq	ConVQ	LowRH	TGrad	SF-ITCZ	P-ITCZ
25°	1	X		X			
	2	X		X			
	4	X		X			
	8	X		X			
	16	X		X			
35°	1	X	X	X			
	2	X		X			
	4	X		X			
	8	X		X			
	16	X		X			
45°	1	X	X	X			
	2	X	X	X			
	4	X		X			
	8	X		X			
	16	X		X			

Table 3.3: Criteria matched by each T_r experiment.
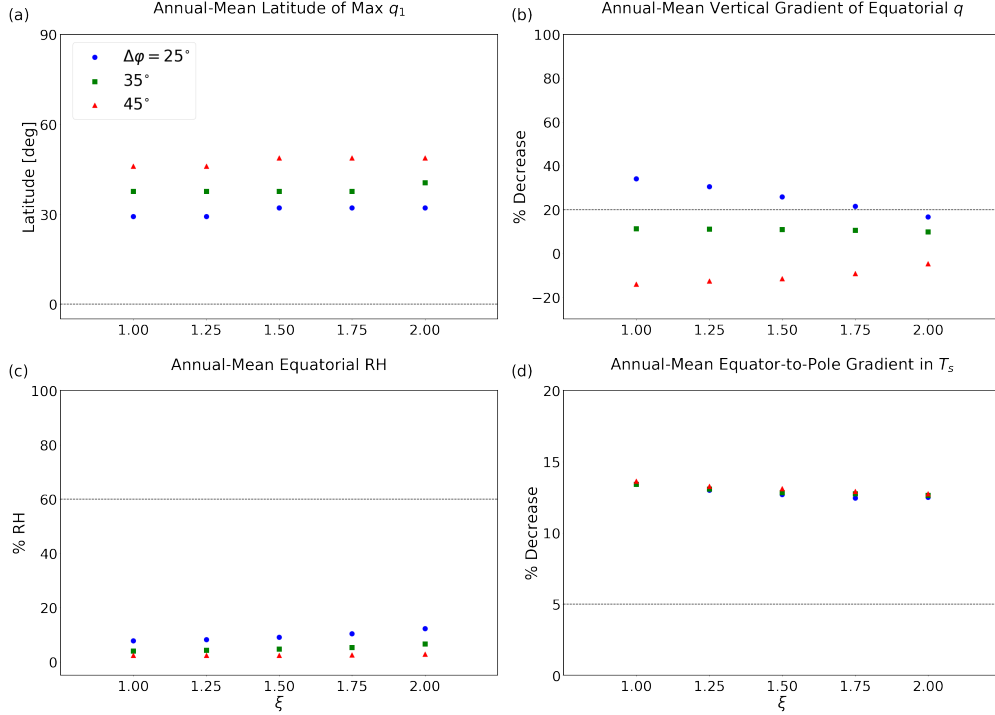
Figure 3.10: As in Figure 3.1, but for the ξ experiments. Experiments are additionally differentiated by $\Delta\varphi$, as described in the legend in (a).

3.2.4 Variable ξ Experiments

Figure 3.10 shows the first four criteria for the ξ experiments. We find little effect on the location of the annual-mean peak in q_1 with increasing ξ (3.10(a)), and minimal effects for equatorial RH (3.10(c)) and the equator-to-pole temperature gradient (3.10(d)). The ConVQ criterion (3.10(b)) shows sensitivity to increasing ξ, although it is not consistent for the three $\Delta\varphi$ values used in this experiment set. The $\Delta\varphi = 25$ cases originally have an equatorial vertical gradient in q larger than the 20% threshold, but this decreases with higher ξ and reaches the threshold for $\xi > 1.75$. In contrast, the $\Delta\varphi = 35$ case has no significant change in its gradient with ξ, while the $\Delta\varphi = 45$ case has its gradient increase (from a negative gradient at $\xi = 1$) with increasing ξ. The experiments thus converge towards each other as ξ increases, suggesting that higher ξ may specifically favor a near-zero gradient rather than a positive or negative one.
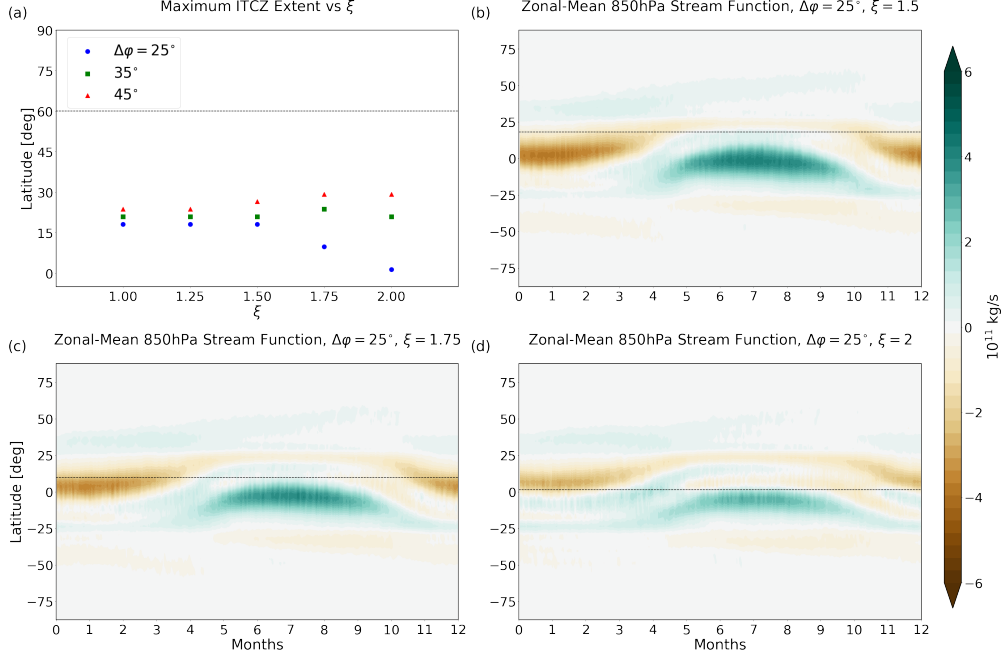
Figure 3.11: As in Figure 3.2, but for the ξ experiments (a) and the cases with $\Delta\varphi = 25°$ and $\xi = 1.5$, 1.75, and 2 (b-d).

As seen in the other experiments with land strips, no cases meet the SF-ITCZ criterion (Figure 3.11(a)). Given the low T_r this is not unexpected, although there is some increase in extent with higher ξ for the cases with $\Delta\varphi \geq 35$. The more unusual result is for the $\Delta\varphi = 25$ cases, which instead have a significant decrease in extent with ξ for $\xi > 1.5$. To demonstrate this decrease we plot the 850hPa climatology of the stream function for three $\Delta\varphi = 25$ experiments. The decrease appears to be due to the formation of a region of negative circulation in the summer tropics that splits the cross-equatorial HC. We explore this phenomenon further in Section 4b.

As with the SF-ITCZ criterin, no experiments meet the P-ITCZ criterion (Figure 3.12(a)). The calculated extents are nearly constant in ξ with some slight increase at the upper end of the range, with the exception of a transition point that occurs between $\xi = 1.25$ and 1.5 in the $\Delta\varphi$ cases. This transition point is demonstrated in Figure 3.12(b-d), which show the transition to be a change in where the dominant seasonal precipitation is located. In the
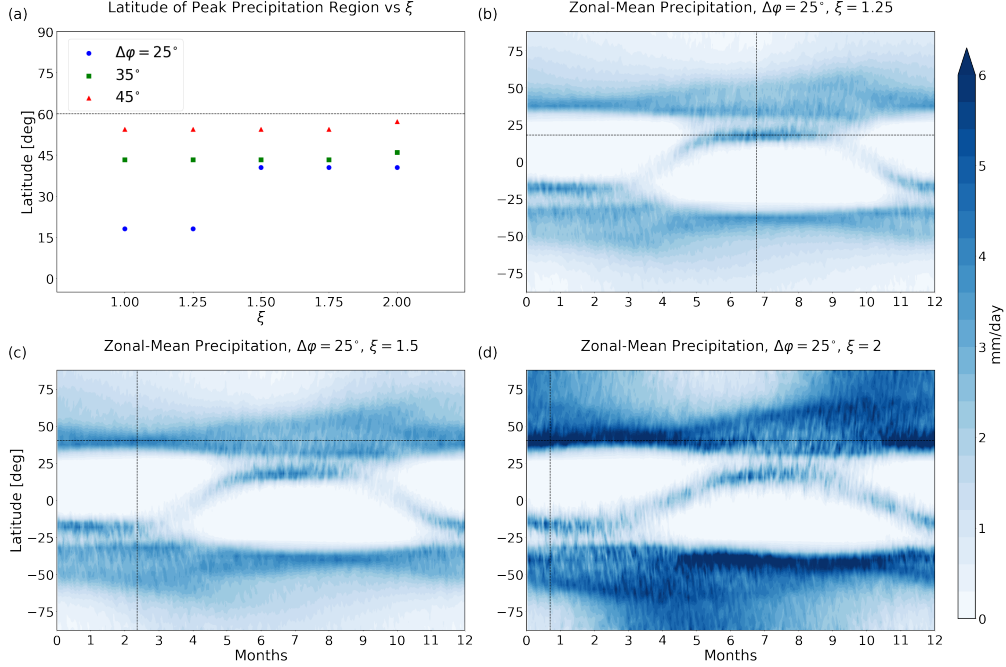
Figure 3.12: As in Figure 3.3, but for the ξ experiments (a) and the cases with $\Delta\varphi = 25°$ and $\xi = 1.25$, 1.5, and 2 (b-d).

$\xi = 1.25$ case, the tropical ITCZ is still the dominant seasonal precipitation, placing the peak extent within the land strip. Once ξ increases to 1.5, the peak location shifts to the winter shoreline, noticeably increasing the peak extent. The shift in dominant precipitation from summer to winter is similar to that observed in the T_r cases in Figure 3.9. Unlike those cases, however, the peak remains in the winter as ξ continues to increase, with the winter shoreline precipitation becoming more dominant over the tropical summer ITCZ. The relative weakening of the summer precipitation may be due to the circulation observed in Figure 3.11, or may be connected to the increased saturation vapor pressure in the high-ξ simulation. If the saturation specific humidity is higher, more moisture is needed to reach condensation and produce the same amount of rain as in the lower-ξ cases. Since the tropical ITCZ is located over the land strip, it is dependent on advected moisture from the shorelines. If the advected moisture does not increase with higher ξ as fast as the saturation specific humidity, the tropical ITCZ would weaken. The shorelines and ocean regions do not have this

limitation, as their moisture source is local evaporation which is directly tied to saturation specific humidity. The seasonal shift from summer to winter may also be connected to the greater difficulty in reaching saturation, as the colder temperatures in winter could be more effective at producing rain. Table 3.4 summarizes the results for the ξ experiments.

$\Delta\varphi$	ξ	Criteria					
		OffEq	ConVQ	LowRH	TGrad	SF-ITCZ	P-ITCZ
25°	1	X		X			
	1.25	X		X			
	1.5	X		X			
	1.75	X		X			
	2	X	X	X			
35°	1	X	X	X			
	1.25	X	X	X			
	1.5	X	X	X			
	1.75	X	X	X			
	2	X	X	X			
45°	1	X	X	X			
	1.25	X	X	X			
	1.5	X	X	X			
	1.75	X	X	X			
	2	X	X	X			

Table 3.4: Criteria matched by each ξ experiment.

3.3 Discussion

3.3.1 Interaction between the Cross-Equatorial HC and Land Strip
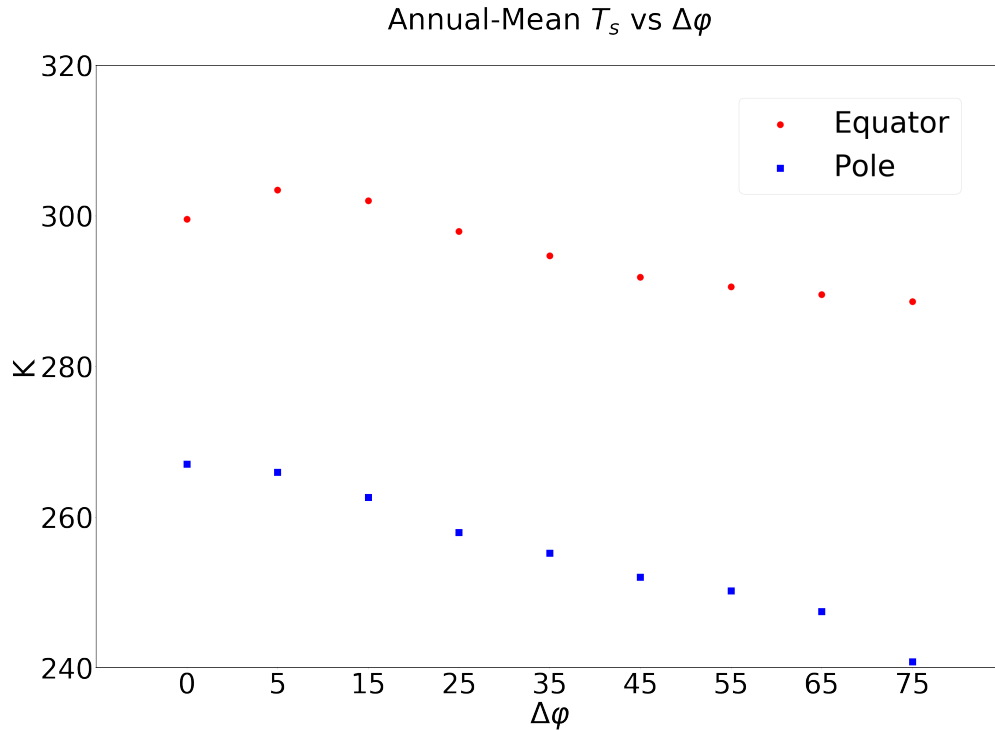
Figure 3.13: Annual-mean equatorial (red circles) and polar (blue squares) T_s for the $\Delta\varphi$ experiments.

One unexpected result was that the addition of a seasonal cycle acted to dry out the equatorial climate in the $\Delta\varphi$ experiments (Figure 3.4). Each of the three criteria applied to the aseasonal experiments (OffEq, ConVQ, and LowRH) showed significantly drier climates in the equivalent seasonal cases, yet there is clear cross-equatorial flow in the summer/winter months (Figure 3.5). In this section we will investigate how this cross-equatorial flow fails to supply moisture to the equator, or instead removes it.

We first compare the annual-mean T_s at the equator and the poles in Figure 3.13. The equatorial temperature is relevant to the LowRH criterion since RH is a function of both q and T. This means the low annual-mean values of equatorial RH in the $\Delta\varphi$ experiments

could primarily be the result of higher T_s rather than lower q. We find that equatorial T_s generally decreases with higher $\Delta\varphi$, ranging from $\sim 305\text{K}$ at its maximum ($\Delta\varphi = 5$) to $\sim 290\text{K}$ at its minimum ($\Delta\varphi = 75$). This is a relatively small change compared to the decrease in RH of $\sim 60\%$ between the same two experiments, with the RH going to $\sim 0\%$ by $\Delta\varphi = 45$. This means the primary driver of the low RH in the higher $\Delta\varphi$ cases is indeed low q. For the equator to be dry in the annual-mean, there must either be a dominant season that is dry or all seasons are dry. If we roughly approximate the aseasonal experiments from Chapter 2 as the spring/fall season, the drier annual-mean in the seasonal experiments must be due to the summer/winter season that is not present in the aseasonal simulations. This is now our focus.
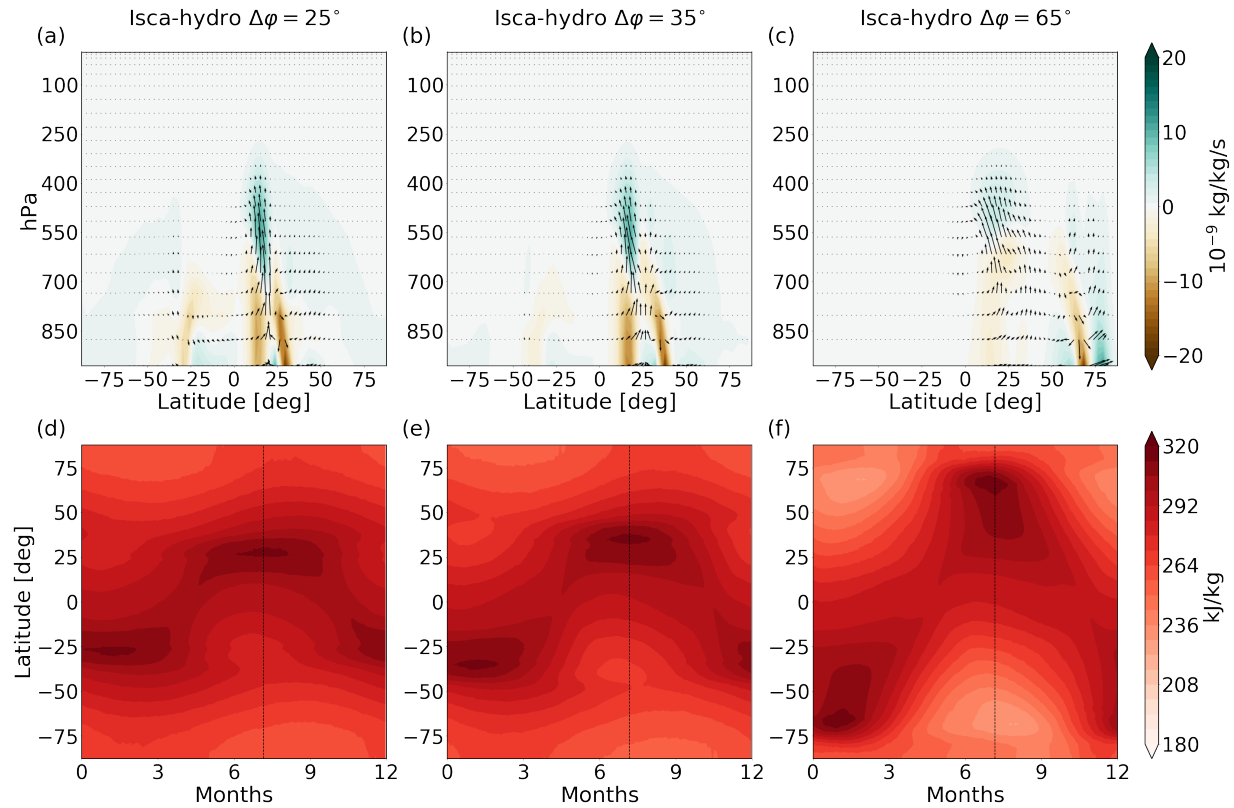
Figure 3.14: Peak summer MFC and moisture fluxes (top) and near-surface MSE climatology (bottom) for the $\Delta\varphi = 25$ (left), 35 (middle), and 65 (right) experiments. The dashed black lines in (d-f) mark the day used to define the "peak summer" period in (a-c).

70

We investigate the summer moisture transport of three $\Delta\varphi$ experiments: 25, 35, and 65 (Figure 3.14). For each experiment we calculate the mean moisture flux convergence (MFC) for the 31-day period centered on the day of maximal ITCZ extent as defined for the SF-ITCZ criterion. We additionally overlay the associated moisture flux vectors. Figure 3.14(a) shows the mean MFC for the $\Delta\varphi = 25$ case. We find clear cross-equatorial moisture transport occurring at low levels, but little positive MFC at the equatorial surface. Positive MFC is instead found south of the equator, inland from the southern shoreline of the land strip. This region of convergence peaks approximately halfway between the shoreline and the equator, suggesting the moisture being advected further north into the equator is being balanced out by advection away from it, towards the ITCZ located around 20°N. The equatorial surface thus appears to be cut off from oceanic moisture even during the peak of the cross-equatorial HC. The situation for the $\Delta\varphi = 35$ case appears to be similar (Figure 3.14(b)). There is a region of weak to moderate positive MFC at the surface, inland of the southern shoreline, which reduces to near-zero at the equator. We find the ITCZ has moved north relative to the $\Delta\varphi = 25$ experiment (3.14(a)), but appears to still be contained by the shoreline at around 25-30°N. The region of negative surface MFC associated with the ITCZ is wider than for $\Delta\varphi = 25$, and appears to just reach the equator.

We hypothesize that the equator can remain dry despite the cross-equatorial flow because the MFC at the equator is approximately equal to, or slightly weaker than, the flux divergence away from the equator. In addition, this process may be more effective at drying the equator for the same $\Delta\varphi$ than the containment of the aseasonal HC in Chapter 2. Since the aseasonal HC always has its ITCZ at the equator, the only direction moisture can be advected away from the equatorial surface is upward, where it is likely to form precipitation and return to the surface. As such the primary constraint on equatorial moisture is whether the winds flowing into the equator from the subtropics could acquire it (via evaporation) before moving over the dry continent, i.e. whether the HC circulation was contained by the land strip. But for the seasonal experiments, the cross-equatorial HC is able to advect moisture both into

and out of the equator at similar magnitudes, meaning the only source of local humidity would be evaporation. Since even the case with the smallest $\Delta\varphi$ has a dry equator, this would allow any land strip to become drier than the equivalent aseasonal case as long as the cross-equatorial regime dominated the annual-mean. We find this to be true in our experiments, as the specific and relative humidities at the equatorial surface are lower in the seasonal cases (Figure 3.4) than in the aseasonal ones (Figures 2.7 and 2.8).

In addition to understanding the dryness at the equator, we also want to look at how the circulation affects moisture in the high $\Delta\varphi$ experiments whose ITCZs extended well into the midlatitudes. Figure 3.14(c) shows the MFC for the $\Delta\varphi = 65$ case, which had the most northern ITCZ extent as calculated for the SF-ITCZ criterion. There is an overall drier circulation with a somewhat unusual shape. There is a region of positive upper-tropospheric MFC that matches the $\Delta\varphi = 25$ and 35 experiments, but the low-level moisture flux appears to have two parts. It converges at $\sim 45°$N, in line with the calculated value in Figure 3.5(a), and flows upwards and back towards the equator to reach the region of positive MFC. Despite the convergence in the flux vectors, the MFC is near-zero throughout the lower troposphere at this latitude. Near the shoreline at $65°$N there is a region of downwelling associated with significant negative MFC at the surface. This feature matches similar downward moisture flux at the shorelines in the $\Delta\varphi = 25$ and 35 cases, but differs in that it is not adjacent to the region of upward flux over the continent. This appears to be due to widening of the summer HC, which has moved its descending branch poleward with the shoreline while the shared rising branch has been restricted to the lower midlatitudes.

Figures 3.14(a-c) shows the near-surface Moist Static Energy (MSE_1) climatology of the $\Delta\varphi = 25$, 35, and 65 experiments, where MSE_1 is defined as,

$$\text{MSE}_1 = c_p T_1 + g z_1 + L_v q_1 \tag{3.1}$$

In all three cases the presence of the land strip is clear, with the dry surface having a more responsive seasonal cycle and greater MSE_1 extremes. In the summer and winter months this can result in strong gradients at the shorelines. In the case of summer, the peak MSE_1

is approximately at the shorelines, which would create an area of local surface convergence just equatorward of the shore even for the $\Delta\varphi = 65$ case. It is possible the strength of this convergence is enough to generate a HC much wider than would otherwise be expected for an experiment with $T_r = 1$.

3.3.2 Impact of T_r and ξ on Summer Moisture Transport
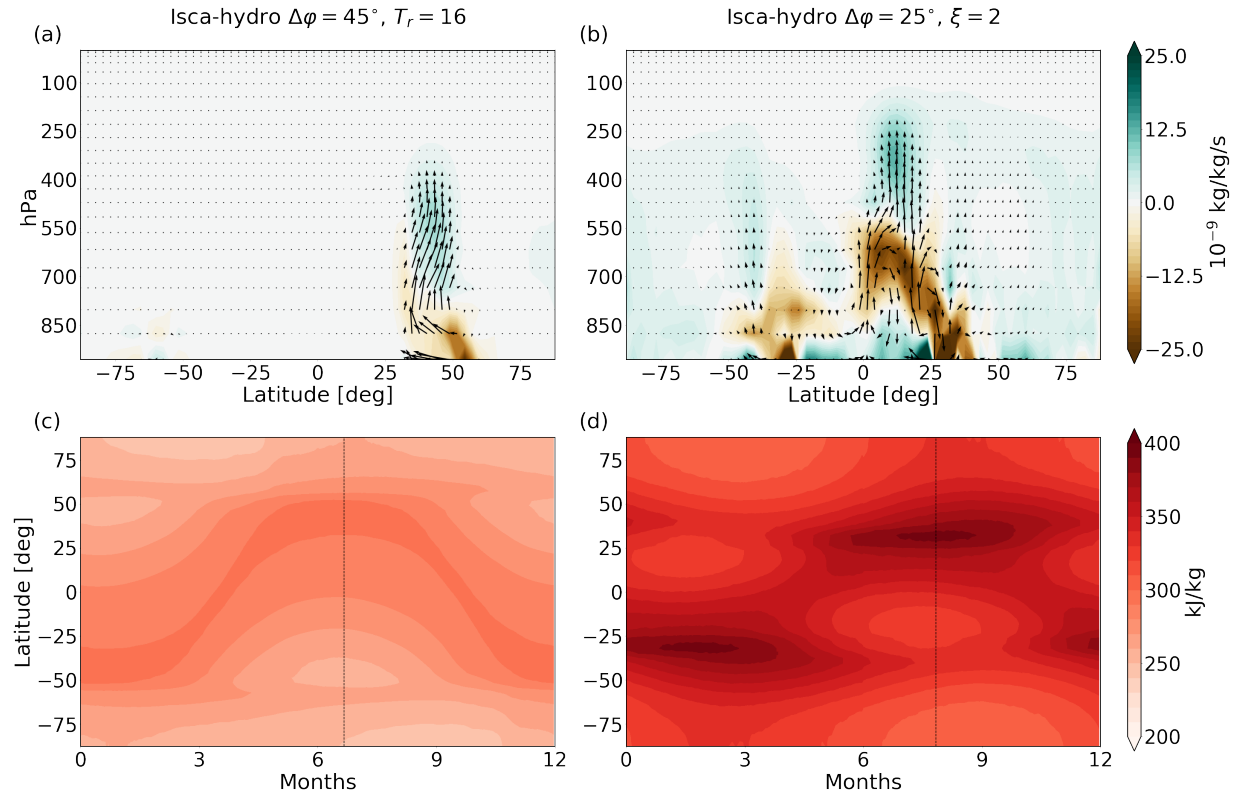
Figure 3.15: Peak summer MFC and moisture fluxes (top) and near-surface MSE climatology (bottom) for the $\Delta\varphi = 45$, $T_r = 16$ experiment (left) and the $\Delta\varphi = 25$, $\xi = 2$ experiment (right). The dashed black lines in (c, d) mark the day used to define the "peak summer" period in (a, b).

Given the large effect on the global circulation and moisture transport from $\Delta\varphi$ alone, it could be hard to gauge how the addition of larger T_r and ξ would further impact the results. As described in Section 3.2.3, multiple criteria were largely insensitive to T_r, including the

two ITCZ criteria. This result was unexpected, and to investigate it further we analyze the MFC and MSE_1 of the $\Delta\varphi = 45$, $T_r = 16$ experiment in Figure 3.15(a,c). This experiment has both the largest $\Delta\varphi$ and largest T_r of the T_r cases, both of which would be expected to push the ITCZ poleward. Yet the latitude of surface flow convergence is approximately 35°N, well within the land strip. The rising branch of air appears to be located over the region of peak summer MSE_1 even with the high T_r. There is no positive MFC at the surface, only a negative region that extends from just north of the shoreline to the inland point of upward flow. The overall picture is that any water vapor of oceanic origin that had made its way over the continent before the summer is removed by the surface flow convergence and gathers in the upper troposphere. The region of positive MFC in the upper levels matches the latitude of peak seasonal P for this experiment (Figure 3.9(a)), showing that even planets with large T_r can have summer P maximize at the midlatitudes.

Perhaps the most unusual results found in the seasonal experiments are the ξ experiments with $\Delta\varphi = 25$. As shown in Figure 3.11(a), while most cases do not have a strong trend in SF-ITCZ extent with higher ξ, those with $\Delta\varphi = 25$ have a marked *decrease* in extent with higher ξ once $\xi > 1.5$. The mechanism for this is not clear, but we analyze the most extreme case in Figure 3.15(b), that with $\xi = 2$. What we find is a fundamentally un-Earth-like circulation with multiple rising and falling branches squeezed within the land strip's summer half. At approximately 20°N latitude is what could be construed as the conventional ITCZ, an area of upward flux from the surface that converges moisture in the upper troposphere. But over the equator is yet another region of upward flux that partially flows into the same upper level region, with the region in between having downward flux towards the tropical surface where it also converges moisture. In summary, the circulation in the summer (northern) hemisphere is both moving moisture from the surface shoreline region to the upper troposphere, but also moving it inland laterally towards the deep tropics. In addition to this, the deep tropics receives downward moisture flux from above that appears to originate in the winter hemisphere. Rather than conventional cross-equatorial flux, the flux

74

from the winter hemisphere reaches a secondary point of convergence and rises at the equator. This is similar to features observed by Pauluis (2004) in experiments with thin boundary layers, but in their results the initial rising motion occurred in the winter hemisphere rather than at the equator. After rising at the equator in our simulation, the flux moves into a region of negative MFC, where it either continues to rise into the upper troposphere or returns to the surface in the summer tropics. This additional source of moisture may explain the slight rise in annual-mean RH with increasing ξ seen in Figure 3.10(c). The presence of positive MFC from downward moisture flux also matches results from the aseasonal high-ξ experiments in Chapter 2, although the physical mechanism behind it is still unclear.

The MSE_1 climatologies of the two cases analyzed in Figure 3.15 are shown in 3.15(c-d). As with Figures 3.14(d-f), the effect of the land strip is clear in each experiment. The experiment with $T_r = 16$ (3.15(c)) has relatively lower MSE_1 than similar experiments with smaller T_r, which may be why the SF-ITCZ extent reduces somewhat as T_r increases. The region of rising flux in Figure 3.15(a) approximately matches the location of peak summer MSE_1, as in the $\Delta\varphi$ cases from Figure 3.14. This correlation does not appear in the $\xi = 2$ experiment (3.15(b,d)), as its peak MSE_1 occurs slightly poleward of its shoreline and both regions of upward flux are over the continent. As might be expected of a high value of ξ, MSE_1 is high even in winter, with the land strip peaking at nearly 400 kJ/kg. This is well above a normal value for Earth, suggesting that only a relatively small change in ξ can have significant effects on an Earth-like planet.

3.3.3   General Comparison between Earth and Titan Endpoints

Within the suite of simulations presented in this chapter, we can identify two that represent "endpoints" of the Earth-Titan climate spectrum. On the Earth side there is the $r_E = 0\%$ aquaplanet simulation (subsequently Aqua-Earth), which is the closest approximation to an Earth-like global climate. On the Titan side there is the $\Delta\varphi = 65$ experiment (subsequently $\Delta\varphi65$-Earth), which met the most of our Titan-like criteria (as did the $\Delta\varphi = 55$ and 75
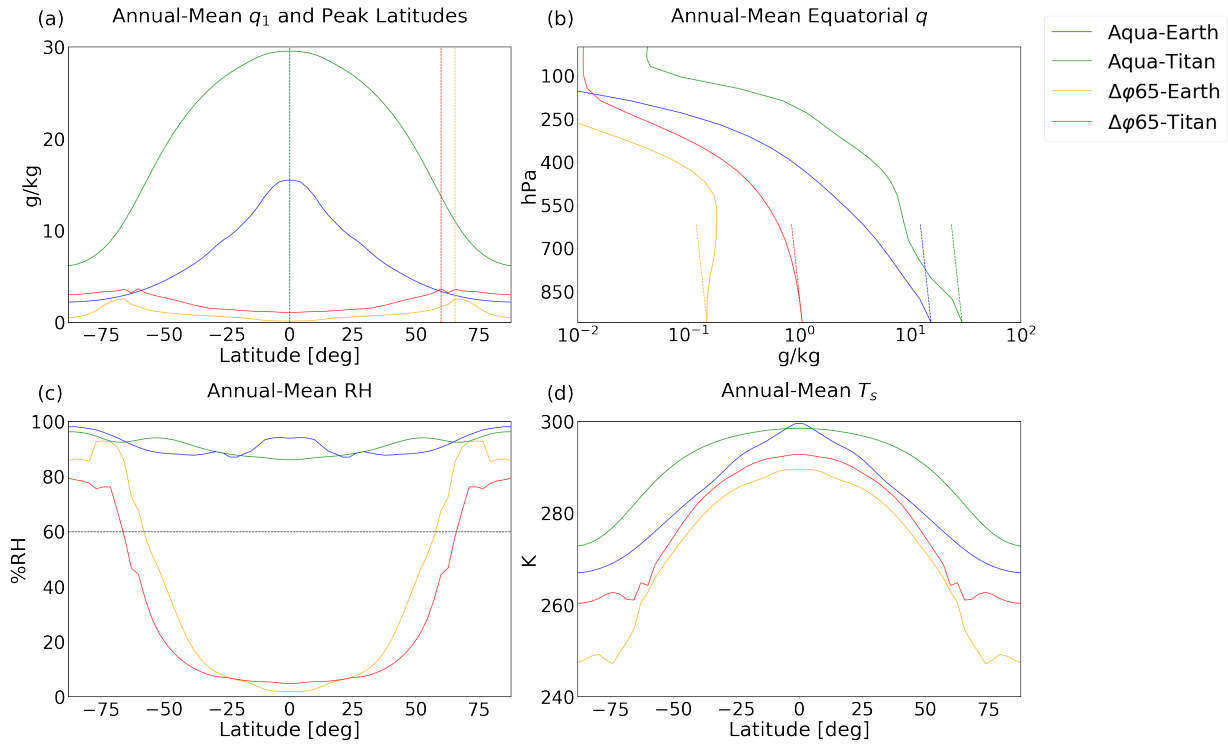
Figure 3.16: Comparison of Earth- and Titan-like endpoint simulations. (a) shows the zonal- and annual-mean q_1, with vertical dashed lines showing the latitude of the peak values. (b) shows the annual-mean vertical profile of q at the equator, with dashed lines representing the 20% decrease threshold of the ConVQ criterion. Only the $\Delta\varphi 65$-Earth case decreases more slowly than its associated dashed line, meaning it meets the ConVQ criterion. (c) shows the zonal- and annual-mean near-surface RH, with the horizontal dashed line marking the 60% RH threshold to meet the LowRH criterion. (d) shows the zonal- and annual-mean T_s. While the two $\Delta\varphi 65$ cases have similar temperatures over the land strip, the polar temperatures differ substantially.

cases). These two experiments both have $T_r = 1$ and $\xi = 1$, meaning their only difference is the presence of the land strip. As such we have run two additional simulations. The first is an aquaplanet equivalent to the $r_E = 0\%$ case but with $T_r = 16$ and $\xi = 2$ (subsequently Aqua-Titan). The second is an experiment with $\Delta\varphi = 65$, $T_r = 16$, and $\xi = 2.5$ (subsequently $\Delta\varphi65$-Titan). These two experiments will represent the combined affects of high T_r and ξ on the global climate, as would be expected under true Titan-like conditions.

Figure 3.16 shows the comparisons of the OffEq (3.16(a)), ConVQ (3.16(b)), LowRH (3.16(c)), and TGrad (3.16(d)) criteria for the endpoint simulations. The $\Delta\varphi65$-Earth case is notable for being drier than the equivalent Titan case, and being the only one of the four cases to meet the ConVQ criterion. It also has lower RH at the equator than $\Delta\varphi65$-Titan, despite higher RH everywhere outside the deep tropics and much lower ξ. Tropical T_s is similar between all four experiments, but the $\Delta\varphi65$-Earth simulation has much cooler poles than even $\Delta\varphi65$-Titan. This may be from its low polar specific humidity (3.16(a)) leading to a weaker water vapor feedback and greater cooling during polar night.

Figure 3.17 compares the zonal-mean 850mb stream function climatology for each endpoint case. There is a clear increase in the summer extent of the HC circulation (horizontal dashed lines) with higher T_r for both the aquaplanet and $\Delta\varphi65$ cases, suggesting Titan's rotation is important to its climate despite our T_r experiments meeting few Titan-like criteria. Of note is that no experiment in Figure 3.17 has a truly global extent, with the most poleward being $\sim 45°$ latitude. This presents an interesting contrast to the precipitation climatologies in Figure 3.18. The peak summer precipitation corresponds fairly closely with the HC extent in most cases, but not for the $\Delta\varphi65$-Earth case. $\Delta\varphi65$-Earth has its summer precipitation concentrated near its poles (3.18(c)) while its HC extent only reaches $\sim 30°$. This means its precipitation distribution is a close match to observed clouds on Titan and simulated precipitation with TAM (Figure 1.2). The increase in tropical precipitation between $\Delta\varphi65$-Earth and $\Delta\varphi65$-Titan is surprising given that more Titan-like planetary parameters have moved the climate away from Titan-like conditions. This may suggest our methods of determining
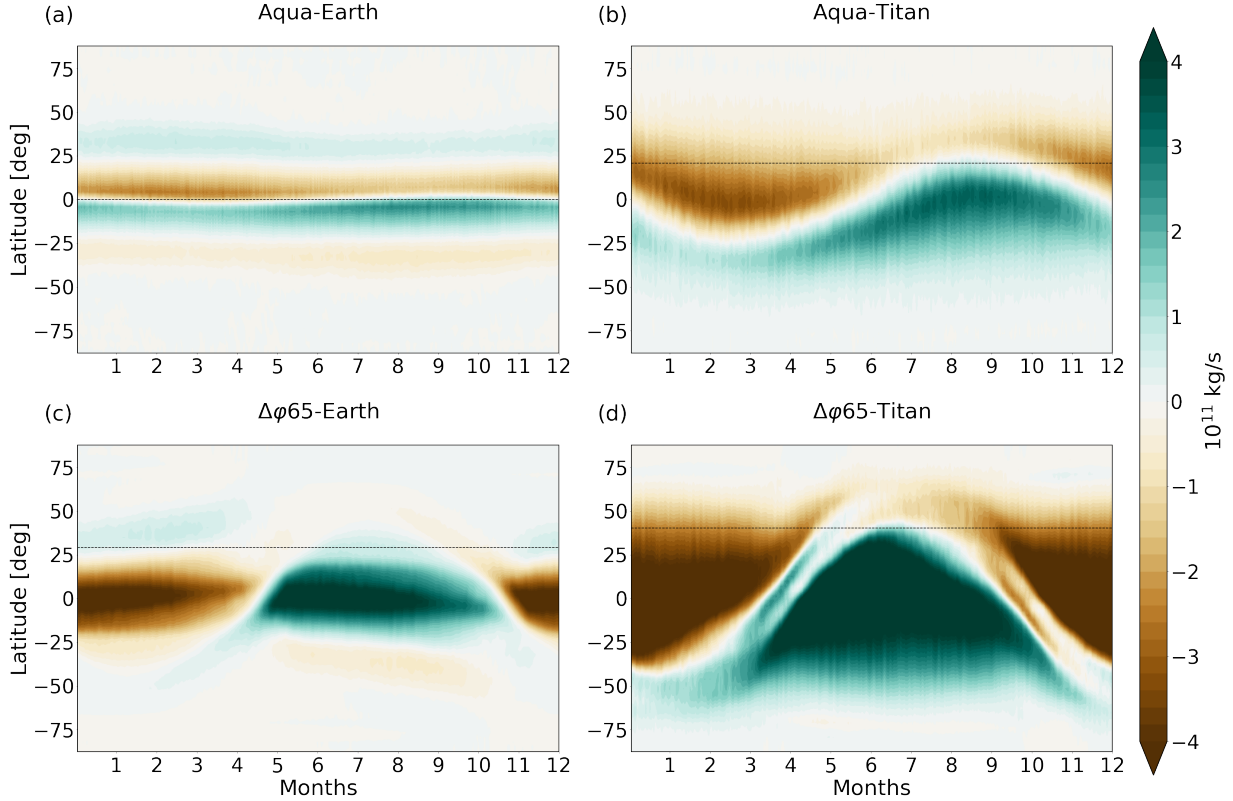
Figure 3.17: Zonal-mean 850hPa level stream function comparison of Earth- and Titan-like endpoint simulations over an average year. "Earth" experiments have $T_r = 1$ and $\xi = 1$, while the "Titan" experiments have $T_r = 16$ and $\xi = 2$ (Aqua-Titan) or $\xi = 2.5$ ($\Delta\varphi 65$-Titan).

Titan-like conditions need refinement, and in Chapter 4 we apply them to TAM simulations to determine if they are robust at identifying Titan-like climates.

3.4   Summary & Conclusions

We have paralleled the suite of idealized GCM experiments from Chapter 2 while adding a seasonal cycle to more robustly understand the transition to a Titan-like climate at the surface of an Earth-like planet. We added three new criteria to determine if the climate was Titan-like: (1) The annual-mean equator-to-pole gradient in T_s is small, $\leq 5\%$ (TGrad); (2)
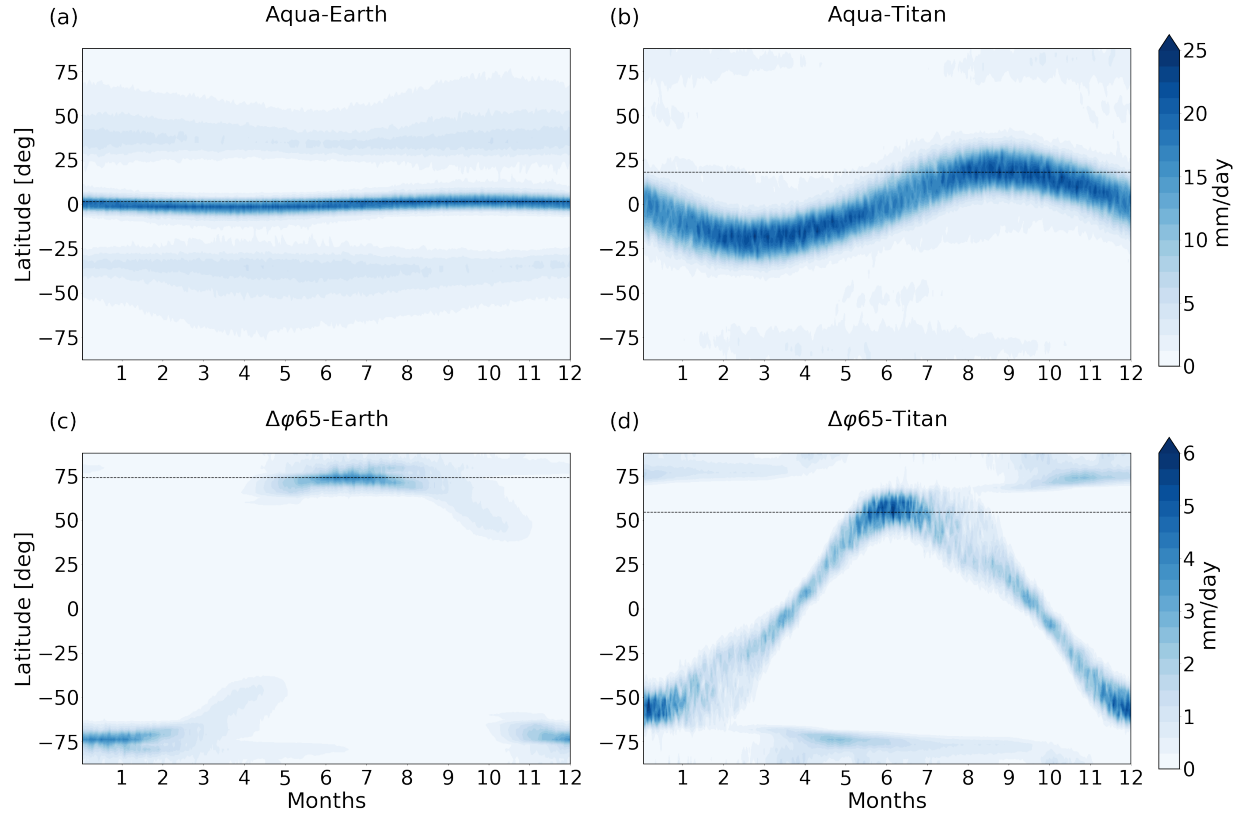
Figure 3.18: Zonal-mean precipitation comparison of Earth- and Titan-like endpoint simulations over an average year.

The ITCZ, as calculated at the 850hPa level stream function, extends beyond 60° latitude in summer (SF-ITCZ); (3) The peak seasonal precipitation is located at 60° latitude or poleward (P-ITCZ). We found that varying the land strip ($\Delta\varphi$) had the most impact on whether experiments met both the three criteria from Chapter 2 and the three new ones. The only experiments to meet any of the new criteria were those with $\Delta\varphi \geq 55$, which met the P-ITCZ criterion. Similar to our results in Chapter 2, experiments with low T_r met more Titan-like criteria, which contradicts Titan's high T_r relative to Earth. We found that varying T_r had little impact on meeting the three new criteria, including the two related to ITCZ extent. The ITCZ appears to be primarily constrained by $\Delta\varphi$, meaning large T_r would need to be combined with large $\Delta\varphi$ to achieve a global HC. We found that varying ξ also

did not have much effect on which experiments met most criteria. There is a transition to a different HC structure in the cases with $\xi \geq 1.75$ (Figure 3.15), but this transition does not push the experiment towards Titan-like conditions in any of our criteria and so is beyond the scope of this work.

We come away from this work with several follow-up questions, including:

1. Is the apparent constraint of the ITCZ by $\Delta\varphi$ affecting Titan? Can we reproduce the effect in a Titan-based GCM?

2. If large $\Delta\varphi$ is the primary constraint on summer precipitation moving between the two poles, does that mean a past Earth or Mars could have experienced a similar climate with the appropriate topographic arrangement?

3. The observed gradients in MSE_1 at the shorelines may create something like a reverse monsoon, where the large-scale sea breeze it generates opposes the cross-equatorial HC circulation. Is it possible that such a phenomenon was present in Earth's past climates, where different continental arrangements could allow for the same processes as observed in our simulations?

As we found in our experiments, it is not difficult to produce distinctly Titan-like features on an otherwise Earth-like planet with minimal changes to its fundamental parameters. This suggests that Earth could have a large range of global climate states throughout its history just through its changing topography. Similarly, Titan may have experienced several climate states in its history, some potentially Earth-like. There is much left to explored in the parameter space of possible climates on a terrestrial planet.

CHAPTER 4

Analysis of Titan GCM Simulations

In Chapters 2 and 3 we applied multiple criteria to determine whether a particular simulation's climate was Titan-like. These criteria were based on both observations of Titan and previous simulations with Titan GCMs. In order to support our results and conclusions from the previous chapters, we will use output from one such GCM and analyze the robustness of our Titan-like criteria when applied to a truly Titan-like climate.

4.1   Methods

We use data from three experiments using the Titan Atmosphere Model (TAM; Lora et al., 2015). The first experiment is an aquaplanet, with the entire surface covered in a shallow methane sea (referred to herein as the aquaplanet experiment; Lora et al., 2015). The second experiment initializes surface liquid only at latitudes greater than 60°, mimicking Titan's surface liquid distribution (referred to herein as the wetlands experiment; Lora et al., 2019). The third experiment utilizes the full hydrology scheme described in Faulk et al. (2020), allowing surface liquid to self-consistently move around the surface based on the topography and to infiltrate into a flowing subsurface reservoir (referred to herein as the hydro experiment). The aquaplanet case was run for 10 Titan years, the wetlands case for 20, and the hydro case for 250, with the last year used for analysis. We apply the same criteria as used in Chapters 2 and 3, with the exception of the LowRH criterion (as we do not have access to RH outputs for these experiments), to assess their robustness at determining Titan-like conditions in a 3D GCM. The five criteria we assess are:

1. OffEq, if the annual-mean peak in q_1 is not at the equator,

2. ConVQ, if the annual-mean equatorial q at the 600hPa level is at least 80% of the near-surface value,

3. TGrad, if the annual-mean T_s at the poles is at least 80% of the equatorial value,

4. SF-ITCZ, if the peak poleward extent of the HC circulation is at least 60° in latitude, as calculated for the 850hPa level,

5. and P-ITCZ, if the region of largest precipitation during an average year is at or poleward of 60° latitude.

4.2   Results
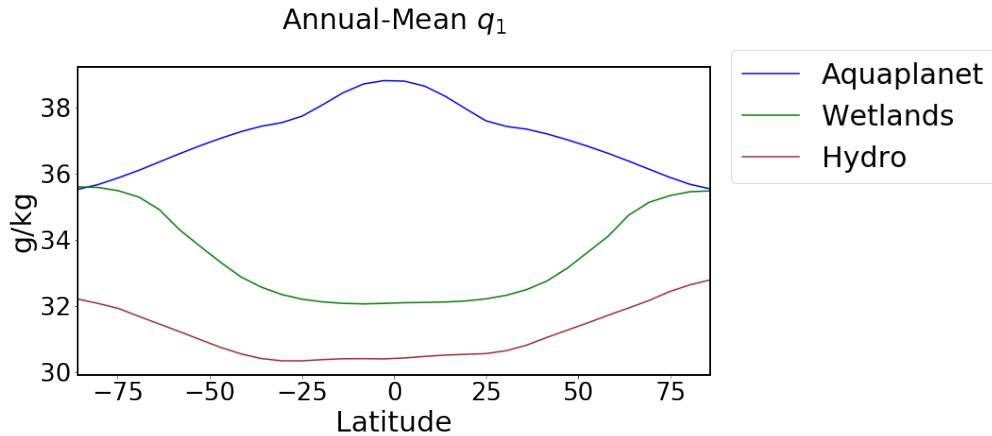
Figure 4.1: Zonal- and annual-mean q_1 for each TAM experiment.

Figure 4.1 shows the zonal- and annual-mean q_1 for each TAM experiment. The aquaplanet experiment peaks at the equator, while the other two peak at the poles. This matches well with the OffEq criterion, as the more Titan-like experiments with a dry tropics meet the criterion while the more Earth-like aquaplanet case does not. The wetlands and hydro cases are much drier than the aquaplanet case, driven largely by the dry tropics and subtropics.

The hydro case is additionally drier than the wetlands case, as it was initialized with less condensable methane to better match Titan's approximate surface reservoir (Faulk et al., 2020).
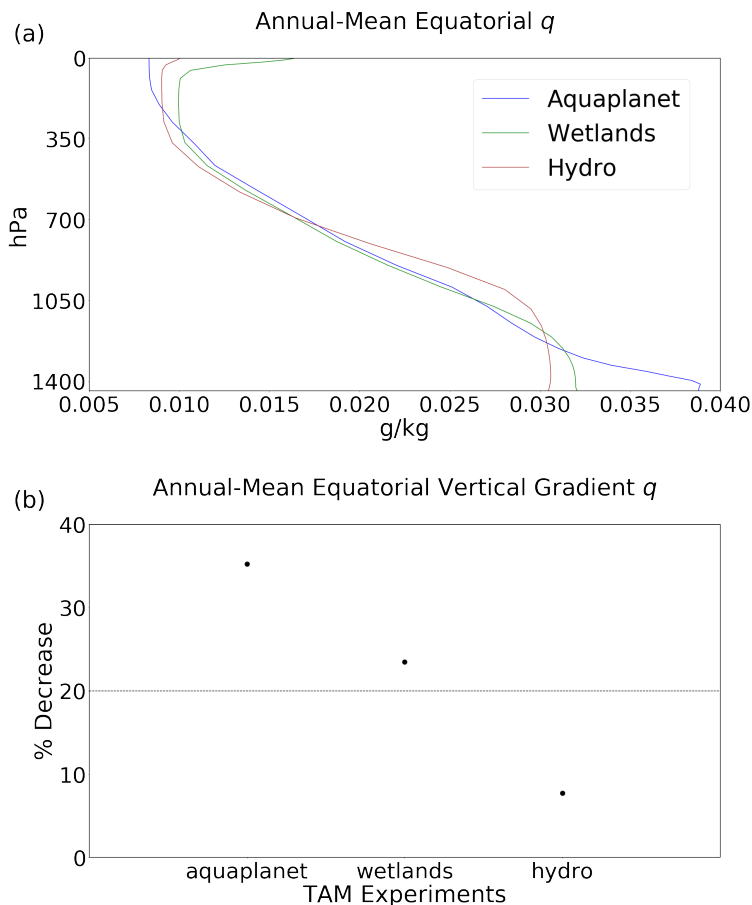
Figure 4.2: Annual-mean vertical profile of equatorial q for each TAM experiment (a) and the corresponding ConVQ criterion analysis (b).

We plot the vertical profile of annual-mean q at the equator in Figure 4.2(a). We find the vertical gradient of q in the lower troposphere decreases significantly as the simulations become drier at the surface, with both the wetlands and hydro cases having a region of near-constant q going up from the surface through the lower troposphere. Only the hydro case is able to meet the 20% threshold of the ConVQ criterion 4.2(b), but the wetlands case is very close ($< 25\%$). This suggests the ConVQ criterion is a robust determiner of a Titan-like

equatorial climate.
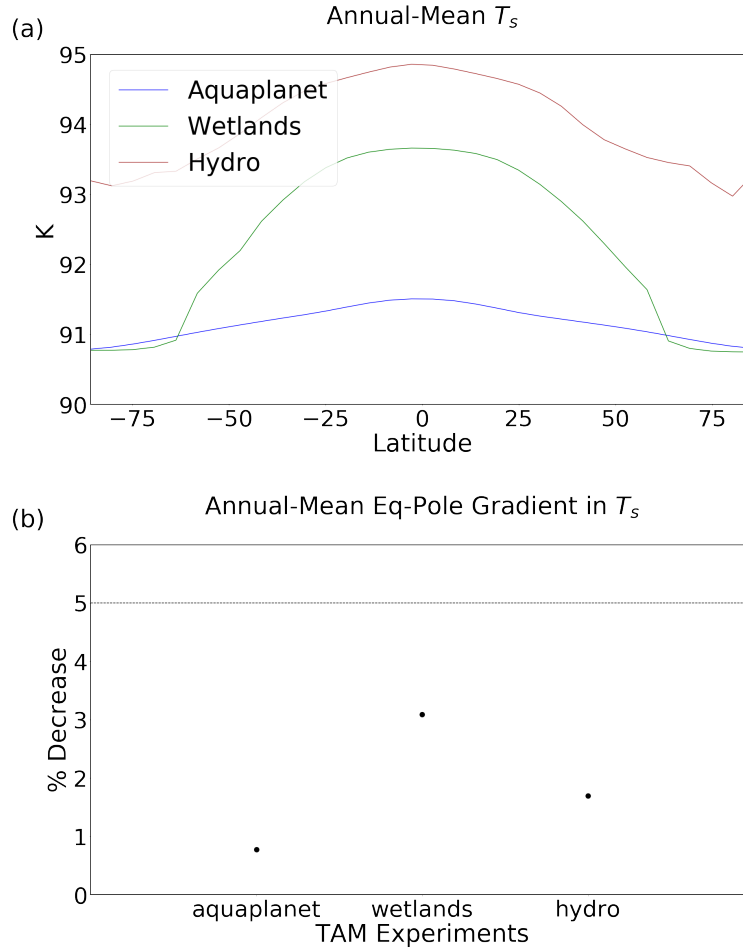
Figure 4.3: Zonal- and annual-mean surface temperature (T_s) for each TAM experiment (a) and the TGrad criterion analysis for each TAM experiment (b).

The TGrad criterion is assessed in Figure 4.3. The top plot shows the zonal- and annual-mean T_s for each case. The drier cases are preferentially warmer, with the wetlands case having the largest change between the equator and poles (4.3(b)). In general, areas with more surface liquid are cooler in all experiments, which allows the wetlands case to have the largest gradient due to its combination of a dry tropics and deep polar seas. Despite this, all experiments meet the TGrad criterion, and in fact the experiment with the smallest temperature gradient is the aquaplanet case. This means that the presence of dry land at

the equator and surface liquid at high latitudes makes an experiment less likely to meet this criterion, suggesting it may not be an effective measure of a Titan-like climate. The hydro case avoids this somewhat by having a relatively shallow surface liquid reservoir even at the poles, which may point to the primary factor in meeting the TGrad criterion being the difference in surface properties between the equator and poles.
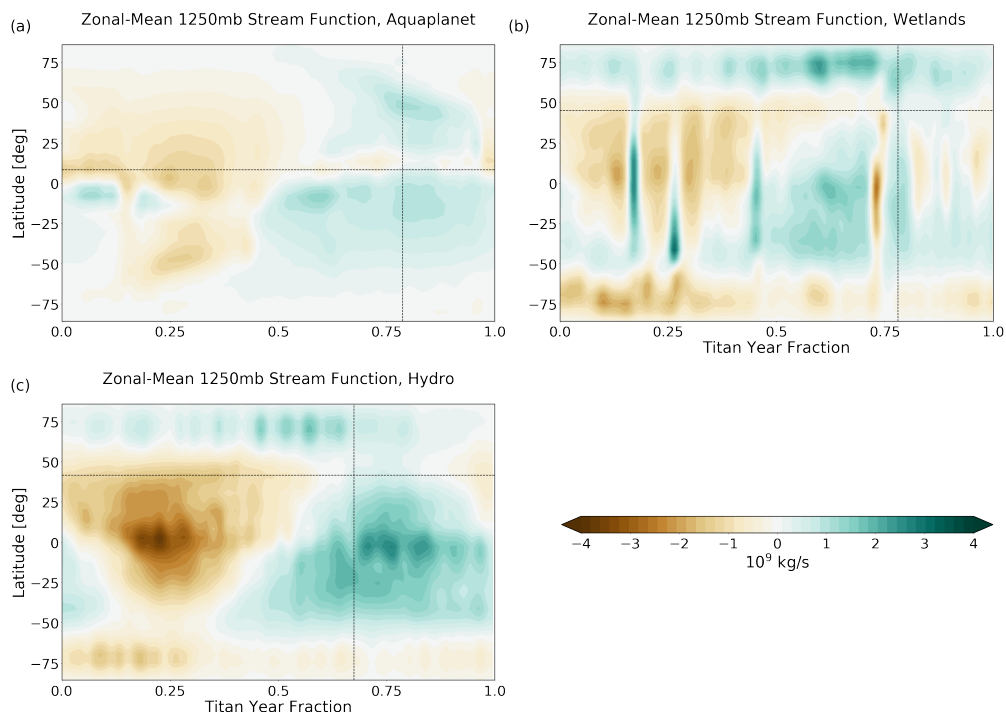
Figure 4.4: Zonal-mean 1250hPa level stream function climatology for each TAM experiment over a Titan year.

In Chapter 3, we found that the width of an equatorial land strip $(\Delta\varphi)$ had the largest effect on the location of peak ITCZ extent, both when measured using the low-level stream function and using precipitation. Figure 4.4 shows the zonal-mean climatology of stream function taken at the 1250hPa level for each TAM experiment. The horizontal dashed line shows the approximate northernmost extent of the cross-equatorial HC, while the vertical dashed line represents the approximate time this extent was reached. No experiments meet the SF-ITCZ criterion, but both the wetlands and hydro cases are close. These two cases

seem to hit a similar limit to the $\Delta\varphi$ cases in Chapter 3, where despite large rotation periods (T_r), the ITCZ can only extend to the edge of the dry surface region. In these two TAM cases that corresponds to roughly 60°N, a bit north of the extent estimates. This suggests Titan itself may not meet the SF-ITCZ criterion if the boundary between its dry and wet regions is at a low enough latitude.
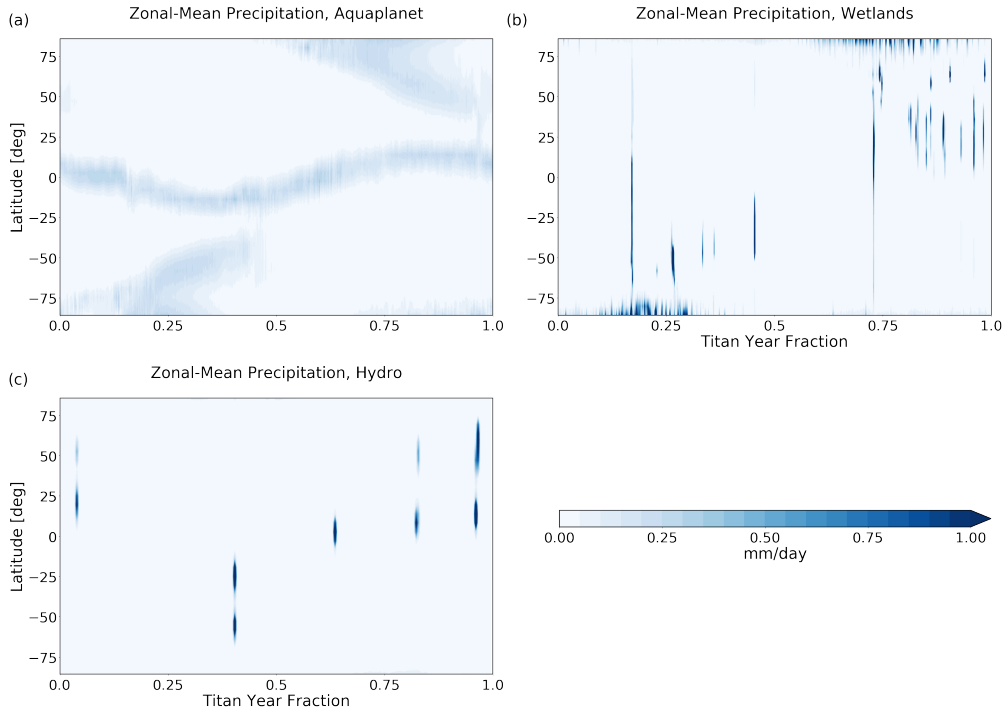
Figure 4.5: Zonal-mean precipitation climatology for each TAM experiment over a Titan year.

The precipitation in the TAM experiments (Figure 4.5) shows some similar characteristics to the stream function, but the aquaplanet case is fairly distinct. It has what appears to be a tropical ITCZ oscillating between 25°N and S, as well as a region of midlatitude/polar precipitation in the summer hemisphere that extends towards the tropical ITCZ as it reaches its peak extent. All experiments meet the P-ITCZ criterion based on the calculation used in Chapter 3, but the wetlands and hydro experiments have primarily isolated and intense rainfall events rather than a consistent region of rain. This may be skewing the calculation

somewhat in favor of placing the peak precipitation at the poles, whereas the ITCZ in both cases appears to only reach roughly 70°N. The wetlands case does have significant precipitation at its summer pole separate from the oscillating ITCZ, reminiscent of the $\Delta\varphi$ experiments that had both an ITCZ over the dry continent and a region of summer precipitation located at the shoreline. In addition, observations of clouds on Titan show significant activity at the summer pole, which suggests the threshold used for the P-ITCZ criterion is robust at identifying Titan-like precipitation.

	Criteria				
	OffEq	ConVQ	TGrad	P-ITCZ	SF-ITCZ
Aquaplanet			X		
Wetlands	X		X	X	
Hydro	X	X	X	X	

Table 4.1: Criteria matched by each TAM experiment.

4.3   Discussion & Conclusions

After assessing the five Titan-like criteria using the TAM experiments, we found that most are effective determiners of a Titan-like climate. Some criteria, namely ConVQ and SF-ITCZ, may benefit from slight adjustments to their thresholds. There is one criterion that may be a poor determiner of a Titan-like state: the TGrad criterion. While this criterion was met by all three TAM experiments, those with a dry tropics had a larger gradient than the aquaplanet case, and more specifically the experiment with the strongest differences in surface properties (the wetlands case) was the closest to not meeting the criterion. It is perhaps no surprise then that our land strip ($\Delta\varphi$) experiments in Chapter 3 failed to meet the TGrad criterion, given the strong contrast between the dry equator and deep high-latitude oceans. At the same time, the presence of a dry tropics and wet poles is a key characteristic

of Titan and one way it is distinguished from Earth. We can hypothesize then that the ability of Titan to meet the TGrad criterion is due to another mechanism that counters the effect of the dry tropics by regulating local heating, meridional heat transport, or both. There did not appear to be such a mechanism operating in the simulations with varying T_r from Chapter 3, where the equator-to-pole T_s gradient was largely insensitive to increasing T_r. One possible explanation is Titan's atmosphere, which is highly optically thick in the visible and infrared spectrums (McKay et al., 1991). The ability of the atmosphere to absorb a large portion of incoming radiation could reduce the localized heating that would occur over the dry tropics while also allowing for easier heat transport to polar latitudes. This would represent a characteristic of Titan not accounted for in our idealized Isca simulations, and one that would be difficult to apply to an otherwise Earth-like planet.
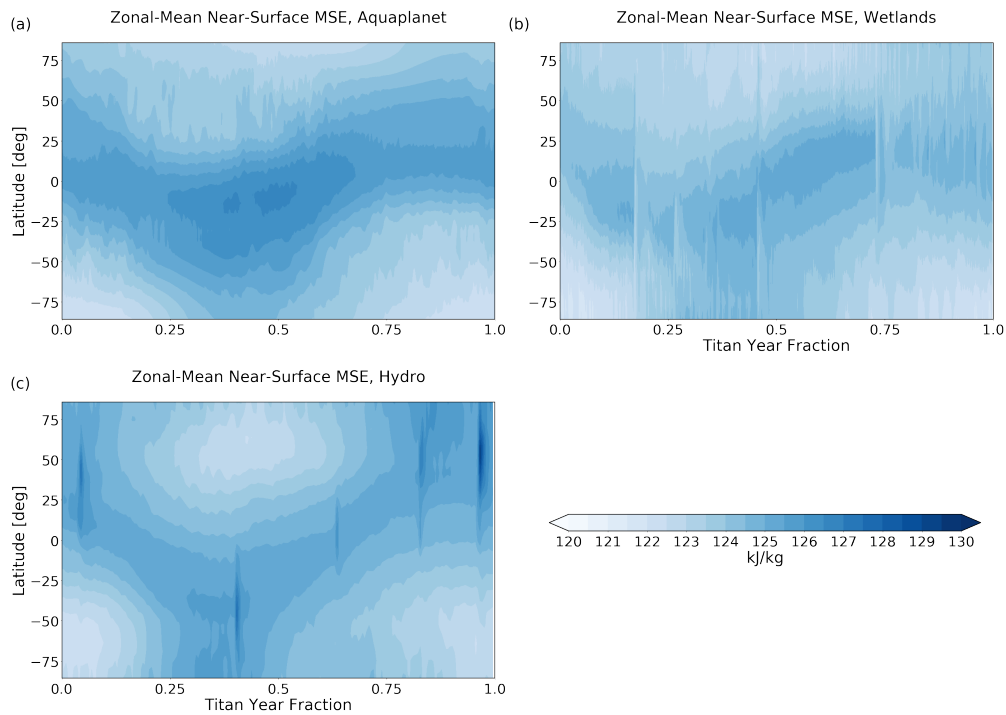

Figure 4.6: Zonal-mean MSE climatology for each TAM experiment over a Titan year.

While the wetlands and hydro experiments did both meet the P-ITCZ criterion, the extent of their summer precipitation still appeared to stop short of the pole. Combined

with both cases failing the SF-ITCZ criterion, it is possible a similar feature observed in the experiments from Chapter 3 is occurring here. In experiments with an equatorial land strip, the peak extent of both the precipitation and cross-equatorial HC were constrained by the location of the shoreline. Even in experiments with $T_r = 16$, peak ITCZ extents were limited to $45°$ as that was the largest $\Delta\varphi$ used for the T_r experiments. The wetlands and hydro TAM cases could be considered as having a "shoreline" in their high latitudes, roughly between 60-75°. Poleward of this latitude there is significant surface liquid, creating a contrast in surface heat capacity as in our idealized simulations. We hypothesize that one mechanism leading to the constrained ITCZ on Titan is this contrast in surface properties, which generates a peak surface temperature off of the pole and locks the summer solstice ITCZ there. Figure 4.6 shows the zonal-mean climatology of Moist Static Energy (MSE) at the lowest model level for each TAM experiment. In all three cases, the peak MSE in the Northern Hemisphere summer occurs south of the pole, even in the aquaplanet case. The hydro case is the closest to having the peak MSE reach the poles, and there are parts of the summer where the peak likely is at the pole. The strongest MSE during the season occurs around $60°N$, corresponding to a large rain event in Figure 4.5(c).

In Figures 3.16-3.18 we looked at four select seasonal simulations representing the Earth- and Titan-like endpoints of the parameter sweep. The most successful of these at meeting the Titan-like criteria was the $\Delta\varphi = 65$ experiment with $T_r = 1$ and $\xi = 1$ (where ξ is the condensable volatility and $\xi = 1$ is equivalent to water on Earth), suggesting that the presence of the land strip was the primary factor in creating Titan-like conditions. The TAM simulations also show a strong dependence on the presence of dry land in the tropics, with the wetlands and hydro cases meeting more criteria than the aquaplanet case. The key exception in both sets of simulations is the gradient in T_s, which is generally larger in cases with greater contrasts in surface properties. Figure 3.16(d) suggests that a larger rotation period and higher condensable volatility may be able to preferentially warm the high latitudes and lower the T_s gradient for the same land strip width, which could explain

Titan's ability to maintain a small gradient. Figure 3.17 shows the zonal-mean climatology of 850mb stream function for the four endpoint cases, which has similar features to Figure 4.4. Peak ITCZ extents are limited to $\sim 50°$ latitude in the most extreme seasonal simulation (3.17(d)) and the TAM wetlands and hydro simulations (4.4(b-c)). This corresponds roughly with the edge of the shorelines (the latitude where the surface becomes significantly wetter in the TAM cases), lending support to the hypothesis from Chapter 3 that the presence of a strong gradient in surface heat capacity, and thus temperature, can prevent the ITCZ from reaching the poles even with a large rotation period. One caveat to this is the TAM aquaplanet case, which also arguably has an ITCZ constrained to the low latitudes in both stream function (Figure 4.4(a)) and precipitation (Figure 4.5(a)). This may be due to high surface heat capacity damping the seasonal heating of the middle and high latitudes, and is similar to the peak extent seen in the most Titan-like aquaplanet seasonal simulation (Figure 3.17(b)).

In contrast to the stream function, the precipitation of the two endpoint simulations with land strips shown in Figure 3.18(c-d) does not match well with the TAM wetlands or hydro cases (Figure 4.5(b-c). These two TAM experiments have primarily intermittent, intense rain in the midlatitudes and tropics as their ITCZ moves between the two poles, whereas the seasonal simulation with $\Delta\varphi = 65$ (3.18(c)) has its precipitation concentrated near the summer shorelines and the equivalent case with $T_r = 16$ and $\xi = 2.5$ (3.18(d)) has a tropical ITCZ that maintains a nearly continuous presence throughout the year. There is some transience in this ITCZ, especially in later summer/early fall of each hemisphere, which could suggest that the $\Delta\varphi = 65$, $T_r = 16$, $\xi = 2.5$ case is in a transition region towards the TAM simulations. The most likely parameter driving this transition is ξ, as it is the only one not fully equaled to Titan's estimated value (~ 3, from Section 2.3.4). Future work on this topic will need to address the ability to stably simulate climates with higher ξ than we were able to achieve.

Our analysis has demonstrated the effectiveness of our Titan-like criteria, while also

identifying new questions regarding how to define a Titan-like climate:

1. How important are the radiative properties of Titan's atmosphere to its distinct climate state?

2. What degree of variation is needed in the surface properties between the tropics and high latitudes to constrain the extent of the summer ITCZ? Could this phenomenon be applied to other planetary archetypes with varied surface properties?

Addressing these questions is important to continue refining our understanding of terrestrial planetary climates. It is quite likely that Earth-like exoplanets could have more optically-thick atmospheres than Earth and any variety of continental arrangements. In a similar vein, Titan-like planets, and Titan itself in the past, may appear much more Earth-like than Titan does today. A less optically-thick atmosphere combined with a stronger contrast in surface properties between the tropics and high latitudes could produce an ITCZ fully contained in the tropics with abundant summer rainfall at the edge of the dry region. This all demonstrates that the specific condensable of a planet is unimportant to its climate archetype, and that there is much more to learn about the possible climates of terrestrial planets.

CHAPTER 5

Conclusion

5.1   Summary & Conclusions

The Solar System contains four terrestrial bodies with large, dense atmospheres, each representing a unique climate archetype:

1. Venus, closest to the Sun, is hot, dry, and slowly rotating. It represents the fate of being too close to the Sun, where the surface condensable eventually evaporates completely and the CO_2 in the atmosphere is no longer returned to the crust via weathering (Ingersoll, 1969).

2. Earth, slightly further out, is cooler and maintains large deposits of surface water while having fast rotation. It represents the middle ground, where temperatures were just right to maintain a liquid condensable.

3. Mars is slightly too far from the Sun, with its atmosphere and water mostly frozen at the winter poles or lost to space, creating a global desert. It represents the opposite extreme to Venus, where temperatures become too cold such that the condensable, and then eventually the atmosphere itself, fully condenses and even freezes onto the surface.

4. Titan, in the outer Solar System, maintains significant deposits of liquid methane but rotates slowly as it orbits Saturn. Titan must also represent a middle ground state

like Earth, just with a different condensable, allowing for a second data point of this planetary climate.

Despite the differences in constituents, these four archetypes can be described as parts of a single continuum of possible climate states (Figure 1.1). In this work, we explored the parameter space between Earth and Titan using the Isca GCM (Vallis et al., 2018). We varied three primary planetary parameters that represent the differences between Earth and Titan:

1. $\Delta\varphi$, the half-width of a dry continent centered on the equator.

2. T_r, the rotation period of the planet.

3. ξ, the volatility of the condensable, a multiplicative factor that increases saturation vapor pressure.

Changing these parameters allowed us to move from distinctly Earth-like planets to distinctly Titan-like planets without changing the fundamental constituents or other parameters in the model.

In Chapter 2 we perform a suite of GCM simulations using these parameters and without imposing a seasonal cycle. We defined three criteria based on observations for determining whether a climate was Titan-like: OffEq if the annual-mean peak of near-surface specific humidity (q_1) was not at the equator; ConVQ if the decrease in annual-mean equatorial specific humidity from the surface to the 600hPa level was $\leq$ 20%; and LowRH if the annual-mean near-surface RH at the equator was $\leq$ 60%. We found that increasing ξ was most effective at meeting all three criteria, while increasing T_r made experiments less likely to meet any criteria. We hypothesized that this effect of T_r was due to the expansion of the Hadley Cell (HC) circulation relative to the width of a fixed $\Delta\varphi$. When T_r increased such that the poleward edge of the HC reached the shorelines, the return flow to the equator

would be able to carry oceanic moisture with it. This resulted in wetter equatorial climates for larger T_r, despite Titan itself having large T_r.

In Chapter 3 we repeat the suite of GCM simulations from Chapter 2 but with the addition of a seasonal cycle to assess its affects on the results. We also added three new observationally-motivated criteria for determining a Titan-like climate: SmallGrad if the annual-mean gradient in equator-to-pole surface temperature was $\leq 5\%$; SF-ITCZ if the extent of the intertropical convergence zone (ITCZ), calculated as the zero point of the 850hPa level stream function, reached at least $60°$ in latitude; and P-ITCZ if the dominant region of precipitation over an average year was located at or poleward of $60°$ latitude. In contrast to the simulations in Chapter 2, we found the most important parameter for meeting the Titan-like criteria was $\Delta\varphi$. The presence of even small land strips, $\Delta\varphi \leq 25$, resulted in a very dry equator (Figure 3.4), and experiments with $\Delta\varphi \geq 55$ met the most criteria. This included the P-ITCZ criterion, meaning it was possible to have what appeared to be an ITCZ move between the two polar regions even with Earth's rotation (Figure 3.6(d)). Once again, high T_r was largely ineffective at creating a more Titan-like climate, while ξ also had minimal impact outside of the ConVQ criterion. The contrast in surface properties between the dry land and ocean at the shorelines appeared to both allow for significant high-latitude precipitation when $\Delta\varphi$ was large and to constrain the HC extent to within the shorelines regardless of T_r. We concluded that the presence of a large dry region centered on the equator was the primary driver of a Titan-like climate, with high T_r and ξ acting as more minor additional influences.

In Chapter 4 we applied the Titan-like criteria used in Chapter 3 to output from the Titan Atmosphere Model (TAM) to determine their robustness at identifying Titan-like climates. We use three TAM simulations: an aquaplanet simulation (aquaplanet); a simulation using prescribed wetlands poleward of $60°$ (wetlands); and a simulation with full surface hydrology (hydro). We find that most criteria correctly identify Titan-like characteristics in the TAM simulations, with some needing small adjustments. Notably, the criteria did not always

capture the qualitative features of the TAM simulations, especially the precipitation (Figure 4.5); the midlatitudes and tropics in the wetlands and hydro cases experience only transient, intense precipitation as the ITCZ moves over, in contrast to the $\Delta\varphi = 65$ case shown in Figure 3.18(c) that has minimal precipitation over its dry region. The TAM wetlands and hydro cases also do not match the additional $\Delta\varphi = 65$, $T_r = 16$, $\xi = 2.5$ case analyzed in Figure 3.18(d), which has a nearly-continuous ITCZ throughout the seasonal cycle. We hypothesized that the high ξ of Titan (estimated to be ~ 3) could move the precipitation towards the transient, singularly-intense storms seen in the TAM output.

5.2   Future Work

Our work has opened up multiple outstanding questions for future work:

1. How significant is the effect of the surface property difference between the dry land and ocean, and what degree of difference is enough to have an impact on large-scale dynamics for an Earth-like planet? While modern Earth does not have a circumglobal land strip, it is not unreasonable to expect it could have something similar in its past or future. It is also possible that a circumglobal land strip is not necessary to affect global circulation, meaning we could achieve similar results with more conventional, single continents.

2. What is the true effect of rotation on Titan's climate? In our experiments increasing T_r had little effect on whether a climate was Titan-like, or in some cases made it less Titan-like. This suggests Titan's current climate state might actually be moderated by its slow rotation, i.e. a faster-rotating Titan might have an even drier tropics. Exploring this question will require a Titan GCM, and can be paired with equivalent simulations in an Earth GCM to identify possible points of divergence in how the two planets may respond to changes in T_r with the same surface properties.

3. How does very high ξ affect an Earth-like climate? Our simulations were limited in maximum ξ due to model stability under high water vapor feedback, and as such were not able to fully reach Titan's effective ξ value (~ 3, formally defined in Section 2.3.4). Expanding this work to other GCMs that can go to higher ξ will allow us to better understand Titan's climate state.

Bibliography

Adam, O., T. Bischoff, and T. Schneider, 2016: Seasonal and Interannual Variations of the Energy Flux Equator and ITCZ. Part I: Zonally Averaged ITCZ Position. *Journal of Climate*, **29 (9)**, 3219–3230, https://doi.org/10.1175/JCLI-D-15-0512.1, URL http://journals.ametsoc.org/doi/10.1175/JCLI-D-15-0512.1.

Ádámkovics, M., and Coauthors, 2016: Meridional Variation in Tropospheric Methane on Titan Observed with AO Spectroscopy at Keck and VLT. *Icarus*, **270**, 376–388.

Betts, A., and M. Miller, 1986: A New Convective Adjustment Scheme. Part II: Single Column Tests Using GATE Wave, BOMEX, ATEX and Arctic Air-Mass Data Sets. *Quarterly Journal of the Royal Meteorological Society*, **112 (473)**, 693–709.

Betts, A. K., 1986: A New Convective Adjustment Scheme. Part I: Observational and Theoretical Basis. *Quarterly Journal of the Royal Meteorological Society*, **112 (473)**, 677–691.

Bordoni, S., and T. Schneider, 2008: Monsoons as eddy-mediated regime transitions of the tropical overturning circulation. *Nature Geoscience*, **1 (8)**, 515–519, https://doi.org/10.1038/ngeo248, URL http://www.nature.com/articles/ngeo248.

Caballero, R., R. T. Pierrehumbert, and J. L. Mitchell, 2008: Axisymmetric, nearly inviscid circulations in non-condensing radiative-convective atmospheres. *Quarterly Journal of the Royal Meteorological Society*, **134 (634)**, 1269–1285, https://doi.org/10.1002/qj.271, URL https://onlinelibrary.wiley.com/doi/10.1002/qj.271.

Edwards, J., and A. Slingo, 1996: Studies with a Flexible New Radiation Code. I: Choosing a Configuration for a Large-Scale Model. *Quarterly Journal of the Royal Meteorological Society*, **122 (531)**, 689–719.

Emanuel, K. A., 1995: On Thermally Direct Circulations in Moist Atmospheres. *Journal of the Atmospheric Sciences*, **52 (9)**, 1529–1534, https://doi.org/10.1175/

1520-0469(1995)052⟨1529:OTDCIM⟩2.0.CO;2, URL http://journals.ametsoc.org/doi/10.1175/1520-0469(1995)052%3C1529:OTDCIM%3E2.0.CO;2.

Emanuel, K. A., J. David Neelin, and C. S. Bretherton, 1994: On large-scale circulations in convecting atmospheres. *Quarterly Journal of the Royal Meteorological Society*, **120 (519)**, 1111–1143, https://doi.org/10.1002/qj.49712051902, URL http://doi.wiley.com/10.1256/qj.03.130https://onlinelibrary.wiley.com/doi/10.1002/qj.49712051902.

Fan, B., Z. Tan, T. A. Shaw, and E. S. Kite, 2021: Reducing Surface Wetness Leads to Tropical Hydrological Cycle Regime Transition. *Geophysical Research Letters*, **48 (8)**, e2020GL090 746.

Faulk, S., J. Mitchell, and S. Bordoni, 2017: Effects of Rotation Rate and Seasonal Forcing on the ITCZ Extent in Planetary Atmospheres. *Journal of the Atmospheric Sciences*, **74 (3)**, 665–678, https://doi.org/10.1175/JAS-D-16-0014.1, URL http://journals.ametsoc.org/doi/10.1175/JAS-D-16-0014.1https://journals.ametsoc.org/doi/10.1175/JAS-D-16-0014.1.

Faulk, S. P., J. M. Lora, J. L. Mitchell, and P. Milly, 2020: Titan's Climate Patterns and Surface Methane Distribution Due to the Coupling of Land Hydrology and Atmosphere. *Nature Astronomy*, **4 (4)**, 390–398.

Frierson, D. M., I. M. Held, and P. Zurita-Gotor, 2006: A gray-radiation aquaplanet moist GCM. Part I: Static stability and eddy scale. *Journal of the Atmospheric Sciences*, **63 (10)**, 2548–2566, https://doi.org/10.1175/JAS3753.1.

Griffith, C., J. L. Mitchell, P. Lavvas, and G. Tobie, 2013: Titan's Evolving Climate. *Comparative Climatology of Terrestrial Planets*, 1–27.

Guendelman, I., and Y. Kaspi, 2018: An Axisymmetric Limit for the Width of the Hadley Cell on Planets With Large Obliquity and Long Seasonality. *Geophysical Re-*

search Letters, **45 (24)**, 13,213–13,221, https://doi.org/10.1029/2018GL080752, URL https://onlinelibrary.wiley.com/doi/10.1029/2018GL080752, 1903.11656.

Held, I. M., and A. Y. Hou, 1980: Nonlinear Axially Symmetric Circulations in a Nearly Inviscid Atmosphere. *Journal of the Atmospheric Sciences*, **37 (3)**, 515–533, https://doi.org/10.1175/1520-0469(1980)037⟨0515:NASCIA⟩2.0.CO;2, URL http://journals.ametsoc.org/doi/10.1175/1520-0469(1980)037%3C0515:NASCIA%3E2.0.CO;2.

Held, I. M., and M. J. Suarez, 1994: A Proposal for the Intercomparison of the Dynamical Cores of Atmospheric General Circulation Models. *Bulletin of the American Meteorological Society*, **75 (10)**, 1825–1830, https://doi.org/10.1175/1520-0477(1994)075⟨1825:APFTIO⟩2.0.CO;2, URL http://journals.ametsoc.org/doi/10.1175/1520-0477(1994)075%3C1825:APFTIO%3E2.0.CO;2.

Hide, R., 1969: Dynamics of the Atmospheres of the Major Planets with an Appendix on the Viscous Boundary Layer at the Rigid Bounding Surface of an Electrically-Conducting Rotating Fluid in the Presence of a Magnetic Field. *Journal of the Atmospheric Sciences*, **26 (5)**, 841–853, https://doi.org/10.1175/1520-0469(1969)026⟨0841:DOTAOT⟩2.0.CO;2, URL http://journals.ametsoc.org/doi/10.1175/1520-0469(1969)026%3C0841:DOTAOT%3E2.0.CO;2.

Hill, S., S. Bordoni, and J. Mitchell, 2022: A theory for the Hadley cell descending and ascending edges throughout the annual cycle.

Hill, S. A., S. Bordoni, and J. L. Mitchell, 2019: Axisymmetric Constraints on Cross-Equatorial Hadley Cell Extent. *Journal of the Atmospheric Sciences*, **76 (6)**, 1547–1564, https://doi.org/10.1175/JAS-D-18-0306.1, URL https://journals.ametsoc.org/view/journals/atsc/76/6/jas-d-18-0306.1.xml, 1810.11105.

Hill, S. A., S. Bordoni, and J. L. Mitchell, 2020: Axisymmetric Hadley Cell Theory with a Fixed Tropopause Temperature Rather than Height. *Journal of the Atmo-*

spheric Sciences, **77 (4)**, 1279–1294, https://doi.org/10.1175/JAS-D-19-0169.1, URL http://journals.ametsoc.org/doi/10.1175/JAS-D-19-0169.1.

Hill, S. A., S. Bordoni, and J. L. Mitchell, 2021: Solsticial Hadley Cell ascending edge theory from supercriticality. *Journal of the Atmospheric Sciences*, **76 (6)**, 1999–2011, https://doi.org/10.1175/JAS-D-20-0341.1, URL https://journals.ametsoc.org/view/journals/atsc/aop/JAS-D-20-0341.1/JAS-D-20-0341.1.xml.

Ingersoll, A. P., 1969: The Runaway Greenhouse: A History of Water on Venus. *Journal of the Atmospheric Sciences*, **26 (6)**, 1191–1198, https://doi.org/10.1175/1520-0469(1969)026⟨1191:TRGAHO⟩2.0.CO;2, URL http://journals.ametsoc.org/doi/abs/10.1175/1520-0469%281969%29026%3C1191%3ATRGAHO%3E2.0.CO%3B2.

Jennings, D. E., and Coauthors, 2009: TITAN'S SURFACE BRIGHTNESS TEMPERATURES. *The Astrophysical Journal*, **691 (2)**, L103–L105, https://doi.org/10.1088/0004-637X/691/2/L103, URL https://iopscience.iop.org/article/10.1088/0004-637X/691/2/L103.

Jucker, M., and E. Gerber, 2017: Untangling the Annual Cycle of the Tropical Tropopause Layer with an Idealized Moist Model. *Journal of Climate*, **30 (18)**, 7339–7358.

Kang, S. M., and J. Lu, 2012: Expansion of the Hadley Cell under Global Warming: Winter versus Summer. *Journal of Climate*, **25 (24)**, 8387–8393, https://doi.org/10.1175/JCLI-D-12-00323.1, URL http://journals.ametsoc.org/doi/10.1175/JCLI-D-12-00323.1.

Kaspi, Y., and A. P. Showman, 2015: ATMOSPHERIC DYNAMICS OF TERRESTRIAL EXOPLANETS OVER A WIDE RANGE. *The Astrophysical Journal*, **804 (1)**, 1–18, https://doi.org/10.1088/0004-637X/804/1/60, URL http://dx.doi.org/10.1088/0004-637X/804/1/60.

Lindzen, R. S., and A. V. Hou, 1988: Hadley Circulations for Zonally Averaged Heating Centered off the Equator. *Journal of the Atmospheric Sci-*

ences, **45 (17)**, 2416–2427, https://doi.org/10.1175/1520-0469(1988)045⟨2416:HCFZAH⟩ 2.0.CO;2, URL http://journals.ametsoc.org/doi/10.1175/1520-0469(1988)045%3C2416: HCFZAH%3E2.0.CO;2.

Lora, J. M., and M. Ádámkovics, 2017: The Near-Surface Methane Humidity on Titan. *Icarus*, **286**, 270–279.

Lora, J. M., J. I. Lunine, and J. L. Russell, 2015: GCM Simulations of Titan's Middle and Lower Atmosphere and Comparison to Observations. *Icarus*, **250**, 516–528.

Lora, J. M., and J. L. Mitchell, 2015: Titan's asymmetric lake distribution mediated by methane transport due to atmospheric eddies. *Geophysical Research Letters*, **42 (15)**, 6213–6220, https://doi.org/10.1002/2015GL064912, URL http://doi.wiley.com/10.1002/ 2015GL064912.

Lora, J. M., T. Tokano, J. Vatant d'Ollone, S. Lebonnois, and R. D. Lorenz, 2019: A model intercomparison of Titan's climate and low-latitude environment. *Icarus*, **333 (December 2018)**, 113–126, https://doi.org/10.1016/j.icarus.2019.05. 031, URL https://doi.org/10.1016/j.icarus.2019.05.031https://linkinghub.elsevier.com/ retrieve/pii/S0019103518307838.

Lunine, J. I., and R. D. Lorenz, 2009: Rivers, Lakes, Dunes, and Rain: Crustal Processes in Titan's Methane Cycle. *Annual Review of Earth and Planetary Sciences*, **37**, 299–320.

Manners, J., 2017: SOCRATES (Suite Of Community RAdiative Transfer codes based on Edwards and Slingo). *Technical Guide, Met Office, Exeter, UK.*

McKay, C. P., J. B. Pollack, and R. Courtin, 1991: The Greenhouse and Antigreenhouse Effects on Titan. *Science*, **253 (5024)**, 1118–1121, https://doi.org/10.1126/science. 11538492.

McKinney, M., J. Mitchell, and S. I. Thomson, 2022: Effects of Varying Land Coverage, Rotation Period, and Water Vapor on Equatorial Climates that Bridge the Gap between Earth-like and Titan-like. URL http://arxiv.org/abs/2207.05815, 2207.05815.

Mitchell, J. L., and S. A. Hill, 2021: Constraints from Invariant Subtropical Vertical Velocities on the Scalings of Hadley Cell Strength and Downdraft Width with Rotation Rate. *Journal of the Atmospheric Sciences*, **78 (5)**, 1445–1463, https://doi.org/10.1175/JAS-D-20-0191.1, URL https://journals.ametsoc.org/view/journals/atsc/78/5/JAS-D-20-0191.1.xml.

Mitchell, J. L., and J. M. Lora, 2016: The Climate of Titan. *Annual Review of Earth and Planetary Sciences*, **44 (1)**, 353–380, https://doi.org/10.1146/annurev-earth-060115-012428, URL http://www.annualreviews.org/doi/10.1146/annurev-earth-060115-012428.

Niemann, H., and Coauthors, 2005: The Abundances of Constituents of Titan's Atmosphere From the GCMS Instrument on the Huygens Probe. *Nature*, **438 (7069)**, 779–784.

O'Gorman, P. A., and T. Schneider, 2006: Stochastic Models for the Kinematics of Moisture Transport and Condensation in Homogeneous Turbulent Flows. *Journal of the Atmospheric Sciences*, **63 (11)**, 2992–3005.

Pauluis, O., 2004: Boundary Layer Dynamics and Cross-Equatorial Hadley Circulation. *Journal of the Atmospheric Sciences*, **61 (10)**, 1161–1173, https://doi.org/10.1175/1520-0469(2004)061⟨1161:BLDACH⟩2.0.CO;2, URL http://journals.ametsoc.org/doi/10.1175/1520-0469(2004)061%3C1161:BLDACH%3E2.0.CO;2.

Plumb, R. A., and A. Y. Hou, 1992: The Response of a Zonally Symmetric Atmosphere to Subtropical Thermal Forcing: Threshold Behavior. *Journal of the Atmospheric Sciences*, **49 (19)**, 1790–1799, https://doi.org/10.1175/1520-0469(1992)049⟨1790:

TROAZS⟩2.0.CO;2, URL http://journals.ametsoc.org/doi/10.1175/1520-0469(1992)049%
3C1790:TROAZS%3E2.0.CO;2.

Schneider, E. K., 1977: Axially Symmetric Steady-State Models of the Basic State for Instability and Climate Studies. Part II. Nonlinear Calculations. *Journal of the Atmospheric Sciences*, **34 (2)**, 280–296, https://doi.org/10.1175/1520-0469(1977)034⟨0280: ASSSMO⟩2.0.CO;2, URL http://journals.ametsoc.org/doi/10.1175/1520-0469(1977)034% 3C0280:ASSSMO%3E2.0.CO;2.

Schneider, E. K., 1987: A Simplified Model of the Modified Hadley Circulation. *Journal of the Atmospheric Sciences*, **44 (22)**, 3311–3328, https://doi.org/10.1175/ 1520-0469(1987)044⟨3311:ASMOTM⟩2.0.CO;2, URL http://journals.ametsoc.org/doi/10. 1175/1520-0469(1987)044%3C3311:ASMOTM%3E2.0.CO;2.

Singh, M. S., 2019: Limits on the Extent of the Solsticial Hadley Cell: The Role of Planetary Rotation. *Journal of the Atmospheric Sciences*, **76 (7)**, 1989–2004, https://doi.org/10. 1175/JAS-D-18-0341.1, URL https://journals.ametsoc.org/doi/10.1175/JAS-D-18-0341. 1.

Sobel, A. H., J. Nilsson, and L. M. Polvani, 2001: The Weak Temperature Gradient Approximation and Balanced Tropical Moisture Waves*. *Journal of the Atmospheric Sciences*, **58 (23)**, 3650–3665, https://doi.org/10.1175/1520-0469(2001)058⟨3650:TWTGAA⟩ 2.0.CO;2, URL http://journals.ametsoc.org/doi/10.1175/1520-0469(2001)058%3C3650: TWTGAA%3E2.0.CO;2.

Thomson, S. I., and G. K. Vallis, 2019: Hierarchical Modeling of Solar System Planets with Isca. *Atmosphere*, **10 (12)**, 803.

Tokano, T., C. P. McKay, F. M. Neubauer, S. K. Atreya, F. Ferri, M. Fulchignoni, and H. B. Niemann, 2006: Methane drizzle on Titan. *Nature*, **442 (7101)**, 432–435, https://doi.org/ 10.1038/nature04948.

Turtle, E. P., and Coauthors, 2011: Rapid and Extensive Surface Changes Near Titan's Equator: Evidence of April Showers. *Science*, **331 (6023)**, 1414–1417.

Turtle, E. P., and Coauthors, 2018: Titan's Meteorology Over the Cassini Mission: Evidence for Extensive Subsurface Methane Reservoirs. *Geophysical Research Letters*, **45 (11)**, 5320–5328, https://doi.org/10.1029/2018GL078170, URL https://onlinelibrary. wiley.com/doi/abs/10.1029/2018GL078170.

Vallis, G. K., and Coauthors, 2018: Isca, V1.0: A Framework for the Global Modelling of the Atmospheres of Earth and Other Planets at Varying Levels of Complexity. *Geoscientific Model Development*, **11 (3)**, 843–859.

Walker, C. C., and T. Schneider, 2006: Eddy Influences on Hadley Circulations: Simulations with an Idealized GCM. *Journal of the Atmospheric Sciences*, **63 (12)**, 3333–3350, https://doi.org/10.1175/JAS3821.1, URL http://journals.ametsoc.org/doi/abs/10.1175/ JAS3821.1.

Wolf, E. T., and O. B. Toon, 2015: The evolution of habitable climates under the brightening Sun. *Journal of Geophysical Research: Atmospheres*, **120 (12)**, 5775–5794, https://doi.org/10.1002/2015JD023302, URL http://doi.wiley.com/10.1002/ 2015JD023302.